INSIGHTS OF ENERGY FLEXIBILITY AND VIABILITY ENHANCEMENT FOR OCEAN ENERGY SUPPORTED COASTAL COMMERCIAL BUILDINGS WITH INTELLIGENT CONTROLS IN RESPONDING TO DYNAMIC BUSINESS MODELS AND GRID INCENTIVES

ZHOU SHIJIE

PhD

The Hong Kong Polytechnic University

2025

The Hong Kong Polytechnic University
Department of Building Environment and Energy Engineering

Insights of energy flexibility and viability enhancement for ocean energy supported coastal commercial buildings with intelligent controls in responding to dynamic business models and grid incentives

ZHOU Shijie

A thesis submitted in partial fulfilment of the

requirements for the Degree of Doctor of Philosophy

October 2024

CERTIFICATE OF ORIGINALITY

I hereby declare that this thesis is my own work and that, to the best of my knowledge and belief, it reproduces no material previously published or written, nor material that has been accepted for the award of any other degree or diploma, except where due acknowledgement has been made in the text.

_____(Signed)

ZHOU Shijie (Name of student)

Abstract

Currently, buildings and transportation contribute significantly to global energy consumption, while fossil fuels are still the mainstay of electricity production and may have adverse environmental consequences. Responding to these pressing concerns, the concepts of carbon neutrality, renewable energy utilization and zero-energy buildings have gained popularity. However, several challenges still need further investigation, including feasibility, discrepancy between generation and energy consumption and dependence on feed-in tariffs. Therefore, comprehensive research is needed to study coastal buildings by accomplishing the goal of a zero-energy building using a mixture of ocean energy resources while considering the design of different energy management schemes. The practicability of achieving zero-energy buildings using hybrid ocean energy systems was evaluated. To enhance energy flexibility and implement demand response control, the study explores the use of batteries for energy shifting, reducing peak demand and improving economic performance. Expanding the scale and number of the studied buildings, the research considers massive zero-energy ferry terminal buildings in two cities to establish a cross-harbour system. Attempts are made to contribute to performance enhancement by reaching cross-harbour energy sharing through self-built submarine cables, where relevant commercial policies are also examined to support the zero-energy buildings. Finally, electric ferries and electric cars with transport tasks are transformed into mobile energy storage devices with vehicle-to-building functionality to be able to take part in the energy-sharing responsibilities. Results showed that a sea-source cooling system could achieve high efficiency as well as reduce the energy demand, and a hybrid floating PV and tidal stream generator was feasible to meet the zero-emission building, with matching indicators between 0.4 and 0.7. This zero-emission system could achieve a positive relative net present value, and the high share of the tidal stream generator system reduced the economic performance. Batteries could enhance energy-matching performance, but their inclusion harmed economic and environmental performance. Energy flexibility control of peak shaving and valley filling could be effectively implemented through batteries, and demand charge could be effectively reduced during the peak period. Meanwhile, the energy flexibility-based strategy responded perfectly to the programme's events and obtained incentives, resulting in a remarkable economic enhancement. However, such an enhancement still made it difficult to increase the renewable energy penetration to 30% without relying on feed-in tariff subsidies. Having looked further at a cross-harbour system, in the scenario of two separate systems in the respective region, the capacity of submarine cables could be less than the maximum capacity only if a floating PV system constructed offshore was present. Although the batteries instituted offshore could substitute a partial submarine cable capacity to reduce the dumped energy, the economic performance was compromised. In a scenario where submarine cables connect all sites, the energy-sharing strategy enabled 40% of the maximum submarine cable capacity without the dumped energy, while energy matching and economic performance were significantly improved. Energy sharing in the integrated feed-in tariff policy was more enhanced for economic performance in source-based compared to boundary-based. Electric ferries and electric vehicles

incorporating the vehicle-to-building feature were able to enhance energy sharing further. However, the enhancement was not significant.

Publications during PhD study

Journal papers

[Publication I]. S. Zhou, S. Cao, and S. Wang, "Realisation of a coastal zero-emission office building with the support of hybrid ocean thermal, floating photovoltaics, and tidal stream generators," ***Energy Conversion and Management***, vol. 253, p. 115135, 2022/02/01/ 2022, doi: https://doi.org/10.1016/j.enconman.2021.115135.

[Publication II]. S. Zhou and S. Cao, "Energy flexibility and viability enhancement for an ocean-energy-supported zero-emission office building with respect to both existing and advanced utility business models with dynamic responsive incentives," ***Energy Reports***, vol. 8, pp. 10244-10271, 2022/11/01/ 2022, doi: https://doi.org/10.1016/j.egyr.2022.08.005.

[Publication III]. S. Zhou and S. Cao, "Co-ordinations of ocean energy supported energy sharing between zero-emission cross-harbour buildings in the Greater Bay Area," ***Applied Energy***, vol. 359, p. 122718, 2024/04/01/ 2024, doi: https://doi.org/10.1016/j.apenergy.2024.122718.

[Publication IV]. S. Zhou, X. Guo and S. Cao, " Enhanced energy sharing and management between cross-harbour zero-emission buildings based on a combination of electric ferries and deck-on electric vehicles," (Officially accepted by ***International Journal of Energy Research***).

Acknowledgements

This thesis summarises the results of my four years PhD work under professional guidance and valuable help from experienced researchers and international professors. It is my great honour to take this precious opportunity to show my sincere gratitude for their selfless and help.

First and foremost, I would like to express my deepest appreciation to my chief supervisor, Dr. Cao Sunliang, for his continuous professional guidance, invaluable patience and support throughout my PhD study. His expertise, insightful feedback, and unwavering commitment have been instrumental in shaping my current thesis and inspired me on my future research.

I would also like to extend my heartfelt appreciation to my co-supervisor, Prof. Yang Hongxing, for his valuable knowledge, expertise and constructive discussions on my study.

Furthermore, I would like to sincerely thank all members in our research group for their assistance and collaboration. I am also grateful to all the staffs and the technicians of our department for their services and the financial support from the Hong Kong Polytechnic University.

Lastly, I would like to express my gratitude to my family, particularly my parents, for their unwavering support and encouragement throughout my PhD journey. Their love, understanding, and belief in my abilities have motivated me to overcome challenges and achieve my goals.

Table of Contents

List of Figures

List of Tables

Nomenclature

Abbreviations

AHUCS	Air handling unit cooling system
ANLC:	Average nearshore land cost
B2V	Building-to-vehicle function
COP	Cooling coefficient of performance
CEM Macau:	Companhia de Electricidade de Macau
CLP:	China Light and Power Company Syndicate
DHW:	Domestic hot water
EV	Electric vehicles
FiT:	Feed-in tariff
FPV	Floating photovoltaic system
FSOC	Fractional battery state of charge
GBA	Greater Bay Area
G2V	Grid-to-vehicles function
HVAC	Heating, Ventilation, and Air Conditioning
HKD	Hong Kong dollar
MNLC:	Maximum nearshore land cost
MOP	Macau Pataca
NTU	Number of transfer units
OEFe:	On-site electrical energy fraction
OEMe:	On-site electrical energy matching
OTE	Ocean thermal energy
PV	Photovoltaics
PDM	Peak Demand Management programme
RE	Renewable energy
SC	Space cooling system
TSG	Tidal stream generator system
V2B	Vehicle-to-building function
WMI	Weighted matching index
ZEB:	Zero-emission/energy building

Notations

B_t:	The benefit of period t compared with the reference case (HKD)
C_t:	The cost of period t compared with the reference case (HKD)
CEF_{eg}:	The equivalent CO_2 emission factor of the electric grid (kg $CO_{2,\,eq}$/kWh$_e$)
CE_a:	The annual operational equivalent CO_2 emission (kg $CO_{2,\,eq}$/m^2.a)
$E_{imp,a}$:	annual import energy from the grid (kWh)
$E_{exp,a}$:	annual export energy to the grid (kWh)
$E_{dumped}(t)$:	The dumped energy that cannot be transported through submarine cable (kWh)

$E_{RE,total}(t)$:	The total renewable energy generation of all the nearshore and offshore sites (kWh)
i:	Interest rate (%)
$L_{elec}(t)$:	The total electricity load power of the building (kW)
NPV_{rel}:	Relative net present value (HKD)
n:	The total lifetime (Year)
PSI_{peak}:	Peak shaving indicator
$P_{exp}(t)$	Exported power from the system to the grid (kW)
$P_{imp}(t)$:	Imported power from the system to the grid (kW)
$P_{REe}(t)$:	The electricity power output of the hybrid renewable energy system (kW)
$P_{j,\ p(t)}$	Demand duration of selected case j with flexibility control strategy during the peak period
$P_{ref,\ p(t)}$	Demand duration of reference case during the peak period
$P_{avg,\ ref,\ p(t)}$	Average demand line of the reference case during the peak period
$P_{j,\ op(t)}$	Demand duration curve of selected case j with flexibility control strategy during the off-peak period
$P_{ref,\ op(t)}$	Demand duration curve of reference case during the off-peak period
$P_{avg,\ ref,\ op(t)}$	Average demand line of the reference case during the off-peak period
$r_{energy\ usage}$:	Energy usage ratio (%)
SPP_{rel}	Relative simple payback period (Year)
$t_{p,\ ref}$	Temporal intersection of the demand duration and the average demand line of the reference case during the peak period
$t_{op,\ ref}$	Temporal intersection of the demand duration curve and the average demand line of the reference case during the off-peak period
$VFI_{offpeak}$:	Off-peak valley filling indicator
WMI	Weighted matching index

Chapter 1. Introduction

1.1 Research background

Buildings and transportation collectively contribute a significant share of energy consumption, with buildings accounting for 30% and transportation for 27% [1, 2]. In the highly urbanized cityscape of the Hong Kong Special Administrative Region (HKSAR), the energy consumption value of these two sector can rise to approximately 67% and 29% [3]. The issue of global warming has intensified in recent years, with increased greenhouse gas emissions and the negative environmental impact. Recognizing the urgent need to curb excessive carbon emissions and combat global warming, carbon neutrality emerged as a key topic among countries [4]. In line with the global focus on carbon neutrality, the Hong Kong government released the related policy outlining its commitment to achieving carbon neutrality after 26 years [5]. Consequently, the concept of zero-energy or zero-emission buildings has gained significant importance.

Zero-energy buildings are characterized by their high energy performance and grid connectivity. They are often incorporate with renewable energy generation systems that matches the energy consumed from the grid during critical loading periods [6]. Over the past years, policies have increasingly focused on achieving zero-emission buildings through stringent energy efficiency standards and carbon-neutral construction practices. The European Union mandates that all new buildings meet near-zero energy consumption standards by 2030, focusing on retrofitting existing structures [7]. Similarly, China released the action plan, promoting the use of low-carbon materials, such as cross-laminated timber and recycled steel, alongside advanced insulation techniques to minimize operational emissions [8]. These policies also emphasize lifecycle carbon assessments, ensuring buildings remain sustainable from construction to decommissioning. Governments are also increasingly focused on integrating renewable energy into building designs. The U.S. encourages using solar photovoltaic (PV) systems, wind turbines, and geothermal heat pumps in residential and commercial buildings [9]. These policies are further enhanced by financial incentives, such as tax credits and subsidies, to promote faster adoption of renewable technologies.

However, the large-scale deployment of intermittent renewable energy systems in the future, coupled with fluctuations in the energy market, can pose challenges to the operation and stability of smart grids. This situation introduces uncertainty and instability in the supply and demand of electricity. To ensure consistency between energy generation and consumption, experts from the International Energy Agency (IEA) propose the control of energy usage. Energy flexibility, which involves managing the energy consumption based on user requirements, local climate conditions, and energy network needs, offers an effective approach as it eliminates the need for additional infrastructure. Energy flexibility enhancement can alleviate peak strain on the power grid and enhance the persistence of future energy systems [10]. The energy

generation of current renewable energy facilities often leads to a considerable matching discrepancy between renewable energy generation and energy demand in zero-energy buildings.

Technologies related to advanced metering equipment and smart grid can facilitate the control of demand side management and energy flexibility [11]. Energy flexibility has emerged as a key policy focus, with governments promoting innovative technologies to optimize energy use. The European Union requires buildings to incorporate demand-side management systems, such as smart meters and energy storage solutions, to shift consumption to off-peak periods [12]. The U.S. encourages using thermal storage and advanced HVAC systems to enhance grid stability [13]. These measures aim to reduce peak demand, lower energy costs, and improve resilience against power outages. Investigating methods to enhance flexibility in zero-energy buildings can help mitigate this inconsistency, enlarge the self-consumption of renewable energy within the system, and alleviate peak power pressure on the grid. Therefore, further research in this area is of great significance. Building-based Demand Response refers to a systematic approach in which buildings actively adjust their electricity consumption patterns in response to grid conditions, price fluctuations, or incentive programs to balance energy supply and demand, achieving incentives provided by power company. This involves leveraging building systems such as HVAC, lighting, energy storage, and distributed generation to reduce or shift load during peak periods, enhance grid reliability, lower energy costs, and support renewable energy integration. Building-based demand response relies on automation, real-time data analytics, and smart control technologies to optimize energy use without compromising occupant comfort or operational performance [14] [15]. Energy-sharing presents an approach to reducing mismatches and improving energy utilization in multiple zero-energy buildings or communities. Electric vehicles, with their potential as mobile electrical energy storage devices, offer an opportunity for vehicle-to-building energy-sharing, which can serve as a tool for energy-sharing and help save investment costs. Peer-to-peer energy trading was enabled in the UK within local microgrids, allowing households to share surplus solar power [16]. These initiatives foster community engagement and ensure equitable access to clean energy. However, the impact of electric vehicles with vehicle-to-building functionality on energy-sharing and the techno-economic performance of zero-energy buildings or communities requires further exploration.

1.2 Literature reviews

In this section, a detailed state-of-the-art literature review is conducted on the zero-energy buildings, ocean related renewable energy systems, energy flexibility, demand response and corresponding policy and business model, energy sharing within zero-energy buildings or communities, the application of electric transportation including electric vehicles and electric ferry. Based on the summarised literature reviews, the related research gaps, research novelty and contributions are identified on each aspect.

1.2.1 Literature review on zero-energy building

In the field of academia, researchers have dedicated their efforts to exploring zero-energy buildings as a solution to resolve the issue of energy consumption in the built environment. Various approaches have been proposed, including passive building designs aimed at reducing energy consumption and the implementation of onsite renewable energy systems. De Masi et al. conducted a study using a multi-domain method to assess the overall quality of nearly zero-energy buildings. They examined a case study in a Mediterranean climate to evaluate the feasibility of their approach. The study considered five criteria, including indoor comfort and energy aspects, with different weighting factors based on occupant feedback regarding the relative importance of residential usage criteria [17]. Yoon and Lee introduced a waste upcycling-driven approach to achieve zero-energy buildings. Their method involved additional energy generation through waste-to-energy processes, enhancing building energy efficiency using advanced materials recovered from waste and maintaining assets through earnings from waste upcycling and management. This integrated approach aimed to achieve net zero energy status and eliminate solid waste in landfills throughout the building's life cycle [18]. Oualid et al. investigated the regulatory framework of the energy strategy, performance indicators, definitions and assessment metrics for nearly zero energy buildings in Morocco [19]. Alqaed et al. explored the impact of solar walls integrated with phase change material on enhancing energy efficiency in zero-energy buildings. They utilized larger areas with phase change material-filled compartments to improve the thermal performance of buildings [20]. Ohene et al. proposed an enhancement approach to improve the design of residential buildings, focusing on energy efficiency and renewable energy systems with the goal of achieving net zero energy status. The approach incorporated life cycle cost analysis and demonstrated significant reductions in annual energy consumption, saving more than 30% of energy [21]. Li and Gou compared net-zero energy building approaches and typical cases between developed and developing countries, using the United States, India, and China as examples. Their study aimed to provide recommendations to bridge the gap in net-zero building development strategies and assist in the formulation of effective strategies. [22]. Forrousso et al. utilised a particle swarm optimisation algorithm to design the optimal size of an off grid microgrid system for net zero energy residential buildings in Morocco. The study considered the hourly spatiotemporal variations in solar energy availability and energy demand, aiming to minimize the total cost while determining the optimal capacities of building-integrated photovoltaic systems and battery energy storage installations. [23]. Sady et al. designed a smart control of underground air ducts, optimal microgrid, and Trombe walls using renewable energy systems to achieve net-zero energy building and investigate the dynamic energy simulation performance. Their research aimed to achieve net zero energy buildings and investigate the dynamic energy simulation performance. The study demonstrated that integrating Trombe walls with a coupled geothermal cooling system and air ducts can effectively reduce both heating and cooling loads, consequently decreasing the daily electricity demand of the base building [24].

1.2.2 Literature review on ocean renewable energy

Ocean energy, as a promising renewable energy source, has garnered significant attention from researchers in the academic community. Li et al. presented an innovative energy harvesting device that combines vortex-induced vibration and multi-grating triboelectric nanogenerators. This device harnesses the motion of an up and down floating mechanism to drive the nanogenerators, converting kinetic energy from low-speed ocean currents into electrical energy [25]. Bianchi and Fernandez introduced a systematic methodology for evaluating the economic impact of ocean renewable energy projects on local regions. They applied this approach to a tidal energy farm to assess its economic benefits in the early stages of development, providing valuable insights for understanding the economic viability of ocean renewable energy initiatives [26]. In another study, Bianchi et al. evaluated the life cycle, environmental, and economic performance of a 34.5 MW tidal farm project. Their assessment aimed to advance the understanding of tidal energy converters' economic and environmental aspects, facilitating their integration into the market. The analysis demonstrated the competitiveness of tidal energy in terms of the levelized cost of electricity [27]. To address the nonlinearity and nonstationarity of tidal energy, Yang et al. introduced a multi-stage forecasting system for predicting daily tidal energy generation. This system utilises advanced techniques to improve the accuracy of predictions and has been validated through experimental results in various cities [28]. Mo et al. focused on developing a deep learning-based method to rapidly identify the status of turbine pollutant adhesion in tidal energy generation systems. Such adhesion can lead to marine biofouling and reduced turbine efficiency. By employing different deep learning algorithms and an existing dataset from a tidal stream generation (TSG) system, they enhanced the quality of underwater biofouling images. The suggested method successfully improved the accuracy of pollutant identification, thereby reducing operational costs [29].

Excepting research on ocean energy mechanisation that can be directly converted into electricity, research on ocean thermal energy (OTE) technologies and applications is also receiving attention from researchers. Rashid et al. analysed the energy and economic performance of a potential OTE conversion plant in Bangladesh. They developed a machine learning model to forecast the plant's future lifetime. The annual average energy generation can be more than 100 MW with an 11-year payback period [30]. Fan et al. introduced a solar pond-assisted system in ocean thermal energy conversion, preheating the warm seawater before entering to improve thermal efficiency. Its thermodynamic model was developed, and the pumping depth of cold seawater and the role of temperature extraction on power generation potential were analysed [31]. Zhang et al. established a solar-OTE conversion integrated air-conditioning system with a capacity of 1 kW to provide electrical energy and cooling energy, and the overall performance was analysed based on energy economy, energy, environment and exergy; the results indicate that the system can achieve higher efficiency compared to the system without solar [32]. Gao et al. proposed a cycle assisted by solar aiming to enhance the efficiency of the OTE conversion system

based on the organic Rankine cycle and established the experimental equipment of the conversion system. Through the exergy and energy analysis, they showed that the proposed system achieved improved efficiency compared to the original ocean thermal energy system [33]. Du et al. introduced four different systems to recover the waste heat from offshore gas and oil platforms to improve the efficiency of the OTE conversion system and studied the thermodynamic performance. Their results show that the production water boosting vapor OTE conversion system can obtain larger generation, thermal and exergy efficiency [34]. Chen et al. employed a non-azeotropic mixed working fluid to establish a new cycle of the ocean temperature and the addition of a secondary heat recovery device to promote the generation of the OTE conversion [35].

Photovoltaic (PV) panels are one of the most common renewable energy technologies for solar energy utilisation. However, they require large land areas. Researchers are exploring how installing photovoltaic panels on reservoirs or the sea could reduce land occupation and make them ocean-related renewable energy systems, which is called the floating PV (FPV) system. Zhang et al. discussed the generation, verification, design, and construction of the innovative modular FPV that has been applied in a nearshore floating photovoltaic farm in Singapore. The floating system of the mentioned design can follow the motion of the waves, and can withstand the harsher conditions of the marine environment [36]. Alcañiz et al. introduced a 3D mechanical movement model to determine the impact of the floater dimension on the fluctuation size and evaluate the generation of an FPV system constructed offshore considering the wave impact. Their results showed that fluctuations in seawater reduce PV production over one year on both DC and AC power simulations [37]. Irshad et al. explored the performance of the FPV and pumped hydro storage system, focusing on the load side and capacity factor of pumped hydro storage. The utilisation of a genetic algorithm with multi-objective allowed for the simulation, and the results demonstrated that a hybrid FPV and pump storage hydropower system has the potential to reliably generate clean and stable electricity [38]. C.J. et al. assessed the impact of different parameters such as ambient temperature, height, tilt angle, water temperature and wind on the FPV system. PV panels under the nominal operating cell temperature condition were used as the reference case, and the comparison was conducted using CFD simulation. [39]. Dzamesi et al. compared the advantages and disadvantages of the FPV system with a ground-mounted PV system. Their results showed that FPV systems can achieve lower temperatures, more efficient area cover use, and larger energy generation capabilities. However, one significant challenge associated with FPV systems is the susceptibility to corrosion [40].

1.2.3 Literature review on energy flexibility

Zero-energy buildings are commonly equipped with on-site renewable energy resources. However, due to the inherent characteristics of renewable energy generation, such as intermittency, the energy produced may not always align with the building's energy demand. This match discrepancy can have economic implications for the building and the stability of the

power grid. In response to this challenge, researchers have increasingly focused on energy flexibility as a promising approach to mitigate the mismatch. Torrejon et al. combined the monitored data and an existing rating methodology into design-based flexibility ratings to quantify the energy flexibility in existing buildings. They first checked whether the extant rating methods were acceptable for monitoring data and designed two calculating methods based on the physical models [41]. Maitanova et al. proposed an independent technique to quantify the flexibility potential over time of differentiated energy systems. The proposed method was validated by two case studies [42]. Erfani et al. investigated how the dataset size and excitation method affect the model predictive control to enhance energy flexibility and solve the difference between supply and demand. Their results indicate that model predictive control needs a suitable dataset; otherwise, the potential flexibility may be lost [43]. Afroz et al. utilised the flexibility approach and a virtual battery model to analyse the behaviour of a commercial building energy flexibility with a cooling system in response to price signals. They highlighted the significant influence of HVAC system operation on electricity demand flexibility, emphasising potential cost savings through effective price-response behaviour [44]. Förster et al. focused on the quantification of the potential of dynamic tariffs and explored their ecological and economic implications, particularly during energy crises. Their results indicate that the application of energy flexibility combined with a dynamic electricity tariff can reduce energy costs [45]. Liang et al. combined a quantification workflow for energy flexibility and a model predictive control method. They applied these approaches to maximum energy flexibility in a net-zero energy office building, showcasing their effectiveness in a real-world case study [46]. Zhang et al. established a building clusters model with diverse cluster sizes, compositions, and building types using an archetype-based method to describe the flexibility. Through simulations, they demonstrated that the implementation of strategies can effectively reduce peak demand [47]. Stegemerten et al. proposed an agent-based framework to assess the flexibility potential from the building energy system during the operation based on the impact of dynamic energy price and cost. The results indicate the flexibility is significantly affected by the heat transfer systems, building boundaries and envelope [48]. Fan et al. developed a generalized method to evaluate the flexibility potential of active thermal energy storage systems which include the flexibility indicators and theoretical heat transfer performance model. Their results show that the designed method can assess the flexibility potential of active thermal energy storage systems precisely [49].

1.2.4 Literature review on demand response

Demand response in ordinary or zero-energy buildings is a methodology to manage demand that responds to the demand of the grid to relieve the pressure on the grid, and it is currently receiving a lot of attention in the academic community. Atefi and Gholaminia introduced a flexible demand response featuring a stair-step pricing mechanism to optimise consumer consumption patterns while considering their specific constraints. Their proposed algorithm incentivises consumer participation in energy management programs by accommodating diverse constraints [50]. Sun et al. utilised

demand-side management and microgrids to manage the power system. Their approach focuses on cost reduction and load shifting. The load response program participation can reduce the peak load through the proposed method [51]. Yu et al. presented a combined photovoltaic and thermal coupling system integrating heat pumps and energy storage within a single building. The energy coupling system is combined with demand-side management; the aim is to achieve a balance between energy production and power grid load pressure. Based on the developed simulation, the proposed system and applied management strategy can achieve energy saving [52]. Çakmak designed a low-cost power logger device for collecting and analysing household power demand profiles together with demand-side management. The feasibility and reliability of the proposed prototype are validated by the test [53]. Ireshika and Kepplinger introduced a framework with model predictive control to schedule the charging activity of electric vehicles to solve the uncertainties in the demand side management. They utilised a decentralized demand-side management algorithm based on the uncertainty related to electric vehicle user behaviour, aggregated electric vehicle demand and non-elastic load for the evaluation. The results show that the proposed method is feasible to handle the mentioned uncertainties [54]. Roshan and D suggested a machine learning algorithm based smart energy management strategy among residential consumers to conduct demand side management and utilise supervised learning techniques to classify the daily load profile of residential consumers [55]. Nilges et al. conducted demand-side management through the cost-optimal load shifting to analyse the impact on the variations in emissions. Their results indicate that greenhouse gas emissions can be affected by the load shifting and the electricity generation mix within electric power systems [56]. Manoharan et al. investigated the impact on the renewable energy system by the different combinations of long-term planning decisions, energy saving strategies and system installations, as well as an optimization framework to determine the demand side management and energy storage capacity. The proposed framework was validated by cases and tools [57]. Kumaresan and Jeyaraj introduced a new energy scheduling strategy for smart buildings aiming to enhance energy efficiency while ensuring user comfort. The findings demonstrate that this strategy effectively optimises energy consumption without compromising user satisfaction, making it a reliable solution for managing energy in IoT-enabled smart residential buildings [58].

1.2.5 Literature review on energy sharing strategy and related business model

Energy sharing in multiple zero-energy buildings or zero-energy communities is an approach that can efficiently consume excess renewable energy generation to improve techno-economic performance, and many academics are researching this direction. Meanwhile, business policies and modelling related to energy sharing are also worthy topics for research. Li et al. presented a distant energy sharing between a hotel building and an office building facilitated by an ocean renewable energy system, the objective of which was to maximise environmental and techno-economic benefits for stakeholders. The results demonstrated the efficacy of utilising electric vehicles and renewable energy for distant energy sharing [59]. Minuto et al. investigated the tilt angles for rooftop PV systems that can achieve the best output in renewable energy communities

with energy-sharing functions to maximise the shared energy index [60]. Tiwari et al. utilised the k-Means algorithm for the Voltage Sensitivity Factor based peer clustering to establish a demand response framework with real-time pricing and a multi-objective optimisation model aiming to solve the negative influence of peer-to-peer energy trading and sharing; the demand response potential has also quantified [61]. Bokopane et al. suggested an optimization method for a grid-connected charging station integrated with peer-to-peer vehicle energy-sharing strategies, PV system and battery storage. The results demonstrated significant reductions in energy demand costs [62]. Sayed et al. discussed the feasibility of the existing solar PV systems with interconnections in rural communities to conduct energy sharing, reducing the waste of renewable energy generation due to the limited capacities. Their analysis indicated that peer-to-peer interconnection energy sharing can enhance self-sufficiency and self-consumption, bringing benefits [63]. Minelli et al. examined how to broaden the net-zero energy building concept to evaluate its applicability to energy-sharing models based on the grid, the dynamic sharing status was investigated, and different energy-sharing scenarios were analysed [64]. Bian et al. established a peer-to-peer energy-sharing model combined with shared energy storage, trying to promote flexible energy trading among microgrids and effectively utilise renewable energy generation. They applied an innovative optimal scheduling strategy for the zone of energy sharing and an optimal allocation scheme with multi-objectives, which can reduce the cost of energy [65]. Ji et al. proposed a bi-level optimisation framework that considers economic efficiency and hydraulic stability as objectives for the energy systems of several communities and utilizes energy sharing as the main process. The results demonstrated cost and emission reductions while maintaining hydraulic stability [66]. Zhou and Lund summarised the energy sharing and trading price mechanisms, decision-making in dynamic energy trading and system configurations for peer-to-peer energy trading and sharing, which indicate that the optimal design can bring economic benefit to all related stakeholders [67]. Chen et al. introduced an operation for shared energy storage to achieve the optimal battery capacity. The time-of-use tariff for the photovoltaic battery system connected to the grid in the energy-sharing community was considered. The goal was to maximise the self-consumption ratio, minimise the payback period, and reduce power transportation losses [68].

1.2.6 Literature review on electric transportation

In addition to buildings, transportation constitutes a significant portion of consumed energy and contributes considerably to environmental degradation. The future of electric vehicles (EVs), which offer benefits such as low noise and zero emissions, holds great promise, and research in this area is steadily progressing. Algafri et al. addressed the challenge of effectively allocating EVs to suitable charging stations using a methodology that combines a programming model with a multi-objective goal in the analysis process. [69]. Garau and Torsæter proposed a methodology to obtain the best placement design for renewable generation and electric vehicle charging. The objectives of this methodology are to minimise electric vehicles charging radius coverage, maximising energy generation, the number of energy hub units and distance from power

substations [70]. He et al. predicted the charging load in Okinawa and established an algorithm based on demand response to select the ideal charging time that can minimise the load difference between off-peak and peak periods. Their proposed method reduces energy costs and enhances grid stability [71]. Zhan et al. proposed a framework to predict the penetration level of electric private passenger vehicles and related reductions in emissions. Their analysis shows that optimal intensity incentives based on usage can achieve substantial long-term economic benefits and emission reduction compared to incentives based on purchase [72]. Lyu et al. conducted an evaluation of how electric vehicles affect air quality, utilising the real data of vehicles. Their analysis demonstrated that the emissions could be significantly reduced when replacing gasoline vehicles with battery-electric vehicles [73]. Zand et al. designed a structure to manage energy for EVs, combining a supercapacitor, a main battery coupled with a replaceable battery to extend the driving range and improve efficiency. They proposed a method to allocate power between different sources, optimise the design parameter and minimise weight and losses [74]. Panda and Tindemans introduced a quantification approach for electric vehicle fleets on charging flexibility, which can be tailored to meet the needs of network operators [75].

The emergence of electric vehicles has spurred research interest in electric boats as well. Roy et al. studied a two-stage system to manage power for an electric ferry utilising fuel cell and battery energy storage systems. Their aim was to achieve a balance between generated power and ferry load while minimising hydrogen fuel consumption. Their results indicate the effectiveness of the proposed system in optimising the performance of marine vessels supported by renewable energy [76]. Feng et al. introduced a model to assess the impact of economic, emission and energy and evaluate the decarbonisation potential of electric ships; the impact of climate policies on emissions is also analysed. They also suggested that advanced decarbonisation should focus on energy efficiency and fostering electrification enhancement [77]. Song et al. presented an energy management strategy based on a hybrid penalised proximal policy optimisation algorithm. This strategy aimed to address energy management challenges by integrating the schedule of generation and adjustment on demand for electric ships [78]. Zhang et al. considered factors such as water depth, cargo amount and water speed to establish the model to obtain the energy demand for the electric ship with a swappable battery. They analysed the energy transfer process and designed a method to obtain optimal energy management and schedule of the voyage. The results validated the effectiveness of this approach [79]. Gao et al. proposed a bi-objective optimisation approach for the energy management and sailing routes for all-electric ships considering emission control to balance the emissions and total operational cost, and the impact of emission policies on navigation decisions is involved. The results presented that the model can effectively reduce operational costs and emissions [80]. Ganjian et al. presented a systematic methodology for obtaining the optimal design and energy management strategy of a hybrid fuel cell with an energy storage system in all-electric ships. Their approach considered objectives such as investment costs, fuel consumption, occupied volume of the

power system, and personnel electrical safety to determine the optimal size of the fuel cell and energy storage system [81]. Pang et al. suggested an optimal control strategy to combine the liquified natural gas engine with hybrid electric propulsion to minimise emissions and maximise fuel efficiency; the reduction of battery degradation costs is also considered [82].

1.3 Scientific gaps, research objectives, and contributions

1.3.1 Scientific research gaps

This section aims to provide a concise summary of the scientific gaps identified in the previous subsections, which focused on zero-energy buildings, ocean energy systems, energy flexibility strategies, demand response, business models, energy sharing, and related policies. Based on the comprehensive review of the literature, the following research gaps can be highlighted:

1) Zero-energy buildings research has primarily concentrated on buildings onshore, with a particular focus on small-scale normal residential buildings, as well as small communities comprising this type of buildings. These studies have primarily aimed to develop passive design strategies and implement intelligent controls to minimise building energy demand. Additionally, on-site renewable energy systems on a small scale have been integrated to achieve the objective of zero-energy buildings or communities. Furthermore, current research in the field of ocean energy primarily revolves around enhancing technology performance and efficiency, as well as understanding the impact of these technologies. The focus is on improving the design and methodologies of marine energy facilities, such as tidal and wave energy projects, to increase their viability while mitigating negative impacts. However, there is a notable lack of research on harnessing different ocean or ocean-related renewable energy sources to support coastal office buildings and even large coastal public zero-energy buildings, including ferry terminal buildings and investigate the feasibility of techno-economic performance.
2) Flexibility control in buildings, both conventional and zero-energy, has gained research interest for reducing electricity costs and integrating renewable energy sources to address the variability between demand and generation. However, current research primarily focuses on thermal systems within buildings, such as heating or cooling storage tanks and heat pumps, and the corresponding control. Meanwhile, they are also more focused on how big data or advanced data modelling can be applied to predict and validate the building's demand profile and changes to provide a basis for a better control framework approach. Furthermore, demand response programmes in many areas have been proposed to manage high electricity loads during peak periods. Research has explored the impact of different control strategies and mechanisms on reducing building bills and overall peak loads, primarily in single residential buildings. Economic analyses often focus on changes in annual electricity costs. However, there is limited studies incorporating other energy storage systems like batteries and corresponding controls in larger buildings to align with regional demand

response programmes, then examining their techno-economic performance over the entire life cycle.

3) Current energy-sharing research primarily focuses on small communities with multiple conventional or zero-emission buildings located at close distances. The emphasis lies on developing energy-sharing technologies to reduce the costs of renewable energy systems and enhance energy efficiency. Meanwhile, studies have examined changes in economic policies resulting from technology updates related to energy-sharing, but these investigations have primarily centred around small energy communities in the same location. Limited research on energy sharing between two large public zero-energy buildings situated in separate locations, especially across different special administrative districts, and the impact of different energy-sharing economic policies between distinct locations, particularly across different special administrative regions, or the integration of diverse business models and policies across these regions.
4) While researchers have begun focusing on the performance, energy management, and enhancement methods of electric zero-energy transportation systems and their associated controls, few studies have explored the utilisation of existing electric transportation systems with vehicle-to-building functions to enhance energy sharing. There is a lack of research investigating the impact of such electric transportation on the performance of a cross-harbour zero-emission buildings.

1.3.2 Research objectives

Research objectives of this thesis include:

1) To investigate the feasibility of zero-energy coastal office building using hybrid ocean-related renewable energy systems and the impact of different mixing ratios of ocean energy systems on the energy matching and economic performance of the building.
2) Design specific energy control strategies for demand-side management and energy flexibility based on the combination of the best-performing ocean energy systems in the established coastal zero-energy building and test the economic impact of these controls on the performance of the system and the economic dependence on government subsidies.
3) Expanding the size and number of buildings under study to form a cross-harbour system and designing the system with its own submarine cables for energy sharing, as well as designing an integrated commercial policy that takes into account the different policies of the two areas across the harbour.
4) Incorporate the vehicle-to-building (V2B) function into the car-carrying electric ferry and electric cars that already exist in the cross-harbour ferry terminal building system to enable them to take on the part of the energy-sharing functions and test the impact on system performance.

1.3.3 Research novelty and contributions

The research presented in this study aims to process the scientific gaps demonstrated in the former subsection and

contributes to academics in several ways. Firstly, the study conducts a feasibility analysis of a zero-energy office building situated on the Hong Kong coastline, utilising TRNSYS simulations. Unlike previous research that often focused on a single ocean energy source, this study innovatively explores a hybrid system that integrates multiple ocean-based and ocean-related renewable energy sources to support a zero-emission building. The investigation extends beyond mere feasibility, delving into the impact of various control measures on the system's economic and energy-matching performance. Emphasis is placed on enhancing flexibility by leveraging internal flexibility sources within the system. Furthermore, the research analyses the effects of different control methodologies on the system following the implementation of the PDM programme in the Hong Kong region. In addition to the study on achieving the zero-energy objective of a coastal middle scale building, this research explores the implementation of a hybrid system that encompasses two public zero-energy buildings with larger floor areas located in the cross-harbour cities. Self-built submarine cables have been adopted to explore energy management solutions that optimise the utilisation of renewable energy resources. It aims to improve the wholesale performance of the proposed system in the GBA through energy sharing. Recognising the distinct renewable energy feed-in tariff (FiT) policies of the two GBA cities, the study integrates and compares various approaches to the integration of FiT. This comparison is conducted through diverse energy management control methods and economic performance evaluations. Finally, the study seeks to promote the energy-sharing capabilities of the cross-harbour system by developing the vehicle-to-building function for electric car-carrying ferries and electric cars with transportation functions that are already part of the system. Additionally, the energy stored in the batteries of the ferries and cars will be managed effectively to further support the energy-sharing initiative when required.

1.4 Organization of the thesis

The thesis was organised as follows:

The current research on zero-energy buildings, ocean-related renewable energy systems, energy flexibility, demand response and corresponding policy and business model, energy sharing within zero-energy buildings or communities, and the application of electric transportation, including electric vehicles and electric ferries, were comprehensively reviewed in Chapter 2. Furthermore, research gaps are clearly identified based on the summarised literature reviews, and the research novelty and contribution are also presented to indicate the importance and necessity.

In Chapter 3, the details of each of the essential parts of the system built throughout the study are mainly described. Firstly, it describes the weather conditions in the area where the system is located and the data files necessary for the purpose of the simulation, e.g., the geographic location of the area where it is located and the type of climate. The weather data that also need to be applied to the hybrid ocean energy system are presented one by one, such as sea water temperature, tidal current, and solar radiation. The characteristics of these data and the monthly or time-step conditions are also presented.

Afterwards, the hybrid ocean-related renewable energy system designed in this study as the main energy supplier to reach a zero-energy building is broken down into individual systems to be presented and described. These systems include ocean thermal energy-based seawater cooling systems, floating photovoltaic systems, tidal stream generator systems and wind turbine systems. The characteristics of these systems, their advantages and the reasons why they were chosen for this research system are described in detail. Furthermore, based on each original research paper, the system components included in the research section with different research objectives and directions are also shown. These components include a coastal office building, energy storage equipment for energy flexibility and demand response control, two large-scale coastal harbour buildings in both Macau and Hong Kong, as well as the submarine cables to conduct the energy sharing through the cross-harbour system and the mobile electric transportation including one car carrying ferry and ten electric cars with V2B function for energy sharing.

Meanwhile, the overall and detailed methodology for the entire research and each part of the study is demonstrated in Chapter 4. The most basic energy flow and control of buildings supported by renewable energy systems are presented in the first study, after which the introduction of energy flexibility and demand response related to peak demand management projects with specific control based on a wide range of possible scenarios is also explained in detail. After expanding the study from a single coastal office building to two large ferry terminal buildings in a cross-harbour system, control strategies for submarine cable-based energy sharing are detailed in scenarios with and without intermediate submarine cables. Finally, energy management strategies for electric ferries and electric cars that incorporate V2B functions to take on some of the functions of energy sharing were also demonstrated. The indicators used to assess the environmental, energy matching, energy usage, energy flexibility and economic performance of the studied system were proposed and presented in this chapter.

In Chapter 5, all the simulation results are presented and evaluated. The impact of an OTE-designed sea source cooling system, different mixing ratios of ocean energy systems encompass FPV and TSG systems, as well as through the incorporation of batteries as an energy storage device on the energy matching and economic performance of the studied coastal office building system is shown and analysed in the first subsection. In the subsequent subsection, the impact of the control of the energy flexibility enhancement and Peak Demand Management (PDM) programme, which were carried out using batteries as the main tool, on the performance of the system was also tested and analysed, while several potential policy recommendations based on the energy flexibility and PDM programme were assessed. Moreover, the results obtained from the energy sharing reached through submarine cables in the cross-harbour system, and the integration challenges it poses for feed-in tariff policies in different regions are also shown and discussed. Finally, the performance

caused by the energy sharing from the electric ferry and electric cars with the V2B function with or without the presence of intermediate submarine cable was demonstrated in the last subsection. The conclusions of all parts of the research included in the thesis will be summarised in Chapter 6, along with a mention of possible future research topics and paths. The following structure of this study starting from Chapter 2 is presented in Fig. 1.1.

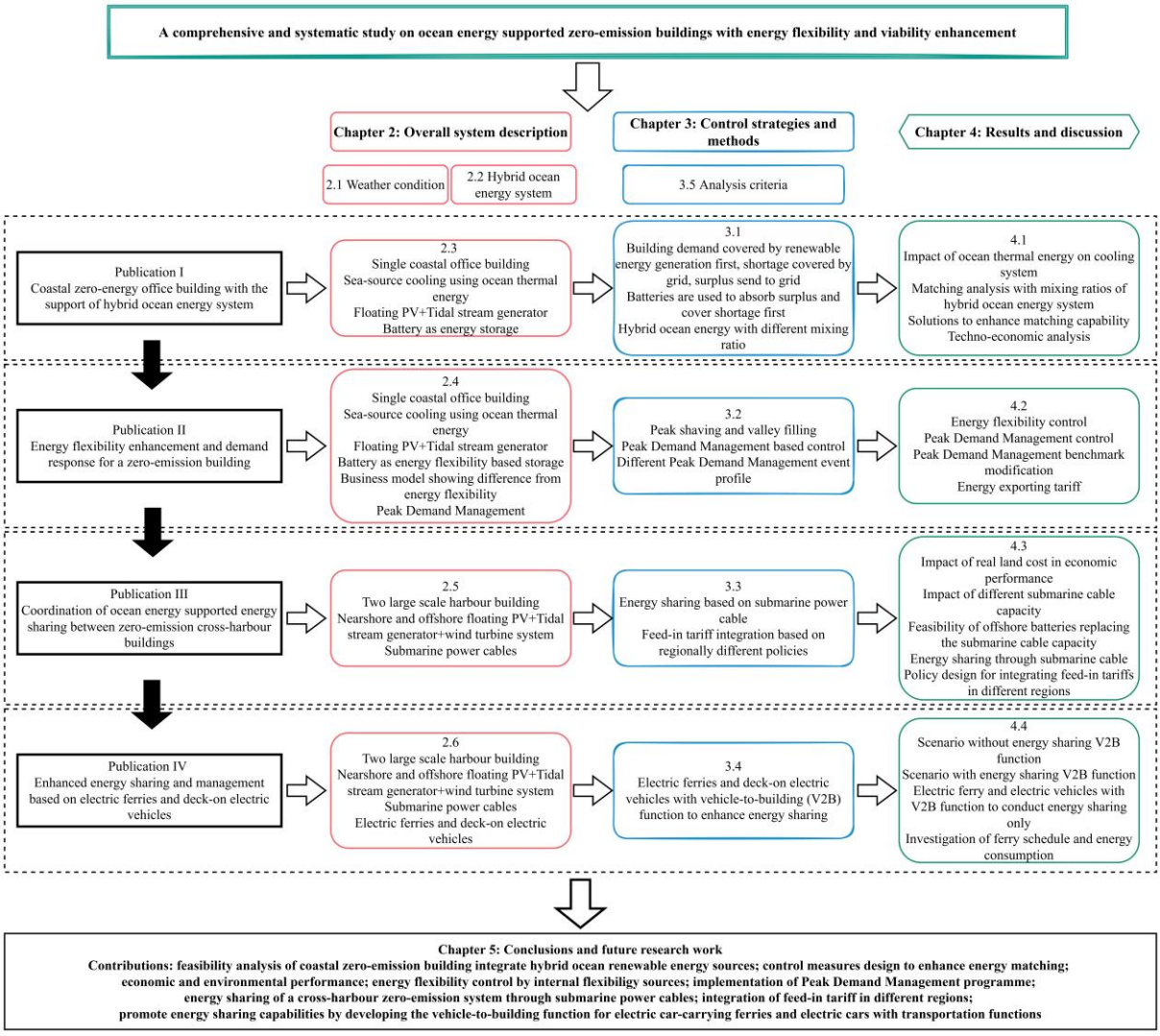

Fig. 1.1 Overall flowchart of the research structure.

The research framework is structured into four interconnected parts, each corresponding to an original academic publication. The first part investigates the feasibility of an ocean energy-supported zero-emission coastal building, establishing foundational technical and economic parameters. Subsequently, the introduction of dynamic electricity pricing mechanisms enables the application of energy flexibility strategies and demand-side management to optimize operational efficiency, thereby enhancing the economic and environmental viability of the system. Furthermore, the third part expands the system's geographical and infrastructural scope by integrating multiple buildings across Hong Kong and Macau, forming a cross-harbour zero-emission network. This interconnected system leverages subsea power cables to facilitate

energy sharing and coordinated energy management between the two regions. Finally, the fourth phase introduces collaboration with a navigation system comprising electric ferries and vehicles, transforming a standalone harbour building into a multimodal transportation hub. This integration strengthens energy resilience through bidirectional power exchange between stationary infrastructure and mobile transport networks. The logical progression from localized feasibility studies to cross-regional system integration reflects a holistic approach to addressing scalability, policy interoperability, and technological adaptability in sustainable urban development. Each phase incrementally addresses technical, economic, and governance challenges, culminating in a comprehensive framework for zero-emission systems in coastal megacities.

Chapter 2. Overall system description

This chapter provides a detailed presentation of the critical components within the studied system based on realistic conditions and modelled using the dynamic energy simulation to test and analyse the performance of the designed zero energy system. The energy management strategy will be presented in detail. The entire simulation system, encompassing the target building and renewable energy systems, was constructed within the TRNSYS 18 simulation environment [83]. TRNSYS 18 offers a highly adaptable, graphically based platform for simulating the behaviour of transient systems, making it particularly well-suited for modelling the daily operations of renewable energy systems and buildings. One of TRNSYS's key strengths lies in its comprehensive library of components. Each component contains a complete set of settings and options to simulate the performance of specific system elements. The standard library encompasses a wide range of models containing basic equipment, complex multi-zone systems, commonly used renewable energy systems, data processors and analysis tools. Furthermore, TRNSYS offers users the flexibility to modify existing components and create custom models for specialised purposes through its equation box feature, thereby extending the capabilities of the simulation environment [84]. TRNSYS includes validated mathematical models and relationships between components. These models have been accepted by the academic community, eliminating the need for further validation when constructing a system within the TRNSYS simulation environment. As a result, users can concentrate on designing the system and developing the control logic without the concern of validating the underlying models. This versatility, combined with the software's ability to perform dynamic energy simulations and techno-economic analyses, made TRNSYS the most suitable choice for this study. To ensure the stability and accuracy of the system model, the time step in the TRNSYS simulation was set to 0.25 hours. This granularity allows for a detailed examination of the system's performance over time, capturing short-term fluctuations and long-term trends in energy production, consumption, and management.

2.1 Weather conditions for the studied system

One of the building service systems that accounts for a substantial portion of the energy consumption within a building is the HVAC system. Therefore, the weather conditions of the location are necessary to be elaborated to obtain the daily

operational energy performance of the targeted building. The studied system is located in two cities in very close proximity Hong Kong and Macau, they share similar geographical coordinates which are approximately 114°E and 22°N and subtropical climates. According to data from the weather database, the total annual solar radiation on the horizontal surface for Macau and Hong Kong is 1425.65 and 1428.74 kWh/m^2, respectively. Wind velocities in both cities reach maximum speeds of 15.28 m/s in Hong Kong and 14.54 m/s in Macau, with monthly averages ranging from 3 to 6 m/s [85] [86]. Seawater temperature plays a vital role in this study, particularly in the utilisation of OTE and the operation of the FPV system. The Hong Kong Observatory provided seawater temperature data, monitored 1 metre below the surface. However, the system's assumed seawater pipe intake in reality is set at a depth of 10 to 20 metres below the sea surface to avoid tidal and wave influences [87]. Preliminary investigations suggest that seawater temperatures do not vary significantly in shallower depths, with a temperature difference of about 2°C between 0 and 10 metres. Given the negligible impact, the lack of reliable seawater temperature data below 1 metre, and the absence of suitable seawater stratification models for the specific location, this study utilises this introduced seawater temperature data. This decision balances the need for accurate modelling with the practical limitations of available data. The variation of seawater temperature in Hong Kong for one year is illustrated in Fig. 2.1.

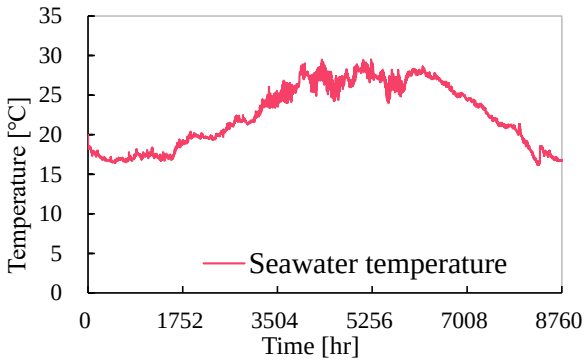

Fig. 2.1 Curve of sea water temperature variation in Hong Kong in a year [Publication II].

2.2 Hybrid ocean-related renewable energy system

2.2.1 Ocean thermal energy utilisation

As a building located in a city with a subtropical climate, the maximum load on the HVAC system comes from the cooling system and ocean thermal energy is considered to play an important role in improving efficiency and reducing cost. Seawater presents a compelling alternative to traditional cooling sources due to its temperature stability and its relatively lower temperature compared to ambient air during summer months when cooling demands peak. This characteristic makes seawater an attractive option for enhancing the efficiency of building cooling systems. Traditional cooling systems typically employ roof-mounted cooling towers to reduce the temperature of condenser cooling water using ambient air.

However, to harness ocean thermal energy more effectively, this study proposes replacing the cooling tower with a sea-source water-to-water heat exchanger. This heat exchanger, featuring condenser cooling water on one side and seawater on the other to replace the cooling tower, transforms the system into a seawater-based cooling mechanism. To optimise the cooling coefficient of performance (COP), large surface areas with substantial cost are generally required for heat exchangers. To address this challenge, this research proposes a heat exchanger design that balances performance improvement with cost-effectiveness. The design incorporates copper spiral tubes with an anti-corrosive coating, which are directly submerged in seawater. This approach mitigates corrosion issues while enhancing heat transfer efficiency. The proposed system integrates chillers with sea-source heat exchangers for both air handling units (AHUCS) and space cooling applications. The parameters for the space and AHUCS chillers were derived from established commercial products, ensuring the model's alignment with real-world performance characteristics [88] [89]. The chiller used for space cooling has a rated COP of 4.7 and a rated capacity of 165.4 kW, while the chiller for AHUCS has a rated COP of 5.53 and a rated capacity of 796 kW. By implementing this seawater-based cooling system, the research aims to demonstrate significant improvements in cooling efficiency compared to conventional air-based systems. This approach not only leverages the natural thermal properties of seawater but also addresses practical considerations such as corrosion resistance and cost-effectiveness. The integration of such systems in coastal urban environments could potentially lead to substantial energy savings and contribute to the overall goal of achieving zero-energy buildings.

2.2.2 Floating photovoltaic system

Solar energy is one of the most common renewable energy sources currently, with photovoltaic panels being the most widely used technology for directly converting solar radiation into electricity. Although it has been developed over a long period of time, its energy conversion efficiency is still not very impressive, and because of the characteristics of the sun's rotation, it still requires a large land area to install photovoltaic panels to meet the needs of a zero-energy building. Currently common installations of PV panels are often chosen for roofs or open ground with no large shadows surrounding them, and as research advances, the building envelope has become a target location for some of the more advanced PV panels.

In bustling metropolises, especially in cities like Hong Kong and Macao, the scarcity and high cost of land pose significant challenges for traditional PV installations and installing PVs on rooftops often prove insufficient to satisfy the energy demands of a high-rise building. Even if there is enough ground to install PV panels, or to consider installing advance PV panels on the building envelope, too many surrounding high-rise or super high-rise buildings can cause shadows to block the sun's rays. Therefore, it is very challenging to equip a single building with a common on-site PV system in such a city and while the application of a floating PV system mounted on the sea surface reduces land use and costs owing to the sea

frontage. Meanwhile, because seawater temperature is relatively more stable than air temperature variations, the temperature of seawater or air near seawater will be cooler in hot weather than air near the ground and roof, in which case FPV systems can achieve higher energy conversion efficiency. [90]. To accurately model the performance of FPV systems, this study employs the building-integrated PV model within the simulation environment. This model incorporates a crucial parameter - the back surface temperature - which allows for the simulation of the cooling effect of seawater on power generation efficiency. To reflect real-world conditions, the FPV panels are modelled with a 0° slope, parallel to the calm sea surface. This configuration minimises the impact of wind and waves on panel orientation and inter-panel shading, enabling the application of building-integrated PV simulation models to FPV systems with minimal modifications. To make the results close to the power output of a realistic floating PV system, the PV parameters in the simulation are derived from an actual purchasable product [91]. This approach grounds the theoretical modelling in practical, real-world considerations, enhancing the validity and applicability of the research findings.

2.2.3 Tidal stream generation system

Tidal energy, a form of hydrokinetic power, harnesses the natural ebb and flow of tides resulting from the gravitational interplay between Earth, the sun, and the moon [92]. This renewable energy source stands out for its high predictability in both quantity and timing, offering a consistent and dependable electricity supply. Such reliability is particularly valuable in the context of developing zero-energy buildings, where consistent energy production is crucial. Two primary technologies have emerged for capturing tidal energy: tidal barrages and tidal stream generators. Tidal barrages employ large dam-like structures to create a barrier between the sea and a tidal basin. While effective, this approach is constrained by stringent locational requirements and potential ecological impacts. TSG systems capitalise on the phenomenon of accelerated water movement through constricted passages, where tidal currents attain sufficient energy for power generation [92]. These systems utilise underwater turbines to extract energy from the kinetic force of moving water masses. The advantages of TSG systems, including lower costs and reduced ecological disruption compared to tidal barrages, make them an attractive option for sustainable urban energy solutions [93, 94]. In this study, the TSG approach was selected as the preferred method for harnessing tidal energy.

This study utilises tidal stream data focusing on a monitoring point located at Kap Shui Mun, adjacent to Ma Wan [95]. The data was generated using the Hong Kong Tidal Stream Prediction System. The Google map screenshot of the selected tidal data monitoring point, as well as the monthly average and maximum values of the tidal data profile, are demonstrated in Fig. 2.2. The tidal characteristics at the study site demonstrate remarkable consistency, with average monthly tidal velocities ranging from 0.76 to 0.84 m/s. However, significant variations are observed in peak velocities, with a maximum of 2.23 m/s recorded in December, while other months exhibit minimum velocities of 0 or 0.01 m/s. This variability

underscores the importance of comprehensive temporal analysis in tidal energy assessments.

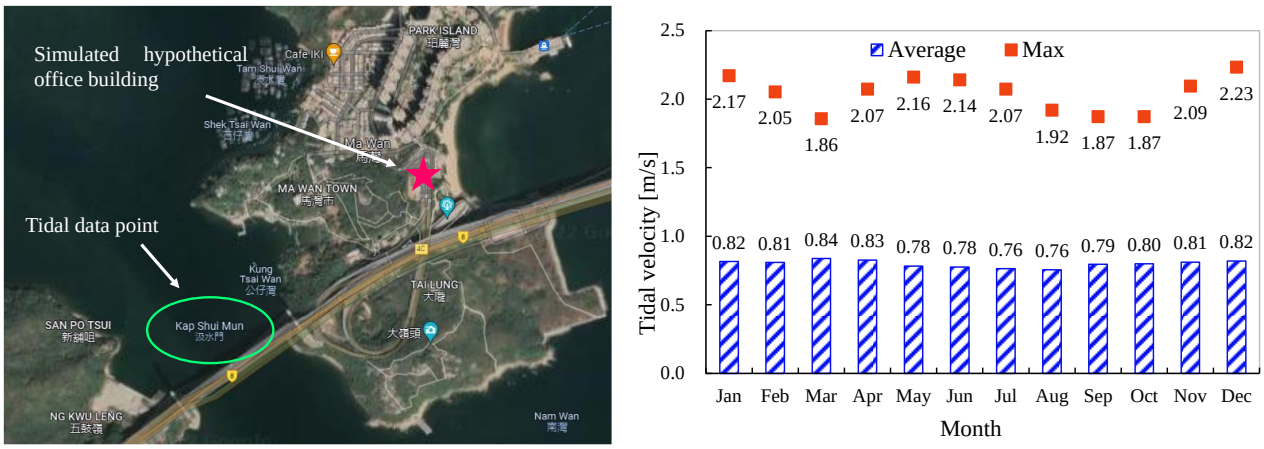

(a) (b)

Fig. 2.2 Display of information related to tidal data: (a) the location of the tidal data point on the map and (b) monthly maximum and average tidal stream velocity at the selected point [Publication II].

Tidal stream generator technology shares similarities with wind turbine technology [96], and exploits these tidal streams to extract energy from moving water masses [97]. A key advantage of TSG systems over wind turbines lies in the significantly higher density of seawater compared to air. This density differential allows TSG systems to generate more power than equivalently sized wind turbines under similar velocity conditions [94]. For this study, floating structure tidal turbines were selected due to their versatility, flexibility, ease of maintenance, and cost-effectiveness [98]. The simulation of the TSG system was conducted employing a power-generation formula derived from a cross-flow tidal stream generator experimental device [99]. This approach was necessitated by the absence of a self-contained TSG model in TRNSYS. The formula for calculating the power output of a 250 kW TSG is expressed as

$$P(t) = \frac{250}{(1 + 5.785e^{-0.122(v-1.3306)})^{1/0.0325}} \quad (1)$$

where P(t) is the instantaneous power-generation output. The economic aspects of TSG implementation were also considered, with an estimated installation cost of 19110 HKD/kW and an annual operation and maintenance cost of 5% of the capital investment [100] [101]. This study was limited to the nearshore sites of Hong Kong, which was imposed to ensure the reliability and consistency of the data used in the analysis.

2.2.4 Wind turbine system

As the research expanded to encompass larger-scale projects, including single expansive buildings and multi-building communities, it became evident that relying solely on FPV and TSG systems might not suffice to meet the energy demands. Consequently, both nearshore and offshore wind turbine systems were introduced as an additional power source. Wind turbines represent a well-established and dependable ocean-integrated renewable energy technology widely adopted in numerous coastal urban areas. To accurately simulate wind turbine performance, parameters from actual commercial wind

turbines were incorporated, including their basic specifications and power-wind speed curves. Given the differing annual energy demands of the buildings in Hong Kong and Macau, distinct wind turbine models were selected for each location. For Hong Kong, a 1 MW wind turbine with a 50 m hub height and a 54.2 m rotor diameter was chosen. This model initiates power generation at a wind speed of 3 m/s and achieves its maximum output of 1005.6 kW at wind speeds below 21 m/s [102]. In contrast, the Macau model boasts a 2.7 MW capacity, with an 89 m hub height and a 122 m rotor diameter. It shares the same cut-in wind speed of 3 m/s but reaches its peak output of 2700 kW at wind speeds under 13 m/s [103]. For both nearshore and offshore installations, a linear arrangement of turbines was envisioned, all facing the same direction. To minimise interference and optimise energy capture, a centre-to-centre distance between turbines equal to four times the rotor diameter was maintained [104]. The economic aspects were also considered, with estimated installation costs of 24843 HKD/kW and annual O&M costs at 0.92% of the capital investment. To ensure a comprehensive understanding of the cost structure, statistics from multiple practical offshore wind turbine projects were referenced, providing insights into the proportion of investment costs attributed to each system component [105].

2.3 Realisation of coastal zero-energy office building with different combinations of hybrid ocean energy system

At the beginning of this study, it was only the single office building that was set up as the subject of the study's objectives and the realisation of the zero-energy aim, and different combinations of the above-mentioned ocean renewable energy systems were used to observe the difference in performance. This building comprised ten floors above ground for office area and one level below for parking, each floor measuring 480 m^2 with a height of 3 meters [106]. The design of this building and a window-to-wall ratio of 0.21, with particular attention given to reducing solar heat gain, was established and assumed as recommended by the guidebook and design code in Hong Kong [107] [108]. The building's energy profile included annual internal gains from lighting systems (58.60 kWh/m^2) and equipment, including devices and lifts (104.30 kWh/m^2). Situated near Ma Wan, the building's location was chosen to facilitate integration with nearshore ocean renewable energy systems. The duration curves of heating, cooling and electrical energy demands for various systems of the original office building supported by the grid are presented in Fig. 2.3.

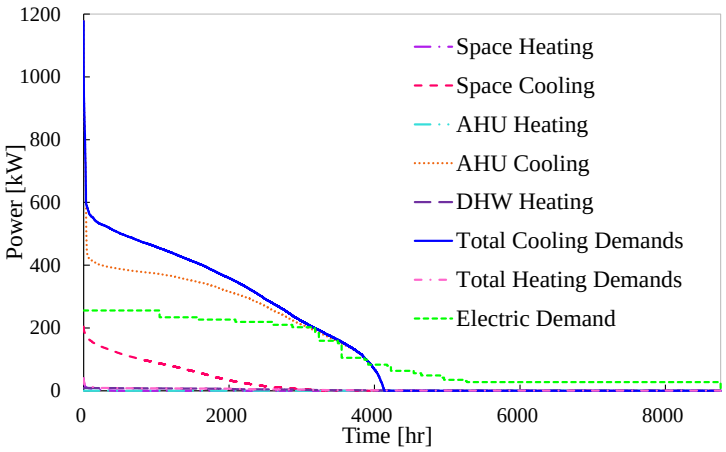

Fig. 2.3 Electrical, heating and cooling power demand duration curves of the coastal office building [Publication II].

To establish a baseline for performance comparisons, the building relying solely on the local power grid, without any renewable energy inputs was modelled as the reference case. To reduce the substantial demand pressure on the total energy requirement from the cooling system, as introduced in the previous subsection, the sea source cooling system that utilises ocean thermal energy was applied. Sea-source chillers also have different designs with different advantages and disadvantages; therefore, three distinct designs for sea-source chillers were proposed. These designs are onshore-based heat exchangers, submerged copper spiral tube heat exchangers, and chillers using seawater directly as cooling water. In TRNSYS, the model Type 91 was used to present the onshore-based heat exchangers, which have constant effectiveness. Furthermore, the on-site stationary batteries were incorporated into the studied system as an energy storage approach as backup equipment. A brief schematic of the designed system, including all the essential components is presented in Fig. 2.4.

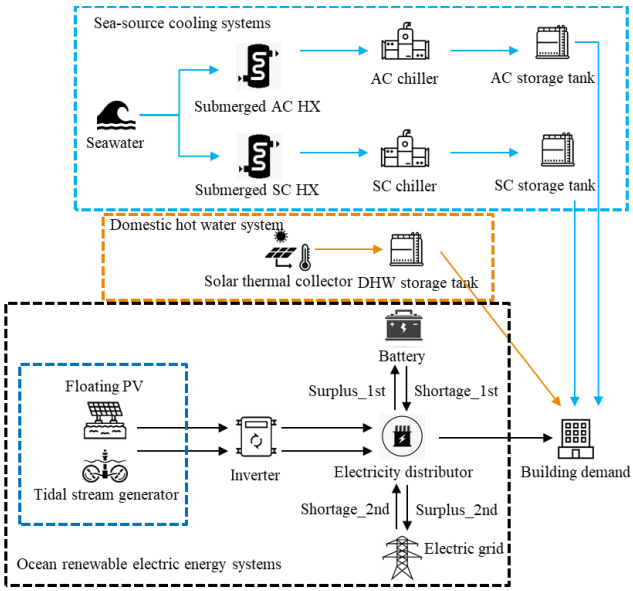

Fig. 2.4 Schematic of utilising the hybrid ocean thermal, floating photovoltaics, and tidal stream generators to support

coastal zero-energy office building [Publication I].

The non-residential tariff from CLP Power Hong Kong, Ltd. was chosen as the business model to calculate the economic performance. This non-residential tariff is mainly based on the energy charge, which is 106 cents per kWh of energy consumption. This tariff also includes fuel cost adjustments, which is 46.3 cents per kWh based on forecasted fuel prices in the latest tariff review [109]. For a system that can generate renewable energy, a feed-in tariff policy is effective in providing a business model. In Hong Kong, the feed-in tariff is considered for renewable energy generation, and the rate is 2.5 HKD per kWh if a capacity exceeds 200 kW.

2.4 Coastal zero-energy office building with energy flexibility-based energy storage equipment

After exploring the performance of office buildings supported only by renewable energy systems with no other strategies, energy flexibility-related management strategies and tariff policies were included in further research and supported by the inclusion of appropriate equipment. These equipment and tariff policies are included in this subsection. The building and the renewable energy system that will help it reach a zero-energy building will have the same components as before, based on the previous study, the best overall performing case was selected as the target of the study to determine the composition of the ocean renewable energy system. The studied ocean renewable energy generation system consists of two TSGs and 3967 FPV panels. The cooling source storage tanks originally present in the system can be used as a support device for energy flexibility. Meanwhile, the on-site stationary batteries mounted near or inside the building that already exists in the previous scenarios can also be the devices to reach energy flexibility and demand side management.

The original business model only included a fixed energy charge, and in the case of such a tariff, the management strategy for energy flexibility, while enhancing energy matching performance, did not have a significant impact on economic performance. To stimulate energy management based on energy flexibility for building stakeholders on an economic level, a more complex tariff that distinguishes between peak and off-peak time periods, as well as between demand and energy charge, was applied in this study instead of the original tariff. This tariff model from CLP was called the bulk tariff. This business model will monitor the maximum demand during peak and off-peak periods each month to calculate the demand charge, the price for the portion of the peak period where the maximum demand does not exceed 650 kVA is 68.4 HKD/kVA, and the price for the portion that exceeds it is 65.4 HKD/kVA. If the off-peak maximum demand does not exceed the peak maximum demand, there will be no charge. If it exceeds, the price of the exceeding part is 26.8 HKD/kVA. They also stipulate the minimum peak billing demand, which is 100 kVA. Meanwhile, the energy consumption of each that does not exceed 200000 kWh of energy during peak periods will be charged 75.3 cents/ kWh for electricity, with the excess priced at 73.7 cents/ kWh and the off-peak energy charge at 67.6 cents/ kWh.

Meanwhile, to encourage users to perform demand-side management to alleviate the pressure on the grid during peak hours, grid companies usually have their own policies to provide incentives. CLP offers its PDM programme, a demand response policy in Hong Kong that provides an incentive mechanism [110]. This PDM programme, accessible to CLP customers, including the studied office building, aims to incentivise commercial consumers to reduce energy consumption during peak demand periods. This initiative not only benefits the grid infrastructure but also provides financial advantages to participating customers. The programme operates through PDM events, which can last up to four hours between 11 am and 10 pm. CLP notifies selected customers in advance about the timing and duration of these events. The incentive structure is tiered based on the notification lead time. If the notification lead time is larger or equal to 24 hours before the event, no matter whether the event is executed or cancelled, the customer can earn 8 HKD per kWh demand reduction. If the notification lead time is less than 24 hours and larger or equal to 4 hours before the PDM event, the customer can earn 13 HKD per kWh demand reduction if the event is executed or 8 HKD per kWh demand reduction if the event is cancelled eventually. The economic impact of the PDM programme on the zero-energy building was analysed based on the original flexibility control. It's worth noting that the utility company establishes a mutually agreed 'target' for hourly demand reduction with each client. While exceeding this target is encouraged, the maximum incentive payment is capped at 150% of the target for each event. To calculate the demand reduction achieved, the utility company compares the actual electricity demand during the event period against a baseline. This baseline is determined by averaging the electricity demand during the same period on the three highest-demand days out of the ten preceding non-event days, ensuring a fair and representative comparison. The integration of such demand response programmes into zero-energy building strategies represents a significant advancement in energy management. By aligning building operations with grid requirements, a more resilient and efficient energy ecosystem can be created.

2.5 Co-ordinations of ocean energy supported energy sharing between zero-emission cross-harbour buildings

After studying the feasibility of a 10-storey office building on the coast to achieve the zero-energy goal through the nearshore ocean energy system and enhancing the performance of the system through energy flexibility and demand response conducted by the stationary batteries, larger buildings meeting zero-energy building targets, and the co-existence of multiple large public zero-energy buildings were considered as objectives for the further study. Meanwhile, the hypothetical case of two zero-energy buildings forming a cross-harbour system in two cities separated by the sea is the subject of the study. The targeted building type is a public terminal building for ferry docking, one located in Hong Kong, and another located in Macau. Public ferry terminal buildings are characterised by a large footprint and a small number of storeys. Based on the available information and the comparison purpose, the actual layout of Taipa ferry terminal in Macau

was adopted, and the plan and 3D structure of two simulated harbour buildings were designed in a simulation environment and assumed to be situated at the actual location of the Taipa and Skypier terminal in Macau and Hong Kong, respectively. This hypothetical ferry terminal harbour building model only has two floors; the first floor and the second floor have an area of 66674 m^2 and 97554 m^2. Each zone has a different occupancy profile, which was determined by the history date in the mentioned two buildings [111] [112]. The building envelopes, insulation, and other service systems of these two buildings were designed based on the building design code and guidelines from Hong Kong and Macau [107]. According to the building design guideline in Macau, the window-to-wall ratio of the east and west external envelope was 0.4, the north was 0.45, and the south was 0.3. The working schedule of the harbour building was 7:30 am to 10 pm in Hong Kong, while the harbour building in Macau operated 24 hours every day. The annual internal gain of the lighting system in the Hong Kong building was 59.56 kWh/m^2 and equipment, including devices and elevators, was 57.24 kWh/m^2, for the Macau building was 120.33 and 94.86 kWh/m^2 respectively. The duration curves are shown in Fig. 2.5.

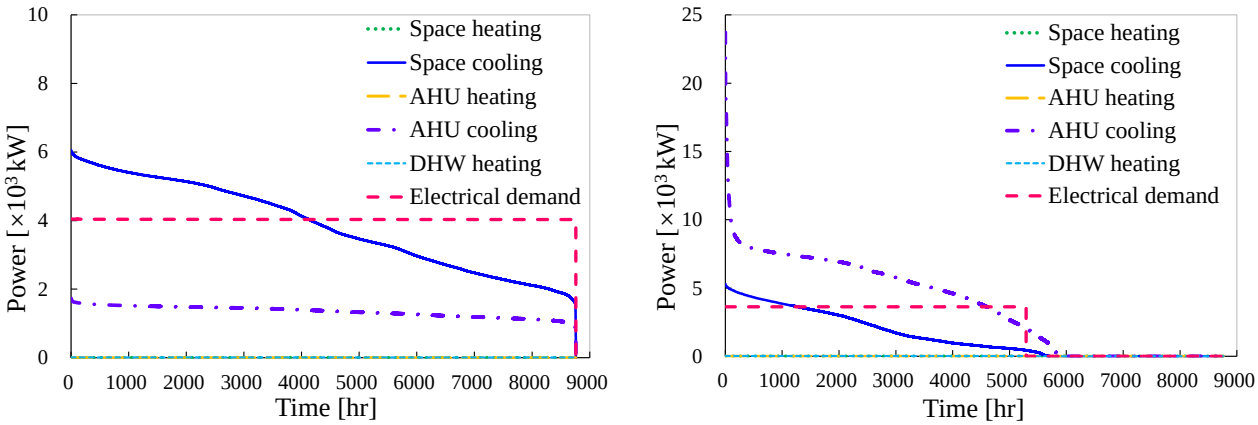

Fig. 2.5 Electrical, heating and cooling power demand duration curves of the buildings in (a) Macau and (b) Hong Kong [Publication III].

As a system controlled by a single stakeholder that incorporates two large public ferry terminal buildings in the cities across the harbour and the accompanying ocean renewable energy systems, how to integrate and collaborate the available resources in the two places will be a key strategy to enhance the techno-economic performance of the whole system. Therefore, energy sharing across the harbour will be an effective energy management strategy to reach energy utilisation and collaboration. Meanwhile, to achieve the zero-energy system, the hybrid ocean related renewable energy system, including a nearshore TSG system, nearshore and offshore FPV and wind turbine system were applied to provide the electricity generation. To reach such an energy management strategy, submarine cables were introduced as a means of energy transmission. Submarine cables have become an important component of the research system in this direction. For comparison purposes, two scenarios were proposed based on the availability of an intermediate submarine cable

connecting the offshore sites, enabling energy from a nearshore or offshore ocean energy system to be transmitted to the ferry terminal building in another city if there is space available in the submarine cable. The submarine cables in this study are assumed that are exclusively used for transmitting renewable energy, electricity from the respective grids cannot be transmitted to other locations via submarine cables. These two scenarios will be introduced in the next chapter. Specifically, the length of the submarine cable on the Hong Kong side is 24 km, while on the Macau side, it is 15 km. Additionally, there are intermediate submarine cables with a length of 8 km.

For the subsystem on the Hong Kong side, the tariff model will continue to use the bulk tariff from CLP, while the Macau subsystem will introduce a new tariff rate that belongs to the Macau electricity company. Tariff Group B3 was selected to calculate the annual electricity cost from CEM Macau and is divided into three parts. First, they also charge for the maximum monthly demand, the price is 21.484 MOP (20.839 HKD) per kW, but there is no distinction between peak and off-peak. The energy charge is divided into two parts, which are called active energy and reactive energy, and distinguishes between full-load hours and low-load hours. Active energy charge in full-load hours and low-load hours are 0.874 MOP (0.848 HKD) per kWh and 0.767 (0.744 HKD) per kWh, respectively. Reactive energy charges in full-load hours and low-load hours are 0.348 MOP (0.338 HKD) per kWh and 0.116 MOP (0.113 HKD) per kWh, respectively. The feed-in tariff policy in Macau differs from that in Hong Kong, as it is based on the energy output from the renewable energy system to the grid, with a feed-in tariff rate of 2.8 MOP per kWh, equivalent to 2.716 HKD per kWh [113].

2.6 Combination of electric ferries and deck-on electric vehicles

Energy sharing through submarine cables, while effective, requires additional investment costs to install the submarine cables. As the stakeholder in the ferry terminal building, it is reasonable to assume that he also owns a company that operates a ferry service from Hong Kong to Macau and owns an electric ferry that can carry electric cars and has no investment costs relative to the reference case. In addition to their own transport tasks, the batteries of electric ferries and electric vehicles themselves can also take on the part of the energy-sharing function as mobile energy storage devices. The transport tasks of the electric ferries and electric vehicles themselves will result in some degree of energy demand. One car-carrying electric ferry and ten deck-on electric vehicles were assumed in this study. This car-carrying electric ferry will travel daily between the ferry terminal buildings and ten electric vehicles must conduct commercial trips on both sides daily. The model of the car-carrying electric ferry was derived from one project [114]. The ferry is assumed to have a battery capacity of 3000 kWh and can carry ten cars and 120 passengers. The speed and energy consumption per kilometre of the car-carrying electric ferry were set according to this project and were 17.6 km/h and 38 kWh/km, respectively. The daily journey of the car-carrying electric ferry started from the Macau ferry terminal building at 7:00 am, firstly arrived at the offshore platform on the Macau side and stayed for 1 hour, then continued the voyage to the offshore platform on the

Hong Kong side and docked for 1 hour, then continued the journey to the Hong Kong ferry terminal building and docked for 3 hours, and then departed at 4:00 pm to return to the Macau ferry terminal building at 9:00 pm via the Hong Kong and Macau offshore platforms, during which time it also docked for 1 hour on both offshore platforms. Based on the above itinerary, this ferry required 1786 kWh of energy one way, meaning 0.6 fractional state of charge (FSOC) of the ferry's batteries would be needed. In addition to the marine journeys that follow the car-carrying electric ferry, the ten electric cars have separate commercial trips in both regions. The data for the model of the electric vehicles used in this study were obtained from the Tesla Model S, which has a speed of 40 km/h and an energy consumption of 0.167 kWh/km [115]. The battery capacity for these electric cars was 95 kWh. When the ferry arrived at the Hong Kong ferry terminal building, the ten electric cars would depart from the harbour building and have a 1-hour drive to the destination, stopping at the Hong Kong destination for 1 hour and then returning to the harbour building after spending 1 hour. When the ferry arrived at Macau at 9 pm, the electric cars would depart from the Macau harbour building and spend half an hour on the road and half an hour at the destination. A single EV consumes 13.36 kWh one-way on the Hong Kong side, requiring an FSOC of 0.14, and 3.34 kWh one-way in Macau, requiring an FSOC of 0.04. The duration curve of the total electrical demand with the inclusion of harbour building, electric ferry and electric vehicles was displayed in Fig. 2.6.

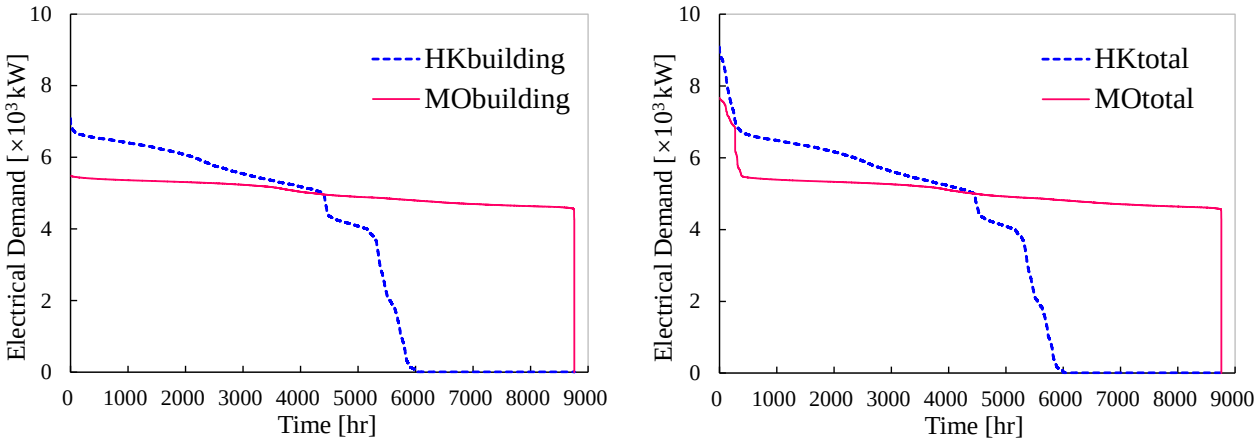

Fig. 2.6 Duration curves of the (a) building demand and (b) overall demand in Hong Kong and Macau regions [Publication IV].

Throughout the study, all inputs and parameters are based on realistic and recognised data. For example, the parameters for the building system are selected to meet local building codes for design criteria and thermal comfort. Similarly, the assumptions regarding the operation and costs of the renewable energy system rely on publicly available data for realistic commodities. This approach ensures that the simulation performance calculations closely reflect real-world conditions. As a result, the system under study closely resembles existing market systems, allowing for meaningful comparisons in terms of economic performance.

Chapter 3. Control strategies and methods

3.1 Coastal zero-energy office building with the support of a hybrid ocean energy system

At the beginning of the study, the entire methodology of energy management was fundamental to explore the feasibility of the zero-energy seafront office building that was designed based on the nearshore hybrid ocean energy system. This approach utilises a combination of renewable energy resources to generate electricity, primarily addressing the building's energy demands. The energy management strategy we developed prioritises the use of locally generated renewable energy. When the system produces surplus energy, it is first stored in on-site battery groups. Any remaining excess is then exported to the grid. Conversely, during periods of energy deficit, the system draws from the stored battery power before resorting to grid imports. This hierarchical approach maximises the utilisation of renewable energy and minimises reliance on the grid. The control logic and the energy flow for this part of the study was shown in Fig. 3.1.

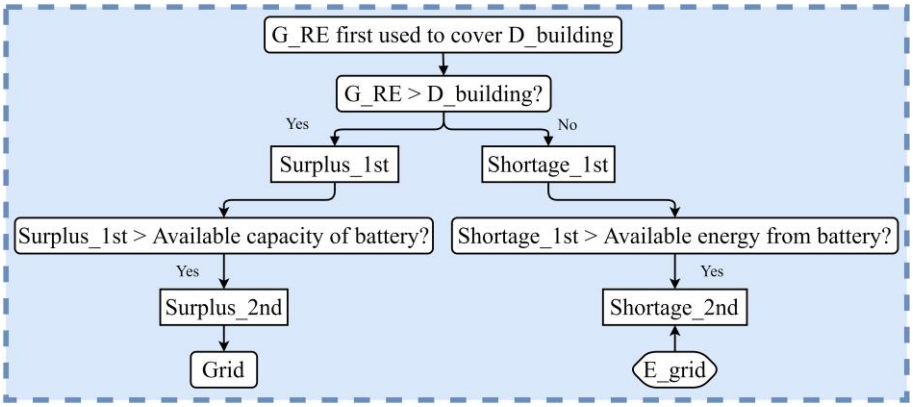

Fig. 3.1 Flow chart of the control methodology and energy flow for the zero-emission office building with batteries.

To analyse in detail the techno-economic and environmental performance of different percentages of FPV and TSG systems for the whole hybrid system, when hypothesizing the scale of renewable energy system for each case, a principle that must be considered is that the annual energy generation of the ocean renewable energy system in a single case should be at least equal to or slightly greater than the annual energy demand of the entire system. This principle will ensure that the system of each case can achieve the goal of a zero-energy system. Therefore, when designing the number of TSGs and FPVs for each case, the quantities will be calculated separately based on the simulated annual energy production of a single device, and marine energy systems with different mixing ratios will be formed. The mixing ratio of both FPV and TSG system will be varied by 10% each time in the different cases. In other words, if from the first to the last case, the percentage of FPV systems goes from 0 to 100 %, increasing by 10 % each time, the proportion of TSG systems will go from 100 %

to 0, decreasing by 10 % each time. Based on the simulations of individual component performance and the building's energy demand, it is determined that a system comprising solely FPV would require 5,055 panels, while a TSG-only system would need ten generators. Using these benchmarks, the appropriate number of FPV panels for each case was calculated as the TSG proportion increased from 0% to 100% from case C1 to C11. The detailed information of the mentioned cases is shown in Table 3.1.

Table 3.1 Cases with mixing ratios based on the design of hybrid ocean energy systems and the corresponding quantities [Publication I].

Cases name	Number of FPV	Percentage of FPV	Number of TSG	Percentage of TSG
C1	5055	100%	0	0%
C2	4511	90%	1	10%
C3	3967	80%	2	20%
C4	3422	70%	3	30%
C5	2878	60%	4	40%
C6	2333	50%	5	50%
C7	1789	40%	6	60%
C8	1245	30%	7	70%
C9	700	20%	8	80%
C10	156	10%	9	90%
C11	0	0%	10	100%

3.2 Energy flexibility enhancement and demand response for an ocean-energy-supported zero-emission office building

The performance of a zero-energy office building supported by a hybrid ocean energy system in the absence of a specific energy management strategy was only investigated in the first part of the study. Therefore, in this part of the study, the focus is on the implications of an energy control methodology based on energy flexibility and demand side management on the system's techno-economic and environmental performance. Although the energy flexibility control based on the cooling storage tank was first considered as one of the approaches, based on the pre-study, such controls have not been very effective and, in some cases, have even had a negative effect, and therefore no longer a priority part of the study. In this hybrid system, the stationary battery serves as the sole dependable source of flexibility. The flexibility control strategy employed in this study focuses on the interplay between the stationary battery, the grid, and renewable energy generation. The aim is to optimise the utilisation of the stationary battery to achieve enhanced flexibility within the system. The core ideas of energy control strategies based on energy flexibility and energy storage devices reached can be summarised as peak shaving and valley filling. Simply defined, in addition to the basic strategy of storing surplus renewable energy in the stationary battery to cover as much of the shortage of the system as possible, the system will be additionally charged during the off-peak period, and this energy will be stored in the stationary battery, and during the peak period, the charging from the grid will be reduced, and the stored energy will be used to compensate for the under-charged energy. While such

a control has the potential to reduce the energy matching performance, there is not only a difference in high demand charge, but the energy charge is also higher. Therefore, it is possible that such a strategy can significantly reduce the operational cost of the system. Since the demand charge in the bulk tariff is based on the maximum value of energy demand per month, it is a cost-minimising control strategy to use all the resources to reduce the power demand of the peak period to the same value as small as possible when implementing energy flexibility control. At the same time, the valley filling strategy in the off-peak period will try to make the value of the power demand that needs to be filled the same and less than the power demand in the peak period every hour. The power demand that needs to be achieved during the off-peak period is known as the charging line, and the target value of power demand that needs to be reduced by renewable energy, battery discharging and grid energy during the peak period is called the discharging line. Electricity billing is based on monthly energy consumption, which is not the same for each month, and two control strategies with different charging line and discharging line values are designed based on different control granularities. In Flexibility Control 1 (FC1), the respective values of the charging line and the discharging line will be the same value for a whole year. In Flexibility Control 2 (FC2), the respective values of the charging line and the discharging line will be set differently for each month for finer control. The values of the charging line and discharging line are not guaranteed to be the same in the same period. Based on the previous study, the hybrid ocean energy case consisting of 3967 FPV panels and two TSGs was the main energy input to the building. In the first scenario, the stationary batteries will be charged only by energy from the grid. Later in the further open design, the batteries will be allowed to interact with the ocean energy system and the grid, where the batteries will first be charged by surplus energy from the ocean energy system, and if there is still space to be charged, the grid will be used to charge the batteries. The control methodology and energy flow for this part of the study were illustrated in Fig. 3.2.

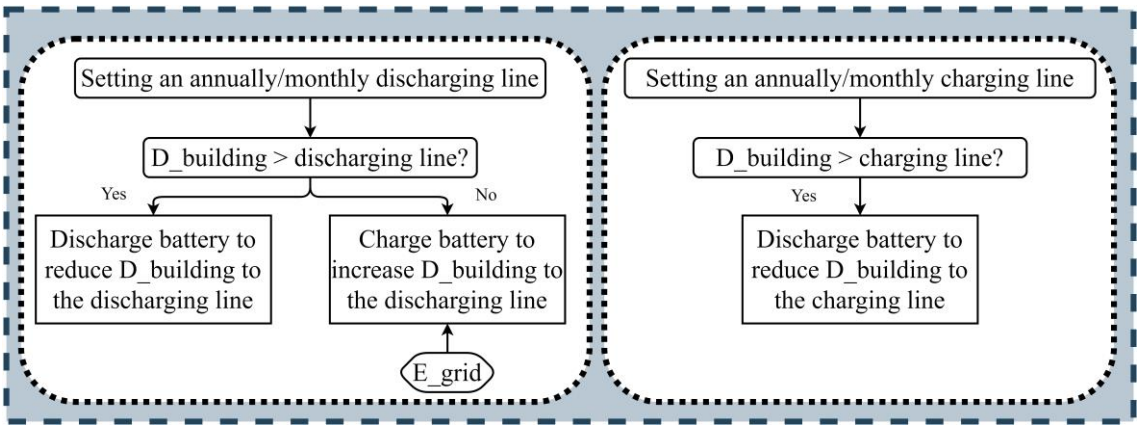

Fig. 3.2 Flow chart of the control methodology and energy flow for the zero-emission office building with energy flexibility.

As mentioned in the previous chapter, the hybrid system can participate in the PDM programme of CLP to alleviate the power pressure. Peak energy consumption and demand can be reduced by discharging the energy stored in the batteries

through extra off-peak charging activity. Incentives can be obtained to strengthen the economic performance of the system with the PDM programme. The variable in different cases is the battery capacity, as the stationary battery is the only energy storage equipment that can effectively conduct the peak shaving and valley filling strategy. Since the control of energy flexibility can also reach the requirement of demand side management to get the incentive, two control methods are designed as a comparison to discover the control method that can get the optimal performance. In PDM Control 1, the energy management strategy will be the same as that of the energy flexibility control, with no specific controls for the PDM programme. In the control known as PDM Control 2, based on the original flexibility control, the off-peak charging line is increased to the maximum power demand and the battery is not discharged so that the battery remains fully charged during the peak period. In this way, the value of the peak discharging line can be further reduced to reach a greater reduction in energy demand and to obtain more rewards when a PDM event happens. Different PDM event profiles determined by low, medium, and high event frequency occurrences were obtained using a random function. The low-frequency profile involved an event every six days, with a probability of 16.67%. The medium-frequency profile had an event every four days, with a probability of 36%. Lastly, the high-frequency profile entailed an event occurring every two days, with a probability of 50%. To determine the specific day, start time, and maintenance time for each event, a stochastic function was utilised. By combining the frequency levels with different notification lead times, C1, C2, C3, C4, C5, and C6 were established as distinct PDM cases. It is important to note that for the annual events, the "target" value in terms of power (kW) was assumed to be unrestricted, which serves as a reference for evaluating and analysing the PDM cases.

3.3 Co-ordinations of ocean energy supported energy sharing between zero-emission cross-harbour buildings

In studying this zero-energy system, which further expands the scale and number of buildings and incorporates energy sharing based on submarine cable transmission of energy, the methodology of the study will consider how to utilise the submarine cable capacity, the difference in energy policies between the two locations, and the investment of the submarine cable can enhance the system performance based on energy sharing. In this study, the focus is on two hypothetical harbour buildings as the energy demand side. The scenario does not include transport or industrial sectors. Consequently, electricity generated from renewable energy sources will primarily supply these two buildings or exported to the local grid or exchanged based on various energy management strategies. Two scenarios based on the connectivity integrity of submarine cables were designed to investigate the requirement of submarine cable capacity and serve as a comparison and are shown in Fig. 3.4 and Fig. 3.5**,** respectively. The first scenario system has no intermediate submarine cables to connect the two closes offshore sites, only two submarine cables connecting the offshore site to the nearshore site. This scenario is named as Scenario 1 (S1). In such a scenario, there is no energy sharing and exchange between the two regions, the offshore generation from the system will only be transmitted via submarine cables to the buildings or grids in the region, and if the

submarine cables do not have enough capacity, it may happen that part of the energy generation cannot be transmitted but only wasted, resulting in negative impacts. The maximum capacity of the submarine cables is generally assumed to equal the total installed capacity of the renewable energy systems they serve. Therefore, the maximum capacity of a single submarine cable connecting two locations differs between Scenario 1 and Scenario 2. In Scenario 1, the maximum capacity of the single submarine cable linking the nearshore area to offshore site of Hong Kong and Macau is equal to the total installed capacity of the renewable energy system on one side. In Scenario 2, all submarine cables have the same maximum capacity, which is equal to the combined installed capacity of the renewable energy systems in Hong Kong and Macau. This assumption ensures that, under maximum cable capacity, no energy will be wasted. The control methodology and energy flow for this part of the study were presented in Fig. 3.3.

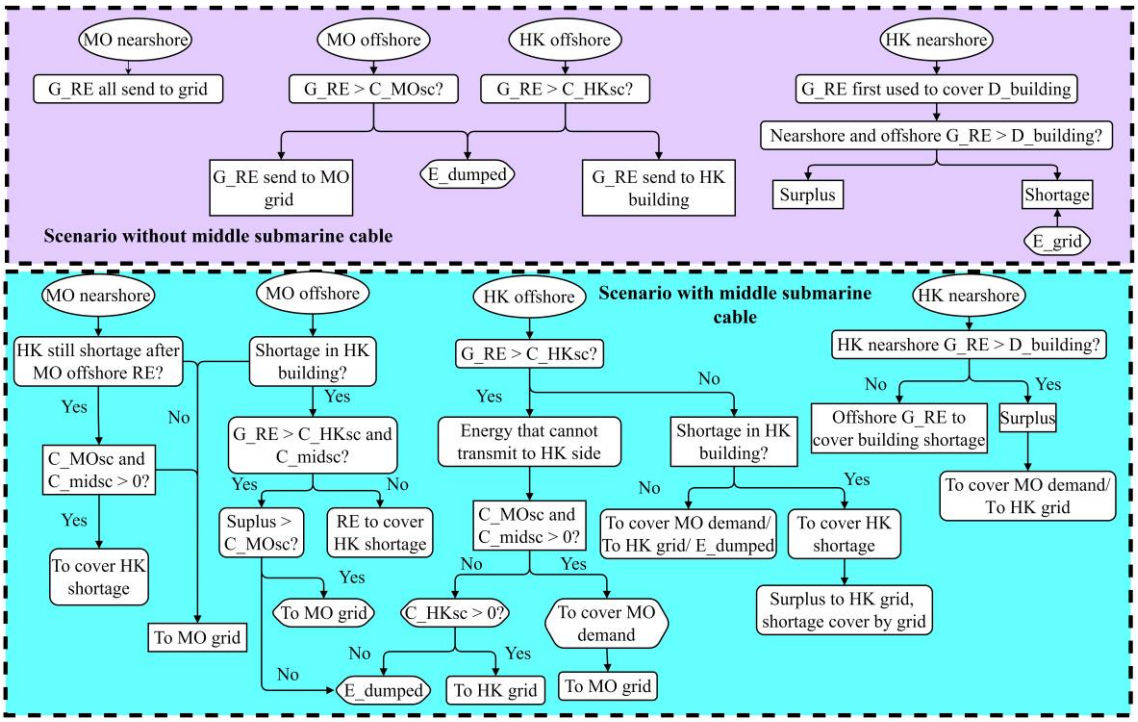

Fig. 3.3 Flow chart of the control methodology and energy flow for the cross-harbour zero-emission system without and with energy sharing.

The business models and policy assumptions integrated into the system encompass electricity tariff for Hong Kong and Macau to estimate annual operational costs, coupled with feed-in tariff policies to evaluate economic benefits. These frameworks exhibit significant regional and sectoral variations. In both Special Administrative Regions, distinct electricity pricing regulations govern different building types, incorporating tiered time-of-use pricing mechanisms based on energy

consumption patterns. Feed-in tariff policies also diverge geographically, reflecting localized energy strategies and market dynamics. Hong Kong's electricity tariff comprises five categories. The residential tariff and non-residential tariff, applicable to general buildings, exclusively employ energy charges. For high-consumption scenarios, three specialized tariffs—bulk tariff, large power tariff, and ice-storage air-conditioning tariff—introduce granular distinctions between on-peak and off-peak periods, alongside differentiated demand charges and energy charges. In contrast, Macau's electricity pricing framework categorizes tariffs into Group A to D, primarily differentiated by voltage levels (e.g., low-voltage for Group A and high-voltage for Group D) and monthly consumption thresholds. For economic calculations, the system assumes Hong Kong's bulk tariff and Macau's Tariff B3, with detailed fee structures outlined in Section 2.5.

The feed-in tariff policies, however, introduce complexities. Hong Kong's feed-in tariff is calculated based on total renewable energy generation, whereas Macau's feed-in tariff depends on the amount exported to the grid. Considering the differences in the feed-in tariff policies of the two regions and the fact that the exchanged energy can only benefit from the feed-in tariff policy once or else there will be an abnormal economic benefit, the establishment of a uniform standard feed-in tariff policy that can be applied in both regions is necessary. Two distinct feed-in tariff policies, the source-based and the boundary-based feed-in tariff, were proposed and analysed. These policies were designed to address the complexities of renewable energy generation and consumption in cross-harbour systems. The source-based feed-in tariff policy operates on the principle that the tariff applied to renewable energy generation is determined by the location of its production, irrespective of where the energy is consumed or exported. This approach ensures consistency in the valuation of energy based on its point of origin. To maintain equity within this framework, energy generated in Macau but transmitted to Hong Kong would be treated as if it were exported to the Macau grid, thus falling under Macau's feed-in tariff scheme. This symmetrical treatment aims to create a balanced system that respects the origin of the energy while accommodating cross-harbour energy flows. In contrast, the boundary-based tariff policy adopts a more territorially focused approach. Under this system, the local feed-in tariff policy is applied when renewable energy is used to fulfil local building demand or exported to the local grid. Energy is subject to the feed-in tariff policy of the receiving region when it moves across regional boundaries. This model more closely aligns with traditional energy market structures, where pricing is typically determined at the point of consumption or grid entry.

In Hong Kong, all the renewable energy produced will initially be transmitted to the harbour building to meet its energy requirements. The surplus will then be sent to the grid. Imported power from the grid will be relied on if the building falls short of electricity. In Macau, since the FiT is different from Hong Kong and is determined based on the exported renewable energy. Two energy management strategies were designed based on whether they were designed to achieve the best energy-

matching performance or the best economic performance. The first type, known as S1C1, energy control will be identical to the subsystem in Hong Kong. S1C2, involves transmitting all the generation directly to the utility and utilising the electrical energy from the utility to fulfil the energy requirements. In S1, the upper limit capacity of a submarine cable matches the total capacity of the renewable energy system it is linked to. Furthermore, the case with the submarine cables capacity reduction while installing stationary batteries at offshore sites to store transient energy generation that cannot be transmitted via submarine cables and retaining the stored energy until the submarine cables have sufficient capacity to transmit the stored energy is considered to compare the impact of batteries and submarine cables. Within scenario S2, a key assumption is made regarding the upper limit of all the submarine cable capacity that links four different locations. This assumption posits that the maximum capacity of these cables is uniform across all connections and matches the combined capacity of the renewable energy systems present on both sides.

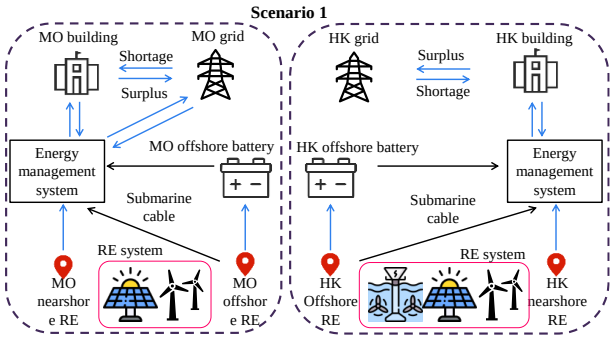

Fig. 3.4 Schematic diagram of scenario S1 that two regions forming separate systems without intermediate submarine cable [Publication III].

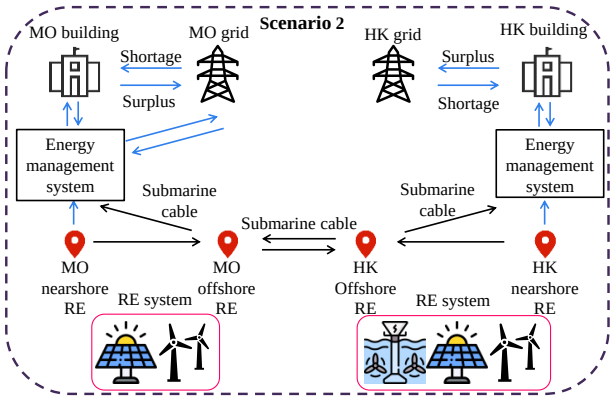

Fig. 3.5 Schematic diagram of the scenario S2 with intermediate submarine cable, the systems in both areas are connected to allow bidirectional energy sharing [Publication III].

In S2, intermediate submarine cables spanning 8 km facilitated the connection between offshore sites were incorporated. This allowed for the transmission and sharing of renewable energy resources between the two regions. Distinct control strategies were developed, three each for the two designed feed-in tariff models. These strategies, designated as S2Csb1-3 for source-based and S2Cbb1-3 for boundary-based, were designed to optimise energy distribution between harbour

buildings and their respective grids. The control strategies prioritise local demand satisfaction before considering energy transmission to the neighbouring region. For instance, in S2Csb1, Hong Kong's renewable energy first meets the demand for its harbour building. Surplus is then evaluated against Macau's harbour building shortage, with transmission occurring only if beneficial, considering submarine cable losses. Similar principles apply to Macau's energy distribution towards Hong Kong. S2Csb2 introduces a variation where both regions initially transmit renewable energy to meet the other's harbour building demand, with the remaining energy directed to local grids or buildings. S2Csb3 further refines this approach, prioritising local demand satisfaction in Hong Kong and grid export in Macau, with cross-border transmission as a secondary consideration. The boundary-based strategies mirror these approaches with subtle differences in grid export priorities and cross-harbour transmission decisions. These variations allow for a comprehensive evaluation of different energy management scenarios. All the control strategies are shown in Fig. 3.6. To account for transmission losses, offshore sites with shorter cable lengths were prioritised when conducting cross-border energy sharing. This approach minimises energy loss and maximises efficiency in the inter-regional energy exchange system.

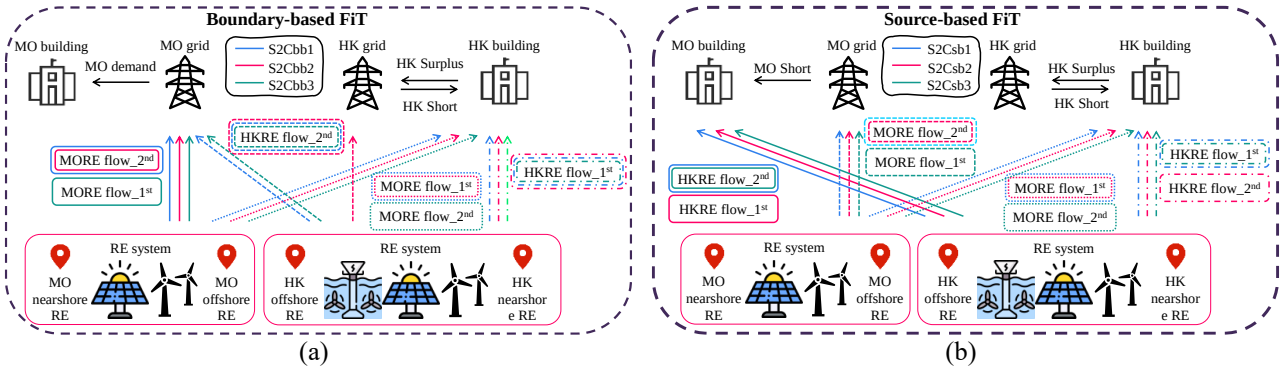

(a) (b)

Fig. 3.6 Schematic diagram of the designed energy control strategies based on two integrated feed-in tariff policies (a) boundary-based FiT and (b) source-based FiT [Publication III].

Simulation analysis was conducted to define representative combinations of renewable energy systems, resulting in the selection of eight combinations, labelled RE1 to RE8 as presented in Table 3.2. These combinations encompass various configurations of offshore and nearshore systems, including wind turbines, FPV panels, and TSGs. The diversity in these combinations allows for a thorough examination of different renewable energy mixes and their impacts on system performance. The number of renewable energy units in each combination was calculated to ensure that annual energy generation from each region could meet its corresponding building's demand. For instance, Hong Kong's energy needs could be met by eight 1 MW wind turbines, or alternatively, by a combination of wind turbines and 150 tidal stream generators, or solely by 60332 FPV panels. Macau's requirements could be satisfied by four 2.7 MW wind turbines or 112749 FPV panels.

Table 3.2 Representative cases of hybrid ocean energy systems for the cross-harbour buildings and the number of nearshore and offshore systems in two regions [Publication III].

Combinations	Macau			Hong Kong			
	Offshore		Nearshore	Nearshore			Offshore
	WT	FPV	WT	FPV	WT	TSG	WT
RE1	0	112749	0	0	0	0	8
RE2	4	0	0	0	0	0	8
RE3	0	0	4	0	6	300	0
RE4	0	0	4	0	7	150	0
RE5	0	0	4	0	8	0	0
RE6	0	0	4	60332	0	0	0
RE7	0	53168	2	0	4	0	4
RE8	2	0	2	0	4	0	4

To enhance the realism of our economic analysis, actual land prices are incorporated. This data allowed us to establish two key metrics: the maximum nearshore land cost (MNLC) of 22.52×10^4 HKD/m^2 and the average nearshore land cost (ANLC) of 11.81×10^4 HKD/m^2 [116]. In the original calculations of the economic performance, we employed a uniform and affordable cost from offshore sites to nearshore sites. Specifically, the same land or sea cost was set at 98.8 HKD/m^2 for land in Macau and 149.9 HKD/m^2 for land in Hong Kong. These values were utilized to estimate the expenses associated with land acquisition for the proposed system. By incorporating the actual land prices, we aimed to capture the potential impact on the NPV_{rel} results.

3.4 Enhanced energy sharing and management between cross-harbour zero-emission buildings based on a combination of electric ferries and deck-on electric vehicles

The cross-harbour zero energy system, based on the previous section, has been expanded to include electrically powered vehicle-carrying ferries and electric vehicles that can reasonably exist between the cross-harbour ferry terminal buildings. In addition to the submarine cables, an electric vehicle ferry with a V2B function and ten electric vehicles have been integrated into the system to perform the energy transport and exchange function. To investigate the changes in the overall system by incorporating electric ferry and electric cars without and with the V2B function for the energy sharing approach and as a comparison, two scenarios are firstly designed which are referred to as Scenario 1 and Scenario 2, both scenarios will directly extend the previous part of the system which contains three segments of submarine cables connecting all the renewable energy venues, and in Scenario 1, the electric ferry and electric cars will have no V2B function and only act as energy demanders, while in Scenario 2, the V2B function will be added so that they can take up part of the energy sharing role. Meanwhile, considering that the presence of intermediate submarine cables may affect the impact of the energy-sharing function of electric vehicles on the overall system, a scenario called Scenario 3 was designed to demonstrate the changes in the V2B function when the system does not include intermediate submarine cables. The basic control methodology of scenarios without and with middle submarine cables for buildings is shown in the upper part of Fig. 3.7.

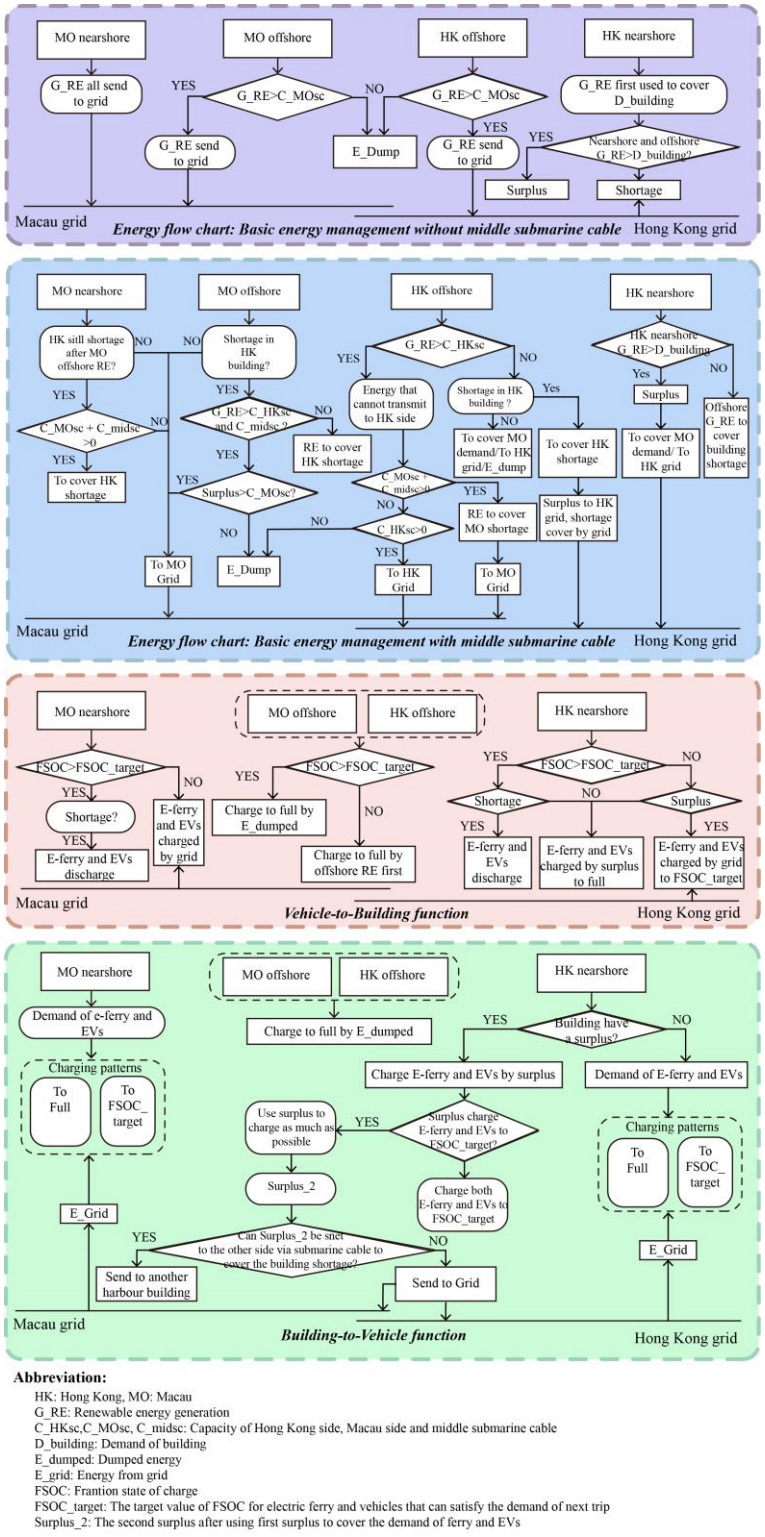

Abbreviation:

HK: Hong Kong, MO: Macau
G_RE: Renewable energy generation
C_HKsc,C_MOsc, C_midsc: Capacity of Hong Kong side, Macau side and middle submarine cable
D_building: Demand of building
E_dumped: Dumped energy
E_grid: Energy from grid
FSOC: Frantion state of charge
FSOC_target: The target value of FSOC for electric ferry and vehicles that can satisfy the demand of next trip
Surplus_2: The second surplus after using first surplus to cover the demand of ferry and EVs

Fig. 3.7 Flow chart of the control methodology for the integrated EV and ferry system [Publication IV].

In the first two scenarios, the energy generation from both regions can be transmitted and shared through both submarine cables and mobile electric transportation. In the previous part of the study, the source-based FiT in the designed integrated FiT was able to achieve better economic performance and was therefore carried over to this part of the study. The electric ferry and the ten electric cars are not only part of the energy demand of the system under study, their own removable

batteries for energy supply can also be used to realise energy sharing. The schematic diagram of these two scenarios is shown in Fig. 3.8. In the first scenario, both the electric ferry and the electric car will only have B2V functions, and they will not be able to deliver the electricity stored in their batteries to the building and the system and will only be used as part of the system's energy requirements, whereas in the second scenario, the V2B function that allows them to deliver the electricity in the batteries that they themselves carry to the building and the system will be realised, thus comparing the impacts that the presence of the V2B function has on the system's performance. The control methodology of the B2V and V2B functions is shown in the lower part of Fig. 3.7.

When only the B2V function is activated and the V2B function is unavailable, electric ferries and cars will only be charged when docked in the harbour buildings and offshore platforms. Upon docking at the harbour building, the energy transferred will first satisfy the building demand. The surplus energy will be used to charge the ferry and EVs, and if there is a surplus after satisfying the demand for the ferry and EVs, it will be exported to the grid. If the generation cannot fulfil the demand for ferries and EVs, electricity from the grid will be used to cover the shortage. When ferries and EVs are charged, their FSOC levels will be charged at least to the level required for the next trip. The specific value depends on the individual controls of each group. When both the B2V and V2B functions are activated, the ferry and EVs will be allowed to discharge the building to cover the building's shortage when docked at the harbour building and the conditions are met. The charging process of the ferry and EVs is consistent with the case where only the B2V function exists, as described above. When the ferry and EVs dock at the harbour building and are about to charge or discharge, they will first check their FSOC level. If the FSOC level is higher than the FSOC level required to meet the next trip and the docked building is experiencing a shortage at this point, then the ferries or EVs will be able to release a portion of the energy stored in their batteries to cover the building's shortage. If the FSOC level is lower than the FSOC level for the next trip, then the ferry or EVs will only be recharged. The charging measures for the B2V charging process include adjusting the target FSOC level for charging and setting different FSOC levels for energy sources, reducing the instantaneous energy demand, and distributing the total energy demand evenly over the entire charging period. The performance of these various charging measures is compared to obtain the optimal charging strategy. For the discharge process of V2B, different discharge strategies are also included. The first is that if there is a shortage in the building and the FSOC level is higher than the level that must be met for the next trip, the ferry and EVs will be fully discharged to cover the shortage. At the same time, the other is a discharge strategy based on energy flexibility, where the discharged energy will be used to reduce the building's energy peaks to reduce the demand charge in the electricity bill.

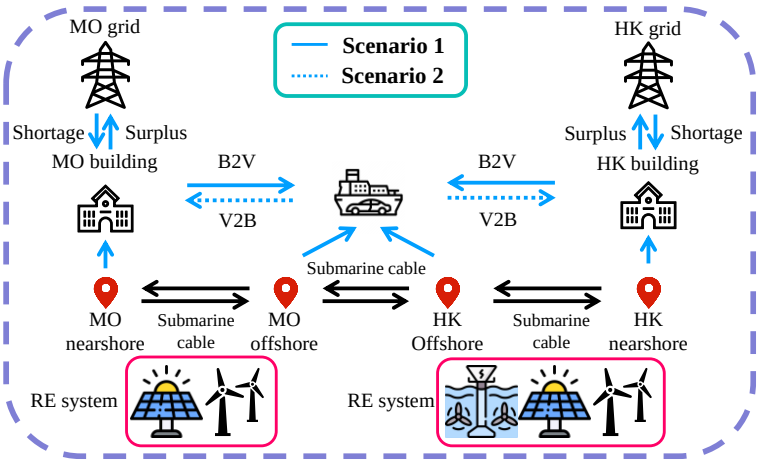

Fig. 3.8 Schematic diagram for Scenario 1 without V2B function and Scenario 2 with V2B function for electric ferry and EVs [Publication IV].

In Scenario 3, the intermediate cable no longer exists, and the energy generation from both regions cannot be shared through the submarine cables, the energy sharing can only be conducted by the mobile electric transportation with V2B function. The submarine cable was assumed to keep at 100% of maximum capacity so that there was no dumped energy. Considering that Macau's FiT policy is calculated based on the amount of output to the grid, to maximise economic benefits, for the Hong Kong side, all renewable energy generated will be first sent to cover building demand. If there is a surplus, it will be exported to the grid, and if there is still a shortage, the grid will cover it. In Macau, all energy will first be sent to the grid, and grid electricity will cover the demand for buildings and EVs. The schematic diagram of scenario 3 is shown in Fig. 3.9.

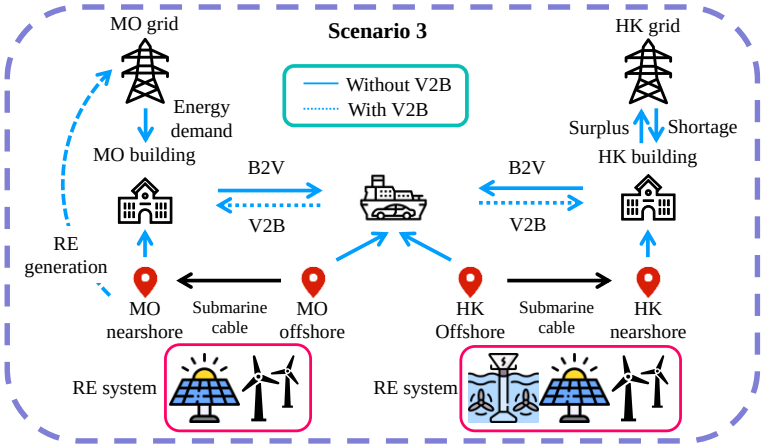

Fig. 3.9 Schematic diagram for Scenario 3 without the intermediate [Publication IV].

A total of 7 representative renewable combinations named RE1 to RE7 listed in Table 3.3 were selected to represent the impacts of different renewable energy system combinations. RE3 is the only case that includes 30 nearshore TSGs in Hong Kong.

Table 3.3 Detailed information of selected renewable energy combinations for the cross-harbour system incorporating electric ferry and EVs [Publication IV].

Combinations	Macau			Hong Kong			
	Offshore		Nearshore	Nearshore			Offshore
	WT	FPV	WT	FPV	WT	TSG	WT
RE1	0	115701	0	0	0	0	9
RE2	4	0	0	0	0	0	9
RE3	0	0	4	0	6	30	0
RE4	0	0	4	0	9	0	0
RE5	0	0	4	63414	0	0	0
RE6	0	56121	2	0	5	0	4
RE7	2	0	2	0	5	0	4

3.5 Analysis criteria

Within this subchapter, a detailed introduction to the analysis criteria employed for assessing and quantifying the environmental, technical, and economic performance of the studied system under various scenarios were provided.

To begin with, it necessitates the determination of the yearly electrical energy exported to and imported from the grid. Based on the study of Cao [106], the two equations of the energy taken out of the grid (i.e. '$E_{exp,a}$') and the energy brought into from grid (i.e. '$E_{imp,a}$') can be expressed as

$$E_{exp,a} = \int_{t_1}^{t_2} P_{exp}(t)dt \quad (1)$$

$$E_{imp,a} = \int_{t_1}^{t_2} P_{imp}(t)dt \quad (2)$$

Here, '$P_{exp}(t)$' and '$P_{imp}(t)$' represent the power taken out of the grid and brought into from grid, respectively. The limitation of these two equations 't_1' and 't_2' denote the start and end times of the investigation period, which, in this study, correspond to the entire duration of one year.

The primary objective of a zero-emission system is to achieve near-zero carbon emissions. Hence, the environmental analysis criteria encompass the annual operational equivalent CO_2 emission (CE_a). This criterion can be expressed as follows:

$$CE_a = \left(E_{imp,a} - E_{exp,a}\right) \times CEF_{eg} \quad (3)$$

Here, 'CEF_{eg}' denotes the equivalent CO_2 emission factor of the power grid.

Furthermore, at the technical level, several methodical criterions are defined to determine the outcomes. The first aspect pertains to the energy-matching performance and capability of the system. Cao et al. [117] introduced two parameters for measuring the energy-matching capability of the system: the on-site electrical energy fraction (OEFe) and on-site electrical

energy matching (OEMe). Enhanced energy matching and renewable energy self-consumption capabilities aim to reduce reliance on the grid and alleviate its burden. Meanwhile, as the feed-in tariff in Hong Kong is calculated based on renewable energy generation, improved energy matching would positively affect the economic performance of the proposed system. The general equations for OEFe and OEMe, specific to this study, are as follows:

$$\mathrm{OEFe} = 1 - \frac{\int_{t_1}^{t_2} \mathrm{P_{imp}(t)dt}}{\int_{t_1}^{t_2} \mathrm{L_{elec}(t)dt}}, 0 \le \mathrm{OEFe} \le 1 \tag{4}$$

$$\mathrm{OEMe} = 1 - \frac{\int_{t_1}^{t_2} \mathrm{P_{exp}(t)dt}}{\int_{t_1}^{t_2} \mathrm{P_{REe}(t)dt}}, 0 \le \mathrm{OEMe} \le 1 \tag{5}$$

Here, $P_{imp}(t)$ represents the imported power from the electric grid. $L_{elec}(t)$ is the total electricity load power of the building. $P_{exp}(t)$ is the exported power from the system to the grid, and $P_{REe}(t)$ is the electricity power output of the hybrid renewable energy system. The integral limits t_1 and t_2 correspond to the start and end times of the investigation period. Higher values of OEMe and OEFe indicate cases with improved energy-matching capability and superior technical performance. The simultaneous presence of two parameters that quantify the performance of energy matches between multiple cases can make comparisons difficult because it is not clear which of the two parameters is more important; therefore, combining the two parameters into a new parameter to facilitate the assessment of the overall energy matching performance that also expresses the importance of each of the two parameters can make case-to-case comparisons easier, a weighted matching index (WMI) was proposed [118]. The equation of WMI can be presented as

$$\mathrm{WMI} = \mathrm{w_1 OEFe} + \mathrm{w_2 OEMe}, \qquad \sum_{i=1}^{2} w_i = 1, 0 \le w_i \le 1, 0 \le \mathrm{WMI} \le 1 \tag{6}$$

In this research, the weighting factors for OEMe and OEFe will have an equal value of 0.5. Higher WMI values indicate better energy-matching performance, with a value of 1 indicating a perfect matching case.

Following the exploration of the energy flexibility enhancement of the building, the technical analysis focuses on evaluating its effectiveness. The aim is to reduce peak demand and energy consumption by shifting power demand from peak to off-peak periods. To demonstrate the performance of flexibility control strategies, two criteria are proposed which are called peak shaving indicator (PSI_{peak}) and off-peak valley filling indicator ($VFI_{offpeak}$). The generalised equations of the mentioned two criteria can be expressed as:

$$\mathrm{PSI_{peak}} = \frac{\int_0^{t_{p,ref}} \left[\mathrm{P_{ref,p(t)} - P_{j,p(t)}}\right] \mathrm{dt}}{\int_0^{t_{p,ref}} \left[\mathrm{P_{ref,p(t)} - P_{avg,ref,peak}}\right] \mathrm{dt}} \tag{7}$$

$$VFI_{offpeak} = \frac{\int_{t_{op,ref}}^{t_{op,end}} [P_{j,op(t)} - P_{ref,op(t)}]dt}{\int_{t_{op,ref}}^{t_{op,end}} [P_{avg,ref,offpeak} - P_{ref,op(t)}]dt} \quad (8)$$

Here, '$P_{j,\ p(t)}$' is the demand duration of selected case j with flexibility control strategy during the peak period, '$P_{ref,\ p(t)}$' is the demand duration of reference case during the peak period, '$P_{avg,\ ref,\ p(t)}$' is the average demand line of the reference case during the peak period, '$t_{p,\ ref}$' represents the temporal intersection of the demand duration and the average demand line of the reference case during the peak period, '$P_{j,\ op(t)}$' is the demand duration curve of selected case j with flexibility control strategy during the off-peak period, '$P_{ref,\ op(t)}$' is the demand duration curve of reference case during the off-peak period, '$P_{avg,\ ref,\ op(t)}$' is the average demand line of the reference case during the off-peak period, '$t_{op,\ ref}$' is the temporal intersection of the demand duration curve and the average demand line of the reference case during the off-peak period. Higher values of PSI_{peak} and $VFI_{offpeak}$ indicate better technical performance in terms of reducing peak demand and filling valleys.

In the designed cross-harbour zero-energy system, energy sharing occurs through self-owned submarine cables. However, variations in the capacity of these cables can pose a challenge. When the instantaneous renewable energy generation exceeds the submarine cable capacity, some of the generation cannot be transferred to the building or the grid and is dumped. This can have a negative impact on the system. Therefore, the energy usage ratio was proposed, and the equation of energy usage is expressed as

$$r_{energy\ usage} = 1 - \frac{\int_{t_1}^{t_2} E_{dumped}(t)dt}{\int_{t_1}^{t_2} E_{RE,total}(t)dt} \quad (9)$$

To ensure optimal performance, it is important to minimise dumped energy. When the energy usage ratio reaches 100%, it means that no energy is wasted, and the system achieves optimum performance.

Furthermore, two economic criteria were included to investigate the economic performance of the studied hybrid system: simple payback period and net present value. A simple payback period (SPP) counts the number of years required to recover the initial funds invested. Net present value (NPV) involves the interest rate in the equation; therefore, it could be considered the time value of money and was included as a more accurate economic analysis parameter, which considers the time value of money through the interest rate. In this study, a reference case was established to exhibit the difference, which did not contain any renewable energy system. Therefore, these economic criteria can be described as relative indicators of SPP_{rel} and NPV_{rel}. The generalised equation of SPP_{rel} and NPV_{rel} can be expressed as

$$SPP_{rel} = \frac{\text{Relative total investment cost}}{\text{Relative net annual returns}} \quad (10)$$

$$\mathrm{NPV_{rel}} = \sum_{t=0}^{n=20} \frac{B_t - C_t}{(1+i)^t} \tag{11}$$

Here, 'n' represents the lifetime of the project, 'B_t' represents the relative benefit during the period t, 'C_t' denote the relative cost during the period t, and 'i' is the interest rate. A positive value of NPV_{rel} signifies that the hybrid system generates a net profit over its life cycle, indicating its financial viability. On the other hand, a negative value of NPV_{rel} indicates that the hybrid system is unable to generate a net profit over the entire life cycle, suggesting financial challenges or limitations.

Chapter 4. Results and discussion

This chapter comprises four subsections that present and analyse the results of each original article. The simulation results from different parts of the entire study are presented separately in each subsection, and the techno-economic and environmental results based on different objectives, scenarios and energy management strategies will be analysed and discussed in terms of the causes of emergence and the phenomena represented. Subsection 5.1 focuses on the findings of original research paper I, subsection 5.2 delivers the results of original research paper II, subsection 5.3 presents and analyses the results obtained from original research paper III, and subsection 5.4 encompasses the results of original research paper IV.

4.1 Coastal zero-energy office building with the support of a hybrid ocean energy system

4.1.1 Impact of ocean thermal energy on the office cooling system

Considering the advantages and disadvantages of the structure and design for the chillers that utilise OTE, three different structures were designed with the aim of exploring the most suitable seawater cooling system. The design of these chiller structures includes the structure of the heat exchange components, their location and the materials from which the heat exchange is primarily derived. Both the first and second designs adopt the structure of copper spiral tubes to expand the heat exchange area and utilise seawater for heat exchange with the cooling water to cool down the cooling water. The first design places the heat exchanger on land and the seawater is transferred to the heat exchanger through pumps and pipes, while the second design installs the heat exchanger directly under the sea surface. In the third formation, seawater is directly introduced into the chiller to serve as a cooling agent for the refrigerant, eliminating the need for intermediate cooling water. In the simulation conducted, the indirect heat exchanger, a key component in the system, was assigned an effectiveness (ε) of 70%. The heat exchange area (A) and effectiveness of the heat exchangers immersed in seawater were determined through the application of the number of transfer units (NTU) method. This approach is widely recognised in the field of thermal engineering for its accuracy in calculating heat transfer rates within exchangers, particularly when fluid temperatures undergo significant changes during the exchange process. It involves multiplying the overall heat

transfer coefficient by the heat exchange area (UA) values of the heat exchangers positioned on the shore. The relationship between the heat exchange area and effectiveness is visually represented in Fig. 4.1, providing a graphical depiction of these key parameters.

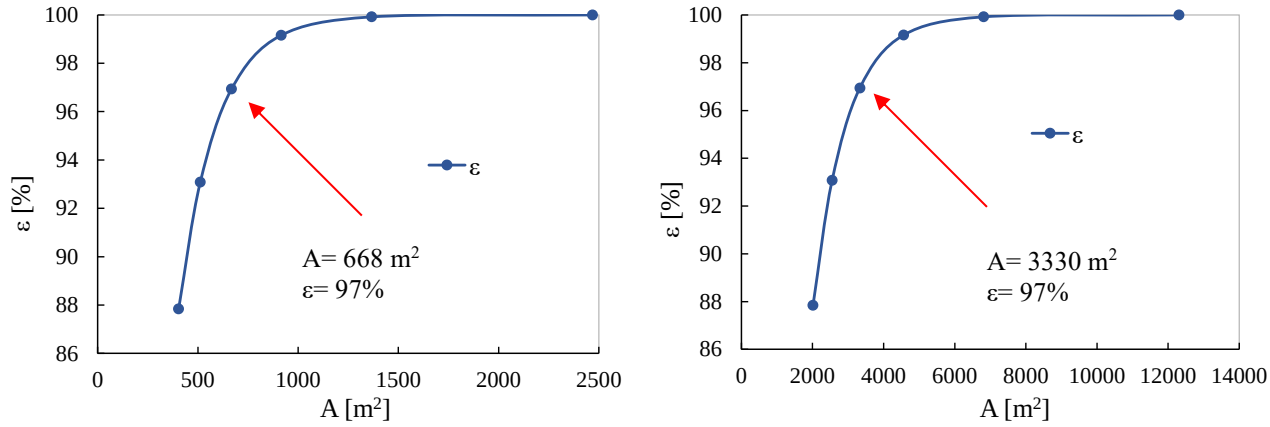

Fig. 4.1 Curves showing the relationship between heat exchange efficiency and heat exchange area in (a) space cooling and (b) AHUCS [Publication I].

The results present that as the heat exchange area continues to increase, the effectiveness approaches 1. However, it is important to note that continuously increasing the heat exchange area would lead to higher costs for the heat exchanger, making it less cost-effective. Upon analysing the trend depicted in the graphs, a point where the trend of the forward and backward curves is outstandingly different occurs between two data points. For the purpose of striking a balance between performing higher effectiveness and minimising the required heat exchange area, the data marked with red arrows in the figure were used. For the AC system, the selected heat exchange area is 3330 m^2, resulting in an effectiveness of 97%. Similarly, for the SC system, the chosen heat exchange area is 668 m^2, also with an effectiveness of 97%. By adopting this design approach, it is possible to achieve an effectiveness of 97% while maintaining a reasonable heat exchange area. Furthermore, implementing this design approach offers the advantage of closely matching the cooling water temperature returning to the condenser with that of the seawater after heat exchange. This alignment in temperatures contributes to the overall improvement of the chiller's performance.

Based on the design of three types of sea source cooling systems introduced previously and the reference case of using a conventional cooling tower, the coefficient of performance (COP) of the chiller and the COP of the whole system for the AC and SC systems are implemented and calculated respectively in the TRNSYS simulation environment to compare and get the design of the cooling system with the best overall performance. In the AC system, the cooling tower case can achieve 6.15 of chiller COP and 4.93 of overall COP. For the sea-source chiller that placed the heat exchanger onshore, chiller COP could be six while overall COP was 4.66. If the heat exchanger was installed under the seawater, the chiller

COP could reach 6.18, and the overall COP would be 4.98. Directly using seawater as the cooling water enables the chiller COP of 6.21 and overall COP of 5. In the SC system, the cooling tower case obtained 7.66 and 5.23 for chiller and overall COP. The onshore heat exchanger achieved 7.64 and 5.31 for the chiller and overall COP. Under seawater, the heat exchanger reached 7.85 and 5.53, while using seawater directly as the cooling water obtained 7.89 and 5.48.

The SC system has a higher COP than the AC system, both in terms of chiller and overall COP. The chiller COP of the SC system can reach more than 7, and the overall COP can reach more than 5. The chiller COP of all sea source cooling designs and reference cases of AC systems is more than 6, and the maximum value of the overall COP is 5. The chiller COP and overall system COP for the AC system, as well as the chiller COP for the SC system, were higher in the cooling tower system of reference case compared to the chillers with onshore indirect heat exchangers. However, the net system COP for the SC system was lower in comparison. The utilisation of chillers with onshore heat exchangers exhibited minor technical performance compared to cooling towers. This outcome can be attributed to insignificant temperature advantage and the use of essential pumps with larger capacities. Chillers with spiral copper tube heat exchangers installed below the sea surface directly utilise seawater as the cooling water has higher chillers and overall system COPs in AC and SC systems compared to the reference case with cooling towers and the design with heat exchanger installed in a building adjacent to the land, which demonstrates better heat exchange efficiency and helps to increase the refrigeration system's efficiency of the cooling system. In these two designs, the sea source cooling system that directly uses seawater as cooling water only obtains smaller result than the design that installs the spiral copper tube heat exchanger in seawater when calculating the overall COP in the SC system, and it is able to obtain higher results in calculating both the chiller and overall COP in the AC system as well as the chiller COP in the SC system for this design. However, the direct transfer of seawater to the chiller to replace the cooling water may cause serious deterioration of the chiller and increase the difficulty and cost of maintenance of the system due to the corrosiveness of seawater. Therefore, installing heat exchangers in seawater to utilise the ocean thermal energy became the best choice for this study building. After utilising the sea-source cooling system, the total energy demand for the entire year amounted to 1.32×10^6 kWh, resulting in an energy use intensity of 250.23 kWh/m^2.

4.1.2 Matching analysis with mixing ratios of FPV-tidal energy generations

The results of the simulations are first used to discuss the respective characteristics of the TSG system and the FPV system. The monthly energy generation performance of both the TSG and FPV system, designed to meet the energy requirement of the target building annually at the same scale of energy generation, was calculated and presented in Fig. 4.2. The TSG system demonstrates more stability in generation, whereas the monthly energy production of the FPV system exhibits greater fluctuations.

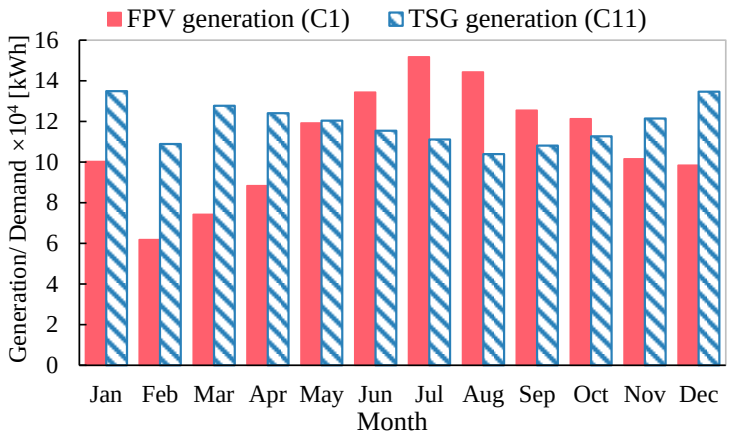

Fig. 4.2 TSG and FPV systems generation in hybrid ocean energy systems with similar annual energy generation in different months [Publication I].

Under the condition of total energy generation, a total of 11 cases with different mix ratios were analysed. Among the cases, C1 and C11 represent the two extreme scenarios, with C11 having ten generators and C1 consisting of 5055 FPV panels. The environmental impact and energy matching curves of each case are visually represented in Fig. 4.3.

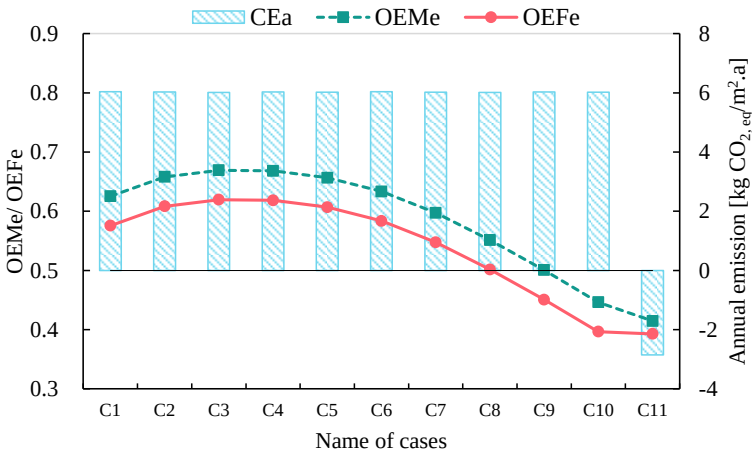

Fig. 4.3 Energy matching performance and environmental performance of 11 cases of ocean energy systems with different mixing ratios [Publication I].

The curves of two energy-matching indicators exhibited similar variations among all the cases, with the OEMe values consistently surpassing the OEFe values. The results ranged from 0.39 to 0.67. Among the cases, C3, which consisted of 3967 FPV panels and two TSGs, demonstrated the maximum OEFe and OEMe values of 0.62 and 0.67, indicating optimal performance within this group. Conversely, C11, comprising 11 tidal stream generators, exhibited the lowest OEFe and OEMe values of 0.39 and 0.42, respectively. The CE_a results for most cases were similar, 6.02 to 6.04 kg/m^2.a, except for C11, which yielded a negative CE_a value.

4.1.3 Solutions to enhance the matching capability of the hybrid FPV-tidal energy system

To further investigate and strengthen the energy-matching capabilities, representative cases were selected for additional simulations. These cases included C1, which utilised only FPV systems; C11, consisting solely of TSG systems; and C3, identified as the optimal performer based on previous technical performance analyses. It was discovered that the values of both indicators were below 0.67. To address this, energy storage devices, specifically batteries, were employed to enhance the system's energy-matching capabilities by absorbing surplus renewable energy and trying to cover part or all shortages. The battery model employed has a single block capacity of 232kWh [119]. Following the addition of batteries, the results are presented and discussed in Fig. 4.4.

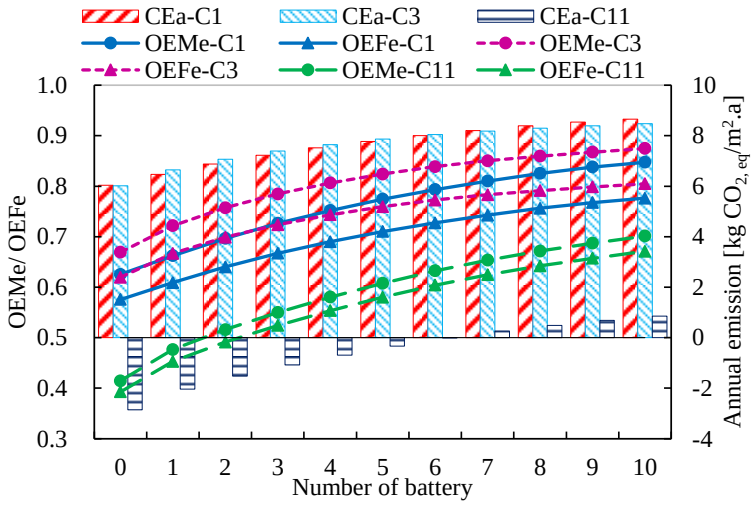

Fig. 4.4 Impact of adding batteries on energy matching and economic performance of selected representative cases [Publication I].

The analysis of the technical performance results revealed that the energy-matching indicators for all selected cases demonstrated a continuous upward trend as the battery number and capacity increased. The OEMe of C3 can reach 0.87 and the OEFe can reach 0.80, and the OEMe of C1 can also be increased to 0.85 while the OEFe can only reach a maximum of 0.78 when the net capacity of the battery group reaches its maximum. The OEMe and OEFe of C11 can only be strengthened to a maximum of 0.70 and 0.67. It can be observed that the OEMe and OEFe results asymptotically approached 1 as the net capacity of the battery group increased. This suggests that the utilisation of batteries can effectively enhance energy-matching capabilities. Furthermore, the emission results specified that batteries had a negative impact on environmental performance. As the net capacity increased, the results of CE_a exhibited an upward trend. This behaviour was attributed to the losses associated with battery storage. Nevertheless, even with the increased values, they remained significantly lower compared to the reference case. The objective of reducing emissions was successfully accomplished.

4.1.4 Techno-economic analysis for cases with mixing ratio and batteries

The techno-economic performance of the studied cases without the presence of batteries is presented in Fig. 4.5, after

incorporating a real commercial electricity tariff model applied to Hong Kong. The economic performance is demonstrated by the parameters SPP_{rel} and NPV_{rel}, while the energy-matching performance is exhibited by the WMI, which combines the parameters OEMe and OEFe. It can be observed that C1, which only consists of the FPV system, achieved the optimum economic performance among all the studied cases, with the highest NPV_{rel} value, 18.74×10^6 HKD and lowest SPP_{rel} 10.5 years. While C11, having the TSG system only, obtained the worst economic performance with the NPV_{rel} value of -27.5×10^6 HKD and the highest SPP_{rel} result of 38 years, reflecting that this case cannot achieve neutral economic performance within the 20-year life cycle. As the proportion of the TSG system in the case's energy supply system increases, the NPV_{rel} gradually decreases while the SPPrel gradually increases, implying that the economic performance of the case is gradually deteriorating. The NPV_{rel} value of C6 remains positive while the NPV_{rel} value of C7 becomes negative, C6 being the last case that still pays for itself over a 20-year life cycle. This circumstance was caused by the higher investment and O&M costs of the TSG system.

The trend observed in the SPP_{rel} curve from C1 to C10 clearly shows a consistent and significant increase. However, the curve between C10 and C11 exhibits a completely different trend compared to the previous cases.

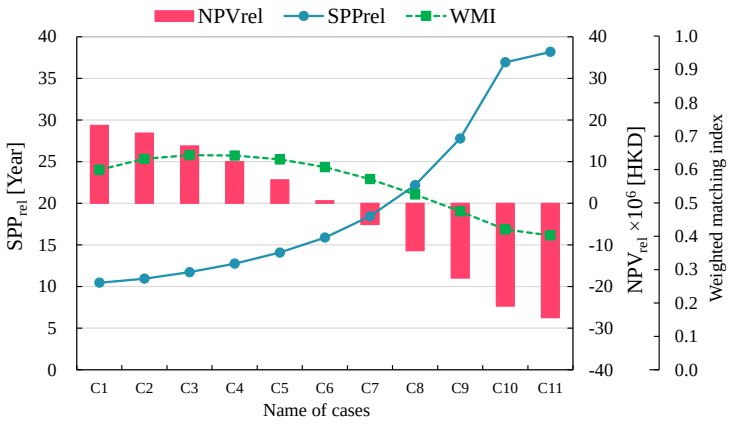

Fig. 4.5 Results for all cases of WMI, representing technical performance, SPP_{rel} and NPV_{rel}, representing economic performance [Publication I].

Similar to the previous technical analysis, the economic performance of the hybrid system was evaluated by selecting three representative cases after incorporating batteries. These cases included C1 utilizing solely FPV system, C11 comprising exclusively TSG system and C3, which is the case with optimum result in the energy matching analysis. The results pertaining to the economic performance of these cases are presented in Fig. 4.6.

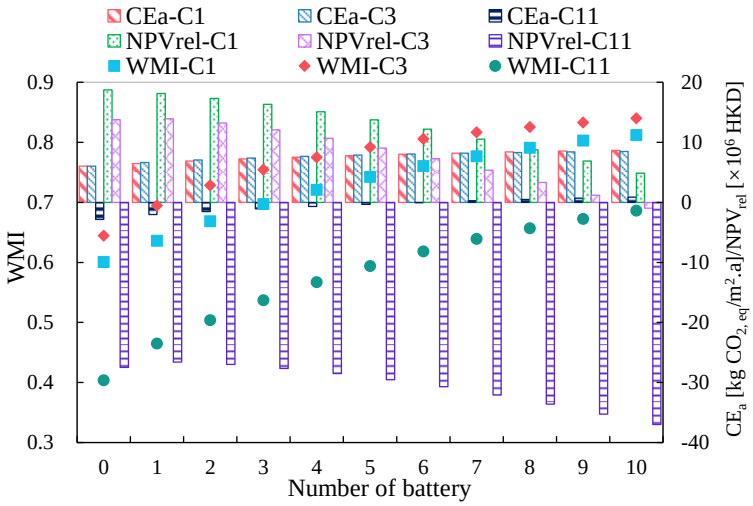

Fig. 4.6 Impact of adding 0 to 10 batteries on the WMI, NPV_{rel} and CE_a results of the selection case [Publication I].

The economic performance of the selected cases remained unchanged after integrating batteries into the system. Among the cases, C1 demonstrated the best economic performance, characterised by the lowest SPP_{rel} values and the highest NPV_{rel} values. On the other hand, C11 exhibited the poorest technical and economic analysis results, with all SPP_{rel} values surpassing 20 years and all NPV_{rel} values being negative. This indicates that even without the use of batteries, C11 would not yield a payback within a 20-year life cycle. These outcomes can be attributed to the higher total capital and annual O&M costs of the TSG system. In C1 and C3, the NPV_{rel} values exhibited a decrease as the net battery capacity increased, while the SPP_{rel} values displayed an increase. This demonstrates the negative economic impact of increasing the net battery capacity. In C11, the economic performance improved only when the net capacity of the battery group increased to 464 kWh, achieving the maximum NPV_{rel} value of -26.6×10^6 HKD. C3 also can obtain the maximum NPV_{rel} value of 13.77×10^6 HKD with the application of one 232 kWh battery. However, when the net capacity of the battery group is increased to the maximum value in this investigation, the NPV_{rel} result becomes negative at -0.95×10^6 HKD.

4.2 Energy flexibility enhancement and demand response for an ocean-energy-supported zero-emission office building

4.2.1 Investigation of flexibility control

The stationary batteries are the only source to conduct energy flexibility control and can be charged by the grid, and the mixing FPV-TSG systems were utilised as the energy supply for the coastal office building. The case referred to as C3 was identified in the previous study, which exhibited the best technical performance. This configuration of this case consisted of 3967 FPV panels and two TSGs. Building upon this foundation, C3 has been selected as the focal point for the further energy flexibility study.

An investigation was conducted focusing on evaluating the impact of varying battery capacities on the performance of

energy flexibility and zero energy building systems with ten distinct battery capacities, ranging from 200 kWh to 2000 kWh, incrementing in intervals of 200 kWh. To determine the effectiveness of the implemented flexibility control, the presented results based on the annual tariff reduction and NPV_{rel} calculation. The obtained results shed light on the performance of the two flexibility control strategies, referred to as FC1 and FC2.

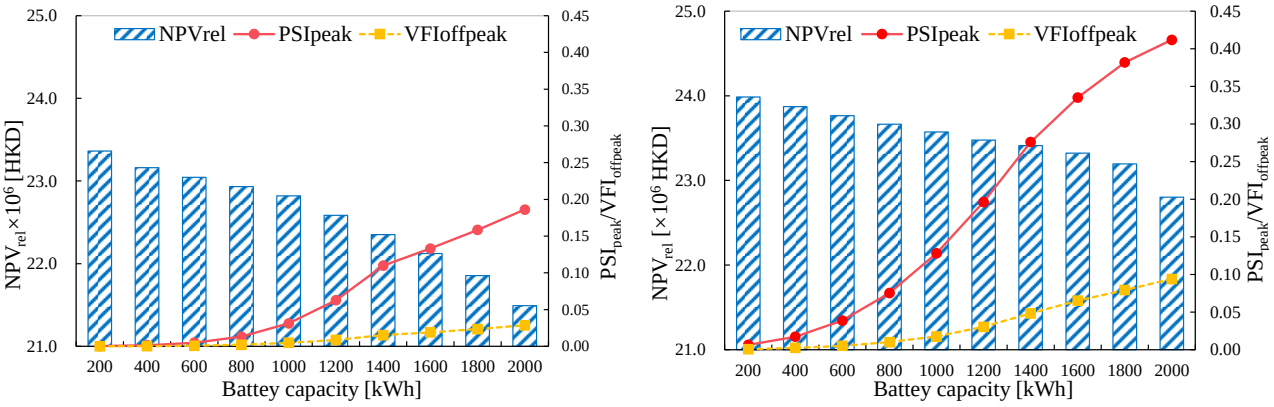

Fig. 4.7 Techno-economic performance based on (a) FC1 and (b) FC2 strategies if the battery can interact with both surplus renewables and the grid [Publication II].

Fig. 4.7 illustrates the economic and energy shifting influence of battery capacity under the control of both charging methods in this scenario. The energy shifting indicators exhibited an upward trend when increasing the battery capacity. Conversely, annual tariff and NPV_{rel} displayed a decreasing trend with increasing battery capacity.

While the tariff reduction signifies enhancement, the substantial capital cost and the need for replacement of the battery resulted in a deterioration of economic performance, as stipulated by the NPV_{rel}. Comparisons between FC2 and FC1 clearly revealed the improvements achieved by FC2. Consequently, both the case acquires the leading technical performance and the case with optimum economic performance employed FC2. The former case utilised a 2000 kWh battery, yielding PSI_{peak} and $VFI_{offpeak}$ values of 0.412 and 0.094, respectively. The latter case employed a battery with 200 kWh, yielding an NPV_{rel} result of 23.985×10^6 HKD. Under the control of FC1 and FC2, the curve slope of the energy flexibility indicators when the capacity increases from 800 to 1400 kWh is larger than the two intervals of 200 to 800 kWh and 1400 to 2000 kWh, implying a higher growth rate. The amount of change in the economic performance parameter NPV_{rel} is relatively smooth, with no greater or lesser amount of change in any of the battery capacity change intervals.

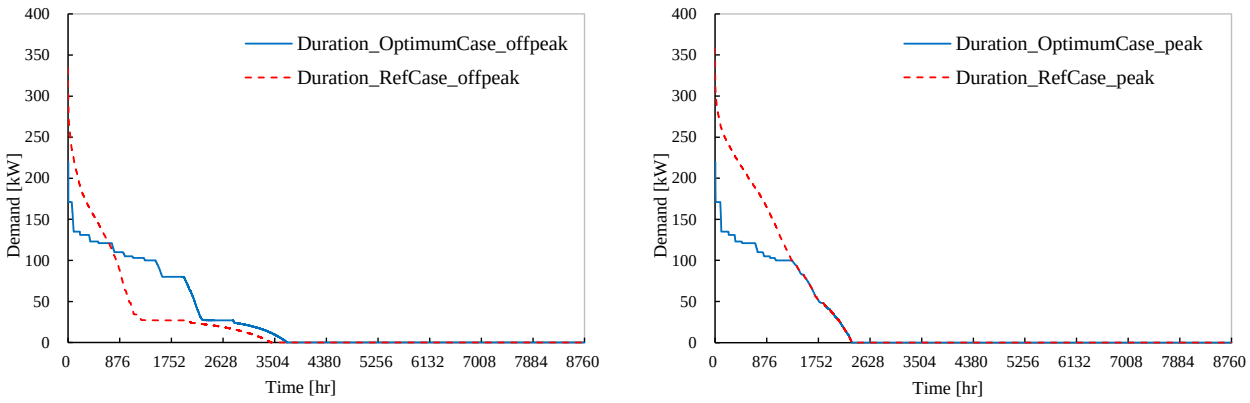

(a) (b)

Fig. 4.8 Duration curves of energy demand in (a) off-peak and (b) peak periods for the best-performing and reference cases [Publication II].

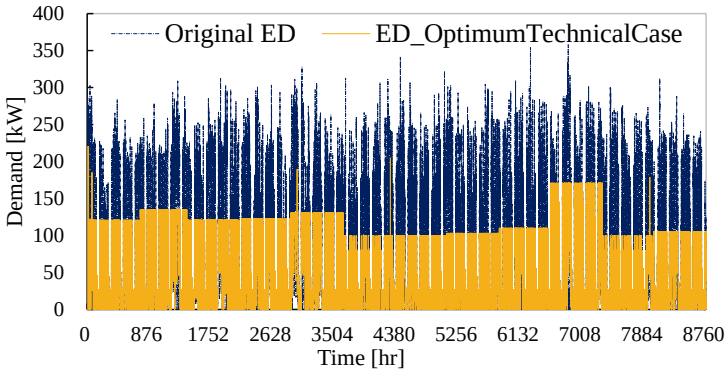

Fig. 4.9 Comparison of annual instantaneous energy demand between the technical best-performing case and the reference case [Publication II].

To further analyse the energy flexibility, the duration curves for the case demonstrating premier energy shifting performance within the defined scenario and the reference case were presented in Fig. 4.8 during both periods. The curves reveal an evident discrepancy which suggests that the power demand was effectively reduced, highlighting the successfulness of FC2 in achieving the energy flexibility control. The comparison between the energy demand (ED) of the chosen case and the original ED without flexibility control throughout the year is depicted in Fig. 4.9.

4.2.2 Investigation of Peak Demand Management

The scenario investigated in the energy flexibility section has also served as the basis for further investigation into the PDM programme. Based on the findings from the previous investigation on flexibility, we proceeded to examine the economic effect of the PDM programme. To achieve this, the battery capacities were systematically increased to the maximum capacity of 2000 kWh in increments of 50 kWh before 200 kWh and in increments of 200 kWh after 200 kWh. The previous analysis considered the NPV_{rel} results based on the feed-in tariff from the government, which resulted in positive NPV_{rel} values. However, it is important to explore the feasibility of zero-energy buildings without relying heavily on feed-in tariffs, which is an incentive without burdens and responsibilities. In line with this focus, this study aims to

investigate the economic performance of the system by leveraging incentives earned and managing the system's energy flexibility. Specifically, PDM Control 2 cases were utilised to examine the renewable energy penetration to gain a positive NPV_{rel} without the presence of a feed-in tariff. This analysis involved studying the NPV_{rel} results for each case, considering a 10% increase to 100%. Table 4.1 provides the particular units of TSGs and FPVs for each penetration of renewable energy generation.

Table 4.1 Specific number of FPV and TSG systems at different renewable energy penetration rates for the selected case [Publication II].

G_{RE} penetration [%]	Number of FPVs	Number of TSGs
0	0	0
10	506	0
20	467	1
30	428	2
40	934	2
50	1440	2
60	1945	2
70	2451	2
80	2956	2
90	3462	2
100	3967	2

The yearly electricity cost and its reduction portion under PDM Controls 1 and 2 are presented in Table 4.2 and Table 4.3, respectively. Additionally, the NPV_{rel} curves under the two controls can be observed in Fig. 4.10. These figures illustrate the changes in NPV_{rel} as battery capacity increases, providing a visual representation of the economic performance trends under the two different PDM control strategies. Across all cases under PDM Control 1, the yearly electricity charge became less initially, then became greater as the battery capacity grew, while the reduction ratio exhibited an increasing and then decreasing trend. The case in C1 to acquire the minimum electricity tariff and maximum reduction ratio was at 800 kWh, resulting in a tariff of 3.139×10^5 HKD and a 59% reduction. The remaining cases accomplished similar outcomes with an 1800 kWh battery. The NPV_{rel} trend with an increase and subsequent decrease as the battery capacity increased, and the largest value occurred at 50 kWh. The maximum NPV_{rel} achieved was 30.426×10^6 HKD with a capacity of 50-kWh in C1.

The yearly electricity cost and its reduction portion of PDM control 2 exhibited a similar pattern. As the battery capacity increased, the annual tariff initially dropped and then rose. The data points with different trends forward and backwards on the curves of C5, C1 and C2 occurred at 1800 kWh. In C3, this data point materialised at 1600 kWh, while in C6 and C4, the turning points were observed at 2000 kWh. The minimum yearly tariff in C1 amounted to 2.161×10^5 HKD, accompanied by 71.8% depletion. These values represented the lowest annual electricity expenditure and the highest reduction portion among all cases. PDM Control 2 realised the economic enhancement by reducing operational costs and increasing NPV_{rel} with a larger capacity, as compared to PDM Control 1. This observation is evident when comparing the

two plots, where the latter parts of the curves for Cases C1, C2, and C3 in Fig. 4.10 (b) are higher than those in Fig. 4.10 (a) for larger battery capacities. The general trend of the NPV_{rel} curve remained consistent for both control methods. The curves for the first three cases exhibited descents and subsequent ascents ranging from 200 to 1400 kWh. However, as the battery capacity exceeded 1400 kWh, the curves dropped again in all three cases. Furthermore, the largest values of NPV_{rel} all arose at 50 kWh, with 30.4 million HKD.

Table 4.2 Results and variations of operational tariffs for six PDM cases based on PDM Control 1 [Publication II].

Battery capacity	**Yearly electricity cost** [$\times 10^5$ HKD]						**Yearly electricity cost reduction** [%]					
[kWh]	C1	C2	C3	C4	C5	C6	C1	C2	C3	C4	C5	C6
0	3.705	5.229	5.286	6.202	6.580	6.999	51.554	31.622	30.876	18.897	13.955	8.484
50	3.439	4.954	5.014	5.923	6.299	6.714	55.029	35.215	34.440	22.545	17.630	12.201
100	3.403	4.916	4.975	5.883	6.258	6.673	55.496	35.721	34.945	23.074	18.165	12.748
150	3.370	4.879	4.938	5.844	6.219	6.633	55.929	36.197	35.428	23.581	18.674	13.271
200	3.339	4.844	4.902	5.806	6.181	6.593	56.339	36.660	35.895	24.079	19.178	13.792
400	3.234	4.715	4.775	5.663	6.034	6.438	57.711	38.348	37.556	25.945	21.105	15.821
600	3.165	4.606	4.672	5.534	5.896	6.287	58.620	39.773	38.904	27.640	22.899	17.791
800	3.139	4.523	4.595	5.419	5.769	6.141	58.953	40.862	39.914	29.145	24.562	19.698
1000	3.168	4.471	4.541	5.316	5.656	6.002	58.577	41.540	40.620	30.489	26.043	21.519
1200	3.249	4.452	4.519	5.233	5.556	5.872	57.512	41.782	40.913	31.567	27.343	23.216
1400	3.361	4.446	4.498	5.146	5.447	5.730	56.052	41.859	41.183	32.709	28.774	25.073
1600	3.389	4.393	4.448	5.045	5.323	5.584	55.691	42.552	41.837	34.026	30.398	26.987
1800	3.364	4.316	4.381	4.942	5.208	5.451	56.016	43.561	42.714	35.375	31.903	28.722
2000	3.528	4.370	4.509	4.974	5.296	5.458	53.869	42.855	41.037	34.959	30.747	28.626

Table 4.3 Results and variations of operational tariffs for six PDM cases based on PDM Control 2 [Publication II].

Battery capacity	**Yearly electricity cost** [$\times 10^5$ HKD]						**Yearly electricity cost reduction** [%]					
[kWh]	C1	C2	C3	C4	C5	C6	C1	C2	C3	C4	C5	C6
0	3.705	5.229	5.286	6.202	6.580	6.999	51.554	31.622	30.876	18.897	13.955	8.484
50	3.479	4.994	5.050	5.959	6.330	6.745	54.506	34.692	33.969	22.074	17.231	11.802
100	3.449	4.961	5.021	5.929	6.304	6.719	54.900	35.124	34.351	22.477	17.564	12.146
150	3.427	4.936	4.993	5.900	6.276	6.689	55.189	35.458	34.706	22.853	17.939	12.536
200	3.410	4.915	4.970	5.875	6.250	6.662	55.414	35.733	35.006	23.182	18.280	12.889
400	3.350	4.843	4.909	5.803	6.169	6.578	56.191	36.672	35.803	24.123	19.332	13.981
600	3.227	4.727	4.809	5.700	6.064	6.474	57.807	38.193	37.123	25.461	20.707	15.349
800	3.040	4.570	4.658	5.566	5.938	6.354	60.253	40.242	39.092	27.218	22.355	16.914
1000	2.802	4.389	4.518	5.460	5.786	6.218	63.363	42.605	40.921	28.605	24.339	18.688
1200	2.511	4.189	4.338	5.326	5.640	6.102	67.161	45.224	43.278	30.355	26.245	20.212
1400	2.174	3.972	4.124	5.174	5.450	5.953	71.576	48.065	46.076	32.348	28.738	22.154
1600	2.161	3.913	4.121	5.133	5.401	5.889	71.748	48.838	46.111	32.881	29.382	23.000
1800	2.209	3.907	4.142	5.116	5.381	5.847	71.117	48.912	45.838	33.107	29.643	23.548
2000	2.281	3.932	4.156	5.094	5.396	5.843	70.171	48.588	45.660	33.394	29.447	23.594

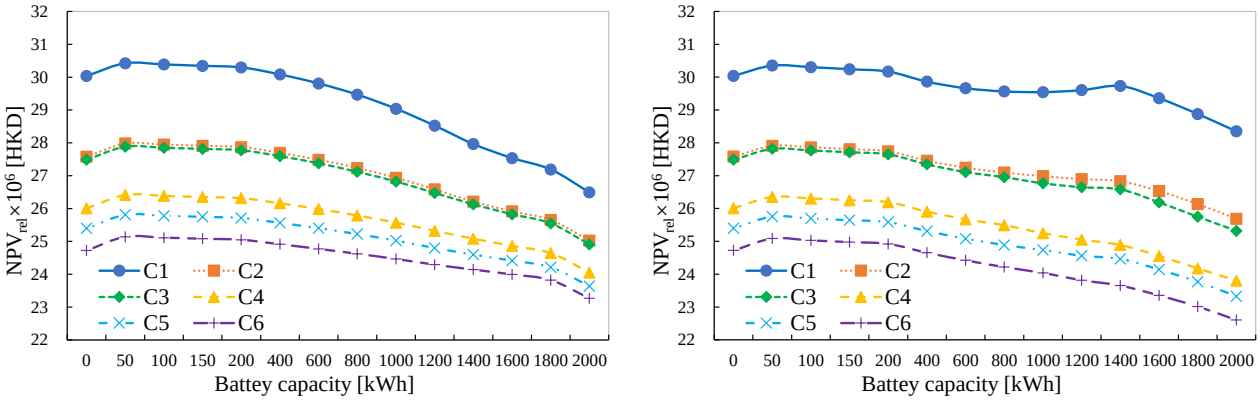

Fig. 4.10 Variation curves of economic parameter NPV_{rel} based on (a) PDM control 1 and (b) PDM control 2 at different battery capacities [Publication II].

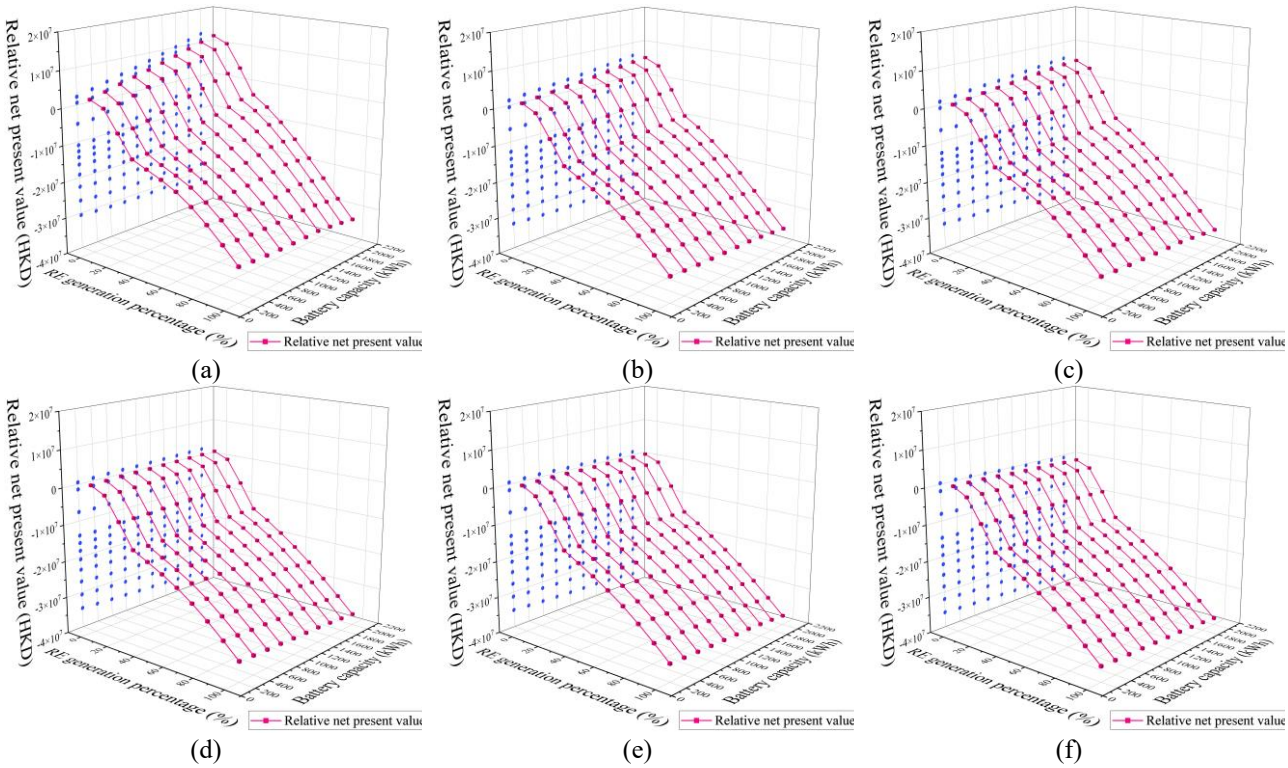

Fig. 4.11 Economic performance of (a) C1, (b) C2, (c) C3, (d) C4, (e) C5, and (f) C6 for different renewable energy penetration rates and different battery capacities [Publication II].

This scenario was examined across all the cases to determine the renewable penetration to accomplish a neutral NPV_{rel} value without a feed-in tariff. Fig. 4.11 illustrates the NPV_{rel} plots settled on the different renewable penetrations and the variations in battery capacity. While specific NPV_{rel} values differed, comparable findings and conclusions were derived compared to the first scenario. The maximum proportion of neutral NPV_{rel} values was greater than 20% and less than 30%. It was observed in C1 with a battery exceeding 1400 kWh. In Cases C2 and C3, when the battery was below 600 kWh, the renewable energy penetration of neutralised NPV_{rel} ranged from 0% to 10%. However, as the battery capacity increased, this range expanded to more than 10%. Neutralised NPV_{rel} values fell within the 0% to 10% range of renewable energy

generation for most battery capacities in C5 and C4. C6, with the smallest PDM incentive, was unable to accomplish a positive NPV_{rel} even without the ocean energy system when the capacity exceeded 1000 kWh due to the high costs associated with battery investments. Consequently, it can be concluded that under the existing utility and PDM model, the office building incorporating the TSG-FPV systems would face challenges in attaining a positive profit over a 20-year lifecycle without a feed-in tariff.

4.2.3 Investigation of Benchmark modifications and energy exporting tariff

Based on previous investigations into the integration of the PDM programme and energy flexibility to minimise electricity costs and gain incentives, it becomes evident that the absence of feed-in tariffs severely limits the penetration of renewable energy. Achieving a zero-energy building becomes economically unfeasible. To enhance economic performance further, two potential strategies for policy or business model modifications are proposed based on the PDM programme and energy flexibility control.

The first strategy involves refining the PDM benchmark for demand reduction calculation. In the original scheme, the customer's electricity demand reduction was determined by the difference between the benchmark and the actual electricity demand during the event period. This benchmark serves as the normalised baseline. However, this setup presents certain issues. The original benchmark will be diminished and affected by both the renewable energy input and the battery-based flexibility control. These factors have implications on the general economic performance of the building, particularly in the absence of a feed-in tariff. To address these challenges and enhance the economic viability of renewable energy without feed-in tariffs, we propose a refinement to the original benchmark, introducing an updated benchmark called Benchmark 2. This updated benchmark is defined as the energy consumption of the office building during the event period without the support of renewable energy resources. For the investigation into benchmark modification, a 200-kWh battery was selected. Fig. 4.12 shows the NPV_{rel} results for this scenario. Significant improvements in NPV_{rel} were observed with the application of Benchmark 2, demonstrating the effectiveness. However, it should be noted that the NPV_{rel} values, which were originally negative, did not reach a neutral value despite the observed improvements.

All the NPV_{rel} curves exhibit noticeable changes in trend at 60% and 30% of penetration. C1 and C3 were adopted to explore the reason and decomposed NPV_{rel} into annual fees, annual income and initial investments as shown in Fig. 4.13. Both the initial capital and annual fee curves exhibited significant changes in trend at 30%, leading to the changes in the trend of NPV_{rel}. The key change between 10% and 30% was the number of TSGs, while the increase from 40% to 100% was solely in the FPV panel quantities. TSG system incurred overpriced capital and O&M costs, resulting in the twists and turns of the curves at 30%. Moreover, after reaching the 60% mark, the slope of the annual benefit curves decreased. This

signifies a slower rate of increase in benefit as the penetration exceeded 60%, leading to another turn at 60%.

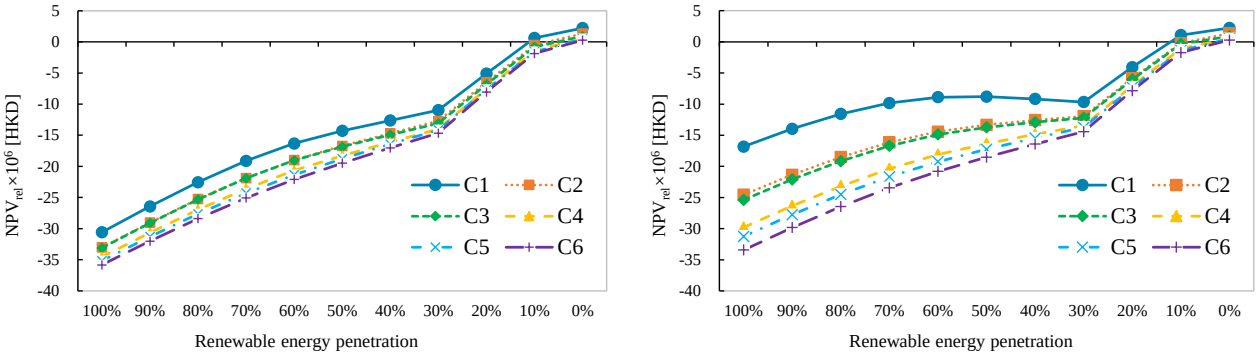

Fig. 4.12 NPV$_{rel}$ variation of all PDM cases with different renewable energy penetration under (a) Benchmark 1 and (b) Benchmark 2 [Publication II].

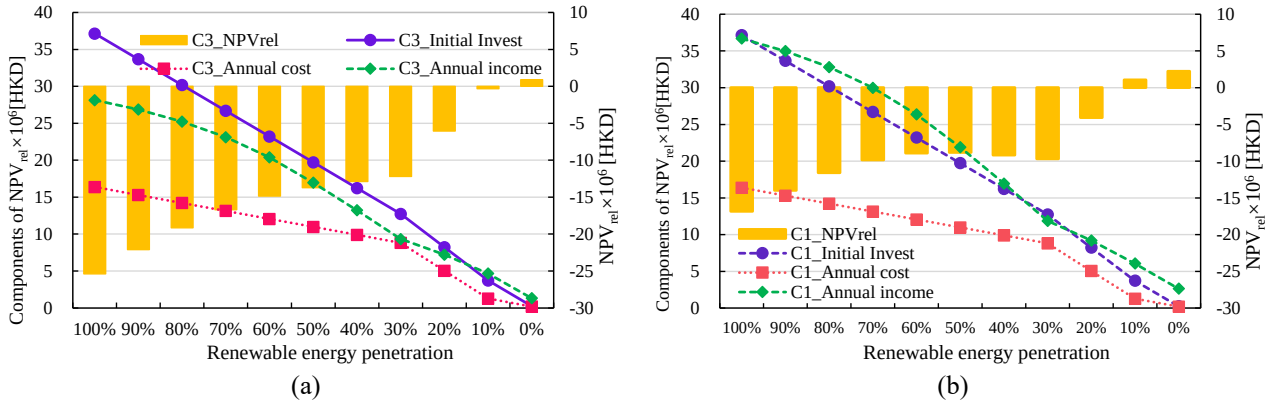

Fig. 4.13 Decomposition of NPV$_{rel}$ for (a) C3 and (b) C1 [Publication II].

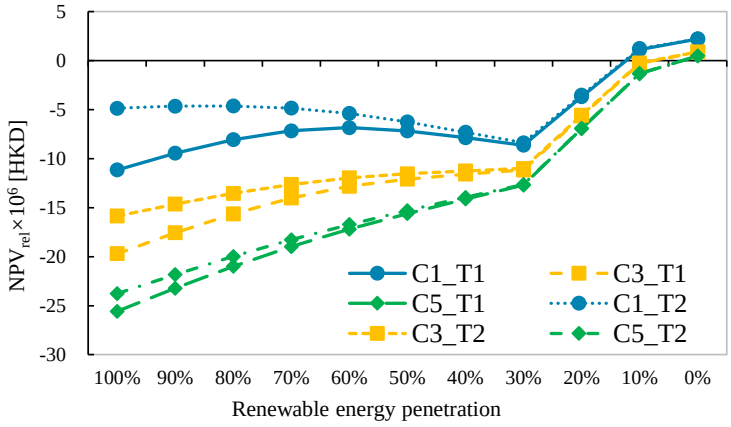

Fig. 4.14 Economic performance of grid exporting tariffs for selected PDM cases [Publication II].

Benchmark 2 can be observed that yielded a further economic improvement compared to Benchmark 1. However, it fell short of achieving a neutral NPV$_{rel}$ value. To address the issue of no earnings from exporting energy to the grid in the absence of a feed-in tariff, two grid exporting tariffs were proposed aimed at enhancing the benefits of energy exporting. The first tariff scheme, named T1, adopts settings derived from the existing electricity tariff model. The electricity export

price during peak periods in T1 is set at 0.737 HKD per kWh, while during off-peak periods, it is 0.676 HKD per kWh. The grid exporting tariff also takes into account the electricity price escalation ratio on an annual basis over the lifetime. The second grid exporting tariff examined the influence of PDM, designated as T2. The exporting price during the PDM event period is set at a fixed rate, which is equal to the minimum PDM incentive. In the non-event period, the cost remains the same as that of T1. Importantly, this incremental exporting cost during the PDM event period will not be affected by the price escalation ratio. For the investigation, we selected C5, C3, and C1, where the modified benchmark was applied and the NPV_{rel} results are presented in Fig. 4.14. These findings indicate that the inclusion of grid exporting tariffs T1 and T2 leads to a remarkable economic improvement. Particularly, when the penetration surpasses 30%, the NPV_{rel} value with T2 is greater than with T1, and the difference is influenced by the PDM event frequency. Meanwhile, as the renewable energy penetration decreases, the difference in NPV_{rel} between a case with T2 and the same case with T1 becomes progressively smaller, and there is almost no difference in the economic results between the two when the renewable energy penetration is reduced to 30% or less. When renewable energy penetration is greater than 50%, C1 with T2 applied achieves the maximum NPV_{rel} at 80% penetration in both scenarios, -4.63 and -4.62 million HKD, respectively. However, despite the considerable increase in NPV_{rel} compared to cases without benefit from energy exporting, neutral NPV_{rel} values remain challenging to achieve, particularly in the penetration up to 20%. As the renewable penetration increases, notwithstanding that the NPV_{rel} significantly improves, reaching a neutral value remains difficult.

4.3 Co-ordinations of ocean energy supported energy sharing between zero-emission cross-harbour buildings

4.3.1 Non-dominated solutions of individual zero-emission harbour buildings

In the scenario denoted as S1, we initially focused on a pair of freestanding zero-emission systems for the port building. In these systems, undersea power cables maintained the upper limit volume, connecting the offshore locations and managing mechanisms discussed earlier were employed. Following the simulation, we compiled the emission and matching results of all suggested combinations in this scenario, as presented in Fig. 4.15. Additionally, the calculation of relative net present value considering the inexpensive cost for the nearshore land, which is equal to the offshore sea fee and ANLC, was included, which is illustrated in Fig. 4.16.

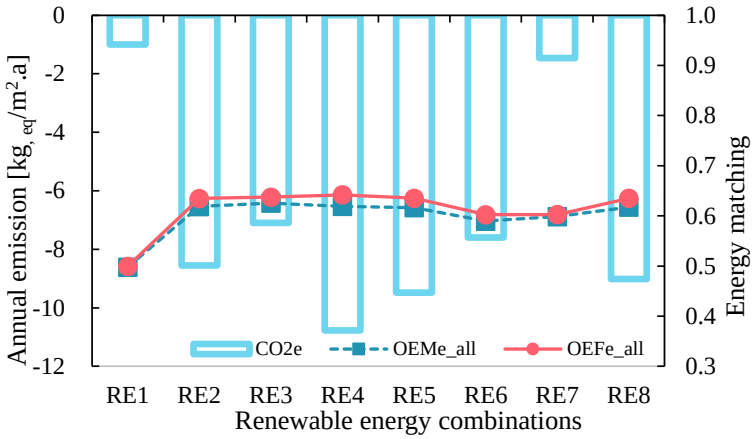

Fig. 4.15 Environmental and energy matching performance of representative cases.

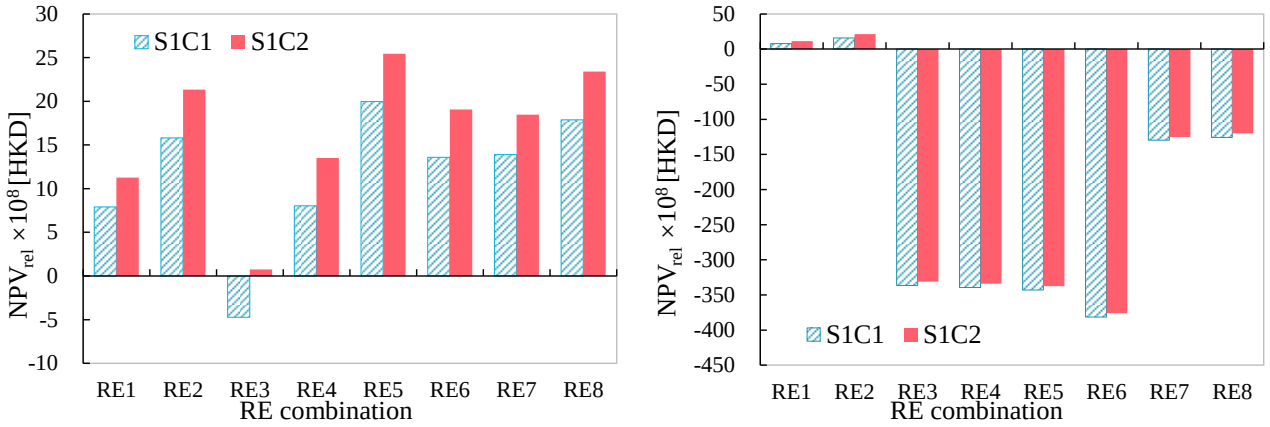

Fig. 4.16 NPV_{rel} results based on two control strategies calculated under (a) the sea cost and (b) ANLC [Publication III].

Comparing the results, all combinations under S1C2 control evinced considerably preferable relative net present values compared to those under S1C1 control can be observed. Except for RE1, which showed a modest increase of 3.365×10^8 HKD for relative net present value, the remaining renewable energy combinations had increases exceeding 450 million HKD. RE1, where the Macau side solely relied on an FPV system situated offshore, displayed poorer economic outcomes compared to RE2, where both the Hong Kong and Macau systems utilised wind turbines established offshore exclusively. Furthermore, the FPV system installed in the offshore points occupied a more sizeable sea area in RE2, resulting in higher sea use costs in terms of investment, which contributed to its inferior economic performance. In terms of combinations with the inexpensive fee, same to the offshore cost of sea use, RE3 exhibited the bottom relative net present value, with -4.723×10^8 HKD under S1C1. The ocean energy system included in this combination was situated nearshore and included ample tidal stream generators. Similarly, although RE4 exhibited a positive outcome, it was in sixth place among all investigated compositions, owing to more than a hundred TSGs. The relatively low annual electricity generation of the TSG system, attributed to substandard tidal stream speed at the chosen locations, necessitated a larger number of units and a higher total capacity compared to the FPV and wind turbine systems. Moreover, the costly investment of the TSG system

contributed to its poorer economic performance compared to other combinations. RE5 demonstrated the finest relative net present value of 1.997×10^9 HKD under S1C1 and 2.546×10^9 HKD under S1C2. The portfolio composed only of wind turbines exhibited the most favourable economic results due to competitive capital and operational costs compared to FPV and TSG systems. Generally, combinations made up of more nearshore systems combined with similar systems yielded better economic performance, as systems located offshore entail dearer capital costs for construction. Upon incorporating the ANLC, except for RE1 and RE2 with the offshore-only system, the relative net present values of portfolios that possess the system established close to shore were negative entirely. This suggests that combinations involving the nearshore renewable energy system are economically uncompetitive based on actual land prices in Hong Kong and Macau. Furthermore, the annual carbon emissions for all portfolios were negative, designating that the intention of zero-emission has been reached.

Meanwhile, the effect of reducing land prices on the economic viability of renewable energy cases involving the system located nearshore was investigated. To quantify this impact, different percentage of MNLC was introduced to examine the level of reduction in real nearshore land prices that would have a chance of making the system under study economically viable. The calculation of relative net present values across a range of top-selling price percentages was investigated, spanning from 1% to 9%. Notably, combinations with the nearshore system achieved neutral or positive NPV_{rel} values within this percentage range. To provide a visual representation of these findings, Fig. 4.17 presents the results for six specific combinations from RE3 to RE8 with nearshore systems, each corresponding to a top-selling price percentage of 0% to 9%.

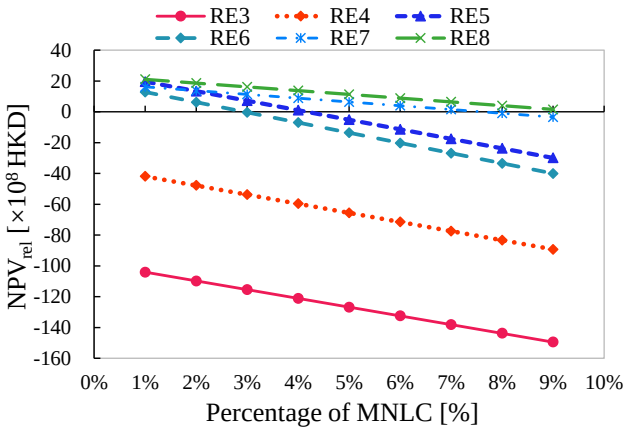

Fig. 4.17 Variations in NPV_{rel} in selected cases based on different MNLC percentages [Publication III].

Distinct patterns for specific combinations were observed. In the case of RE4 and RE3, even if the top selling price was reduced to 1%, every single relative net present value remained negative. Remarkably, the relative net present values for

these cases were consistently lower compared to the other investigated combinations when different highest price percentages were considered. This disparity can be attributed to the composition of these combinations situated in the nearshore of Hong Kong, which included a larger number of TSGs, 300 for RE3 and 150 for RE4 accompanying several wind turbines. Consequently, the larger sea area required for these combinations resulted in higher MNLC calculations, contributing to their inferior economic performance. Positive results were obtained only when the land price was equal to or below 2% of the top-selling price but turned negative at 3% and above in cases of RE6. Similarly, the NPV_{rel} of RE5 transitioned to negative as the fee increased from 4% to 5% of the top-selling price. The relative net present values of RE7 became negative when the nearshore sea fee increased to 8% of MNLC. Lastly, negative results were observed only when the sea cost was reduced to 9% in RE8, while smaller costs for nearshore sea usage resulted in positive economic performance. It is important to note that cases of the last two combinations require a smaller nearshore sea usage for economic calculations compared to the all-nearshore systems. Consequently, the economic performance curves for RE7 and RE8 were higher, and the slopes were flatter. This indicates that the impact of different maximum price percentages on RE7 and RE8 was less significant than the other combinations.

The variation of relative net present value and energy usage as the techno-economic performance of the cross-harbour system is incorporated with the reducing capacity of submarine cable from the maximum submarine cable capacity. The submarine cables will be reduced from 100% of the upper limit capacity continuously to 10%, with a 10% reduction in each case. This discussion is based on the fact that submarine cables also have high investment costs, and that the energy generation is erratic, which may bring the challenge that the volume of undersea cables is not being fully utilised most of the time and is a waste of resources and costs. The hybrid system comprises two distinct systems without any intermediate submarine cables. Two conditions for adjusting the maximum volume portion in the two separate systems were considered. The first condition involved a simultaneous reduction of the maximum capacity portion in both regions, while the second condition maintained the upper limit of capacity on one side and reduced it on the other. To illustrate the effects under the S1C2 control method illustrated in Fig. 4.18, RE2 and RE1 containing the ocean energy system totally located offshore were selected. These combinations demonstrated an improved economic performance.

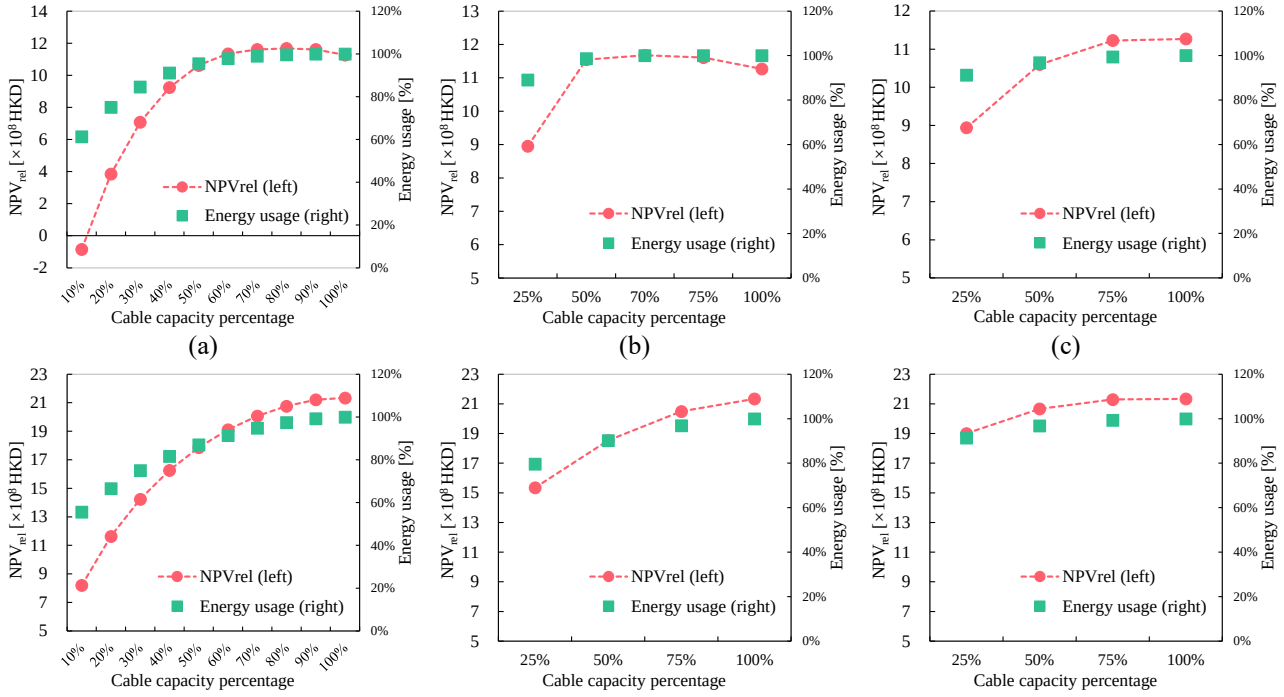

Fig. 4.18 Energy usage and NPV_{rel} results within RE1 (a) when submarine cable capacities in both regions vary, (b) in MO region vary, (c) in HK region vary, in RE2 (d) when submarine cable capacities in both regions vary, (e) in MO region vary and (f) in HK region vary [Publication III].

A comprehensive overview of the results was obtained by simultaneously adjusting the capacity for power cables under the sea on both sides. As the cable capacity increased, the portion of energy usage in RE1 improved from 61% to 100%. The relative net present value initially enlarged from -8.51×10^{7} to 11.675×10^{8} and then decreased to 11.267×10^{8} HKD. At 80% cable capacity, the optimal case achieved an economic result of 11.675×10^{8} HKD and 0.37% of dumped energy. Similarly, increasing the cable volume resulted in reducing dumped energy, from 44.4% to no dumped energy. The relative net present value also increased from 8.197×10^{8} to 2.133×10^{9} HKD. At 100% cable capacity, the most desirable case achieved an economic outcome of 2.133×10^{9} HKD and no dumped energy. When solely modifying the volume of Hong Kong undersea cable, cases exhibited optimal NPV_{rel} at the upper limit of cable. The corresponding fraction of energy usage reached 1, indicating that dumped energy is zero. On the other hand, when adjusting Macau cables capacity on the bottom of the sea, RE1 achieved the 11.68×10^{8} HKD of NPV_{rel} at 70% of the upper limit, which represented the optimal performance for all cases. Simultaneously, the energy usage ratio reached 1. For RE2, maintaining full cable capacity in two regions ensured the best technical and economic performance. Meanwhile, the best economic performance without any dumped energy can only be maintained in RE1 as the capacity was reduced by up to 70%. Therefore, the optimal economic and energy usage outcomes were realised by keeping the full upper limit undersea power cables in the Hong Kong subsystem and reducing the Macau cable volume to 70% of the upper limit. On the other hand, the best performance of RE2 was attained by maintaining full submarine cable volume on both objective systems. This distinction arises from the larger aggregate capacity of the FPV system compared to the wind turbine system despite the greater fluctuations in

energy generation from the FPV system. In contrast, the energy generated by the wind turbine system exhibited greater stability and closely approached the aggregate capacity of the system. Consequently, the FPV systems often operated at lower levels of energy generation, leaving spare unused space in the submarine cables. The submarine cables associated with the wind turbine systems frequently operated at or near maximum load conditions.

In situations where the submarine cable capacity falls below its maximum, there is a risk that the generation at a single time step will surpass the volume of the submarine cable, resulting in dumped energy. To address this issue, the practicability of incorporating batteries to store the energy at the offshore platform, thereby replacing a section of the cables under the ocean, was investigated. Building upon the existing findings, three specific percentages were selected for analysis: 30%, 40%, and 50%. It was determined that the battery capacity range should be between 1×10^4 kWh and 10×10^4 kWh. Taking this into account, the techno-economic performance results are presented in Fig. 4.19. Additionally, Fig. 4.19 also includes the optimal cases, where only cables under the seawater were utilised unaccompanied by the inclusion of batteries.

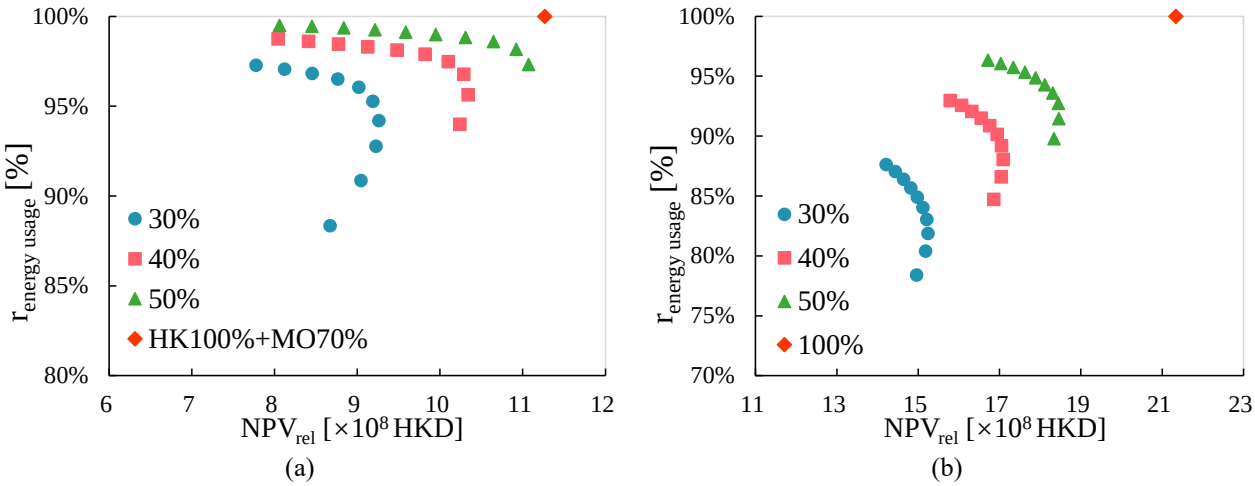

Fig. 4.19 Energy usage and relative net present values in (a) RE1 and (b) RE2 based on different submarine cable capacities and batteries installed offshore as well as best case [Publication III].

The results of the analysis indicate that when the power cable remains persistent, the amount of dumped energy continues to drop as the battery capacity increases. However, the NPV_{rel} exhibits an initial increase followed by a decrease for the RE1 combination when the submarine cable capacity is set at 30% of the maximum value, increasing the battery capacity, which results in 2.72% of dumped energy. NPV_{rel} initially rises from 8.651×10^8 to 9.241×10^8 HKD and afterwards decreases to 7.755×10^8 HKD. Similarly, at 40% of capacity, the $r_{energy\ usage}$ increases from 94% to 98.8%, while the economic result increases from 10.219×10^8 to 10.318×10^8 HKD and next decreases to 8.022×10^8 HKD. At a submarine cable capacity of 50% of the maximum, the $r_{energy\ usage}$ increases from 97% to 99.5%, while economic output decreases

from 11.051×10^8 to 8.039×10^8 HKD. For the RE2 combination, at a submarine cable capacity of 30% of the maximum, the energy usage increases from 78% to 87.6%, while the NPV_{rel} initially rises to 15.210×10^8 HKD and decreases to 14.179×10^8 HKD. At a submarine cable capacity of 40% of the maximum, the $r_{energy\ usage}$ increases from 86% to 93%, while economic outcome initially increases from 16.829×10^8 to 17.058×10^8 HKD and afterwards decreases to 15.757×10^8 HKD. At a submarine cable capacity of 50% of the maximum, the energy usage proportion increases by 96%, while the relative net present value increases to 18.426×10^8 HKD and decreases to 16.683×10^8 HKD with the largest battery in this investigation.

NPV_{rel} shows a distinct peak with the greatest value, and the dumped energy will be diminished as the battery placed offshore is enlarged. Moreover, as the submarine cable capacity increases, the cases tend to move towards the upper right-hand corner of the diagram, representing the best case for the two combinations. For the RE1 combination, the case without batteries, utilising 70% of Macau undersea cable and the uttermost capacity of Hong Kong power cable, demonstrates the best technical and economic performance. Similarly, for the RE2 combination, the optimal case also excludes the battery and utilises full cable capacity on both systems. The inclusion of offshore batteries results in excessive capacity requirements and high investment costs, which weaken economic performance. Given the factors of capital costs and essential requirements, submarine power cables emerge as a more advantageous solution when weighed against batteries.

4.3.2 Non-dominated solutions of coordinated zero-emission harbour buildings in Hong Kong and Macau

The outcomes of the developed control strategies utilizing the source-based feed-in tariff are analysed and demonstrated in Fig. 4.20.

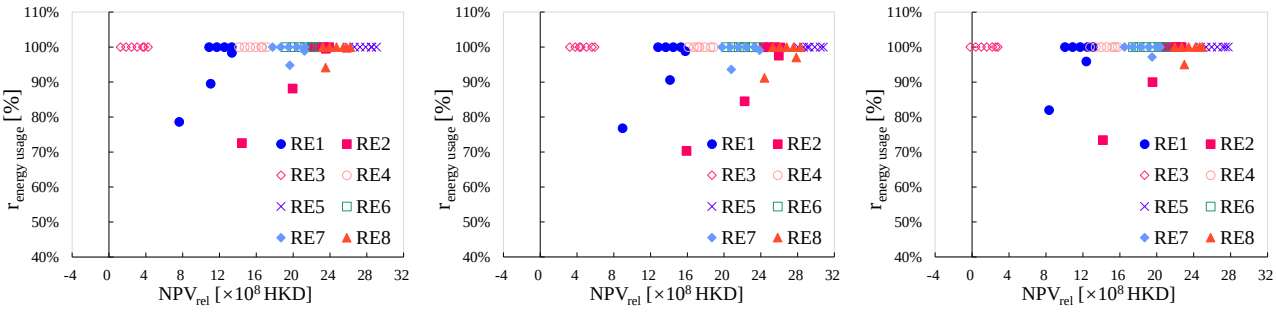

(a) (b) (c)

Fig. 4.20 Techno-economic results based on (a) S2Csb1, (b) S2Csb2, and (c) S2Csb3 for all renewable energy combinations after applying source-based FiT [Publication III].

Among the renewable energy combinations, the slightest energy usage proportions were observed in cases with 5% capacity for RE2, which are 72.56%, 70.33%, and 73.43% corresponding to three control strategies respectively, RE1

(78.63%, 76.84%, and 81.99%), RE7 (94.78%, 93.62%, and 97.13%), and RE8 (94.14%, 91.21%, and 95.01%). The energy usage continuously increased until reaching 100% as the volume of undersea power cables got larger. Overall, S2Csb3 could reach a minimum dumped energy compared to the other two control approaches. The minimum relative net present values were observed in RE1 with 5% cable volume, which is 7.62×10^8, 8.95×10^8, and 8.33×10^8 HKD from the mentioned three control methods. RE3, with the largest quantities of TSGs, exhibited the poorest economic outcomes. Contrariwise, RE5 showed the leading performance. The premier economic outcomes for RE8 and RE1 occurred at 20% submarine cable capacity and appeared at 30% in RE2. The combinations supported by the ocean energy system located nearshore reached their foremost relative net present values at 10% submarine cable capacity. The maximum NPV_{rel} had been realised in RE7 at 20% submarine cable capacity with the application of S2Csb1, and the leading economic outcome was at 10% with the application of S2Csb2 and S2Csb3. The control approach aiming to interchange as much renewable energy as possible between the two regions, S2Csb2, showed the finest economic performance.

The data of cases with the applied ANLC and S2Csb2 are presented in Fig. 4.21. The combinations from RE3 to RE8 which utilize the nearshore ocean energy resource were picked to assess the different MNLC fraction to attain an economic outcome close to zero and are displayed in Fig. 4.22.

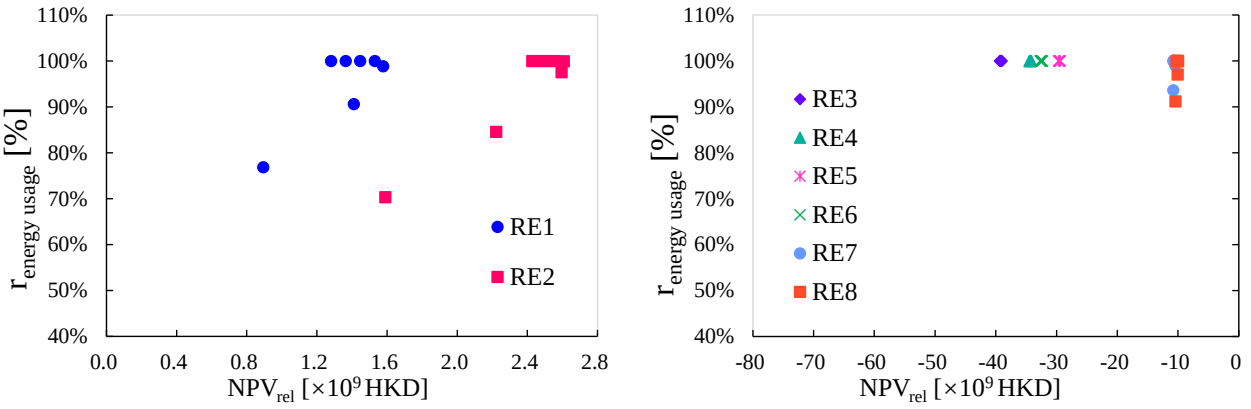

Fig. 4.21 Techno-economic results for (a) RE1 and RE2 and (b) RE3 to RE8 after applying source-based FiT based on ANLC settings and S2Csb2 strategy [Publication III].

With the application of average selling price, the $r_{energy\ usage}$ of all cases involving configurations stayed equable. Similarly, the all-offshore system configurations, RE1 and RE2, which utilised offshore sea prices for calculating sea charges, were unaffected by the inclusion of average selling costs. NPV_{rel} for the configurations involving nearshore systems turned out to be negative. Among the combinations with the application of nearshore ocean energy resources, RE4 and RE3, which incorporated the TSG system, exhibited the poorest economic outcomes. Therefore, these configurations were positioned towards the left side of the diagram, indicating their unfavourable economic outcomes. On the other hand, RE7 and RE8,

which included only half of the system located nearshore and required fewer zones for calculating the fee of nearshore sea usage compared to other configurations only relying on the system nearshore, showcased relatively better performance. However, even these combinations failed to achieve positive NPV_{rel}. These findings underscore the weak economic viability of combinations involving the system situated nearshore when realistic prices of close shore sea usage were taken into account.

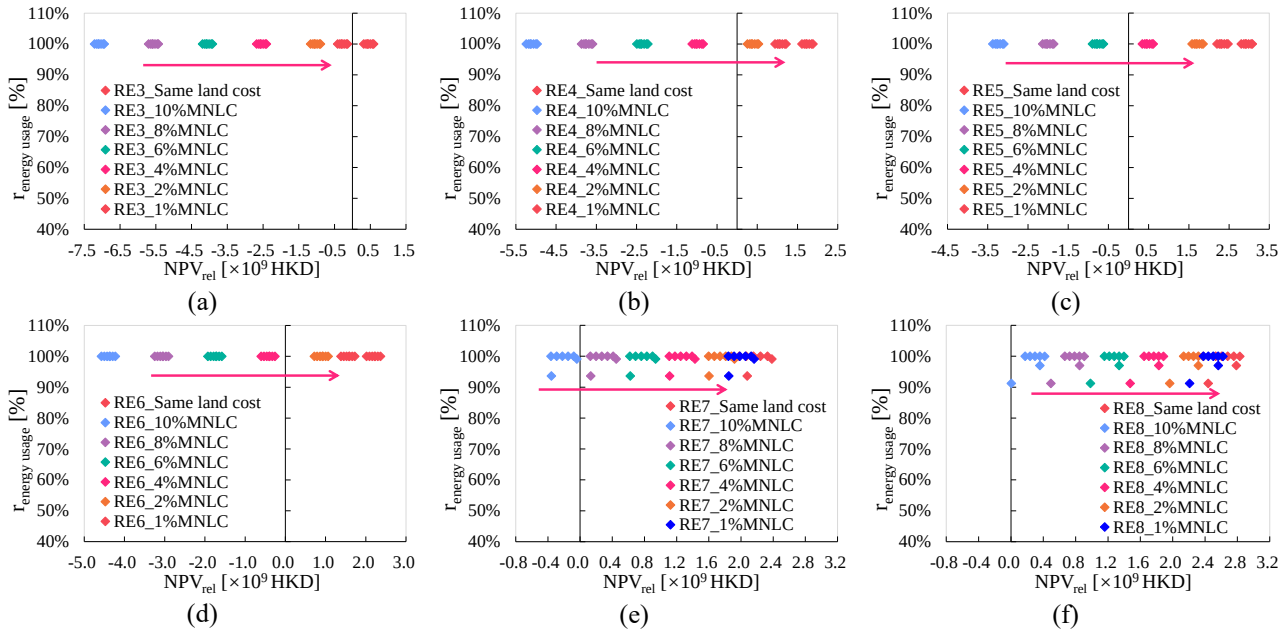

Fig. 4.22 Techno-economic results after applying source-based FiT based on sea cost and 1% to 10% of MNLC in (a) RE3, (b) RE4, (c) RE5, (d) RE6, (e) RE7 and (f) RE8 cases [Publication III].

When the top selling price in the actual existence of the land sale was applied in the economic calculation, the energy usage of all cases involving configurations stayed the same, and the distribution also remained consistent. Among the configurations with the system established nearshore, RE3 was unable to accomplish an economic result larger than zero even if 1% of the top-selling price was exerted. However, as the top-selling price ratio was reduced from 4% to 2%, RE6 and RE4 were able to attain a relative net present value that outweighed zero. This suggests that the top selling price proportion enabling these two configurations to perform an economic result more than zero lies between 2% and 4%. Similarly, as the percentage of top-selling prices decreased to 4%, a positive economic performance could be reached in RE5, indicating that RE5 was able to realise a neutral relative net present value range from 4% to 6% of the top-selling price. In addition, the share of top land sale prices that can be rendered to have an economic outcome greater than 0 in RE7 is greater than 8 % and less than 10 %. Even if the top selling price portion become 10%, they still exhibited positive economic performance. Throughout the variations in land cost, the distribution remained consistent. As the top selling price decreased to 1%, the relative net present values gradually improved, and the distribution shifted gradually to the right, converging with those having the inexpensive fee of offshore sea usage.

Furthermore, the boundary-based FiT and the three related control approaches introduced in the methodology section have also been applied for analysis, and the techno-economic results are shown in Fig. 4.23.

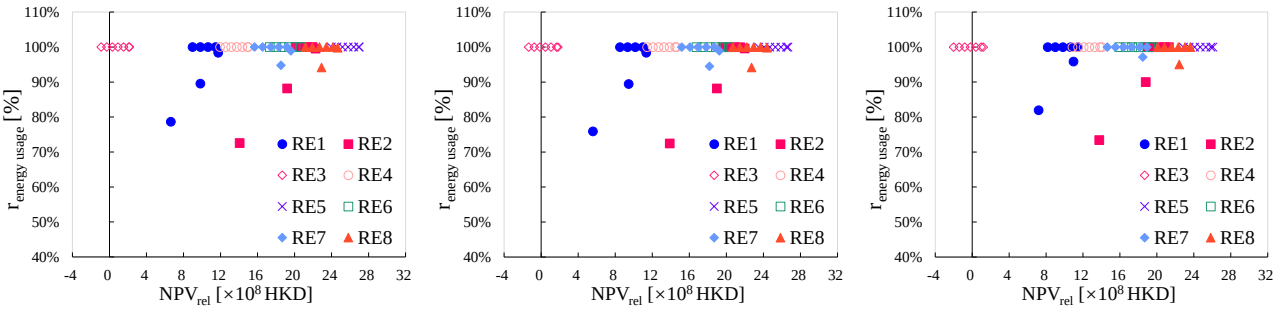

(a) (b) (c)

Fig. 4.23 Techno-economic results based on (a) S2Cbb1, (b) S2Cbb2, and (c) S2Cbb3 for all renewable energy combinations after applying boundary-based FiT [Publication III].

The study revealed that the boundary-based feed-in tariff enables cases to have identical distribution to the source-based feed-in tariff cases. Notably, the combinations RE3 to RE6 involving all-nearshore renewable energy consistently maintained a 100% energy usage ratio. Under these control strategies, the $r_{energy\ usage}$ with the S2Cbb3 control strategy closely matched that of S2Csb3, both could attain the minimum dumped energy. In S2Cbb3, 18.01% of dumped energy existed in RE1 with 5% of undersea power cable upper limit, 26.57% in RE2, 2.87% in RE7 and 5% in RE8. The configuration RE3 displayed the poorest relative net present value because of large quantities of TSGs. Several cases yielded negative NPV_{rel} results, occurring when the undersea cables were increased to 50%, 40%, and 30% of the volume upper limit in S2Cbb1, S2Cbb2, and S2Cbb3, respectively. The scenario with the application of S2Cbb3 and 60% of capacity upper limit had the lowest NPV_{rel} value at -2.016×10^8 HKD.

Enhancing the proportion of wind turbine systems led to enhanced economic viability. Notably, RE5, exclusively utilising nearshore wind turbine systems, emerged as the most economically efficient configuration. Within the range of RE3 to RE6, consisting solely of systems located nearshore, optimal economic results were accomplished at 5% of the maximum submarine cable capacity. However, RE6 under S2Cbb1 bucked this trend by showcasing superior economic outcomes at a 10% capacity upper limit. This trend suggests a gradual decline in economic efficiency as the capacity increases within these configurations. Conversely, other configurations displayed distinctive inflection points where economic performance peaked. For the RE1 and RE2 supported by the systems located offshore, this tipping point materialised at the 20% upper limit of the underwater cables volume. In contrast, for the half-offshore and half-nearshore system pairings of RE7 and RE8, this pivotal juncture occurred at 10% of the maximum submarine cable capacity. These changes in trend signify

critical thresholds where the economic efficiency of each configuration reaches its zenith before potentially diminishing returns set in as capacity increases beyond these thresholds. By comparing the three control strategies, it was found that S2Cbb1 yielded the leading economic outcomes.

After thoroughly discussing and analysing the economic and energy aspects, including energy coordination and sharing, we proceeded to select and compare the non-dominated solutions. Fig. 4.24 illustrates the results concerning economic performance. These findings provide valuable insights into the effectiveness and feasibility of the system under different scenarios.

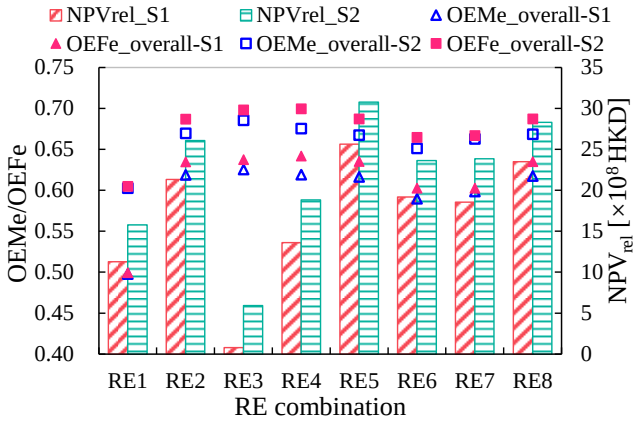

Fig. 4.24 Comparison of the results in scenarios with and without energy sharing [Publication III].

Upon comparing the leading outcomes of the two scenarios, it became evident that the scenario integrating the power cables under seawater connecting the entire cross-harbour locations to facilitate energy coordination exhibited remarkable improvements in the mentioned aspect contrasted to the first scenario, where shared energy could not be implemented. Specifically, the most substantial energy-matching magnification was discovered in RE1, with both indicators of S2 showing a 21% improvement compared to S1. Similarly, RE7 and RE6 witnessed a 0.06 increase, translating to percentage increases of 8% and 11%, respectively. The criteria for remaining configurations increased from 8% to 10%. Meanwhile, the inclusion of energy collaboration and sharing resulted in relative net present value increases exceeding 4×10^8 HKD for each combination. The minor enlargement proportion of 20% became visible in RE8 and RE5. 4.4×10^8 HKD was the minor enlargement of results in RE6, and 5.3×10^8 HKD was the greatest expansion displayed in RE7. These discoveries clearly revealed the viable leveraging sharing renewable energy to enhance the performance of extensive zero-energy buildings. The results highlight the potential benefits and viability of incorporating energy coordination and collaboration strategies in such projects.

4.4 Enhanced energy sharing and management between cross-harbour zero-emission buildings based on a combination of electric ferries and deck-on electric vehicles

4.4.1 Scenario without energy sharing V2B function

Scenario 1 exclusively involves the B2V function, with no presence of the V2B function. In this scenario, both the car carrying ferry and EVs are solely charged within the ferry terminal building, and there is no discharge capability. To facilitate the charging process, three charging measures have been devised. Referred to as S1CS1, this method entails charging the ferry and EVs within the ferry terminal building, irrespective of whether the energy source is renewable or grid power. If the fractional state of charge of the batteries remains below the upper limit of 0.95, the charging process will proceed and continue until reaching the upper limit. To evaluate the performance of this charging method, we have considered energy-matching, economic factors, emissions, and energy usage. The specific results are presented in Table 4.4 and Fig. 4.25, shedding light on the outcomes and implications of this approach.

Table 4.4 Energy matching, operational tariff, relative net present values, energy usage and emission results of the S1CS1 cases [Publication IV].

	WMI	**Operational tariff**	**NPV_{rel}**	**Energy usage ratio**	**CE_a**
		[$\times 10^7$ HKD]	[$\times 10^8$ HKD]	%	kg/m^2. a
20% of submarine cable capacity upper limit					
RE1	0.55	4.56	17.36	99%	-21.31
RE2	0.59	4.15	27.61	98%	-15.55
RE3	0.60	4.16	29.86	100%	-14.86
RE4	0.58	4.16	32.13	100%	-26.31
RE5	0.49	4.95	24.06	100%	-8.78
RE6	0.59	4.18	25.38	100%	-17.68
RE7	0.59	4.15	30.05	100%	-24.47
30% of submarine cable capacity upper limit					
RE1	0.56	4.56	16.81	100%	-24.80
RE2	0.59	4.15	27.74	100%	-24.24
RE3	0.60	4.16	29.28	100%	-15.79
RE4	0.58	4.16	31.51	100%	-26.31
RE5	0.49	4.95	23.35	100%	-8.78
RE6	0.59	4.18	24.65	100%	-17.68
RE7	0.59	4.15	29.29	100%	-24.53
40% of submarine cable capacity upper limit					
RE1	0.56	4.56	15.96	100%	-24.80
RE2	0.59	4.15	27.13	100%	-24.31
RE3	0.60	4.16	28.70	100%	-15.79
RE4	0.58	4.16	30.90	100%	-26.31
RE5	0.49	4.95	22.64	100%	-8.78
RE6	0.59	4.18	23.92	100%	-17.68
RE7	0.59	4.15	28.52	100%	-24.53

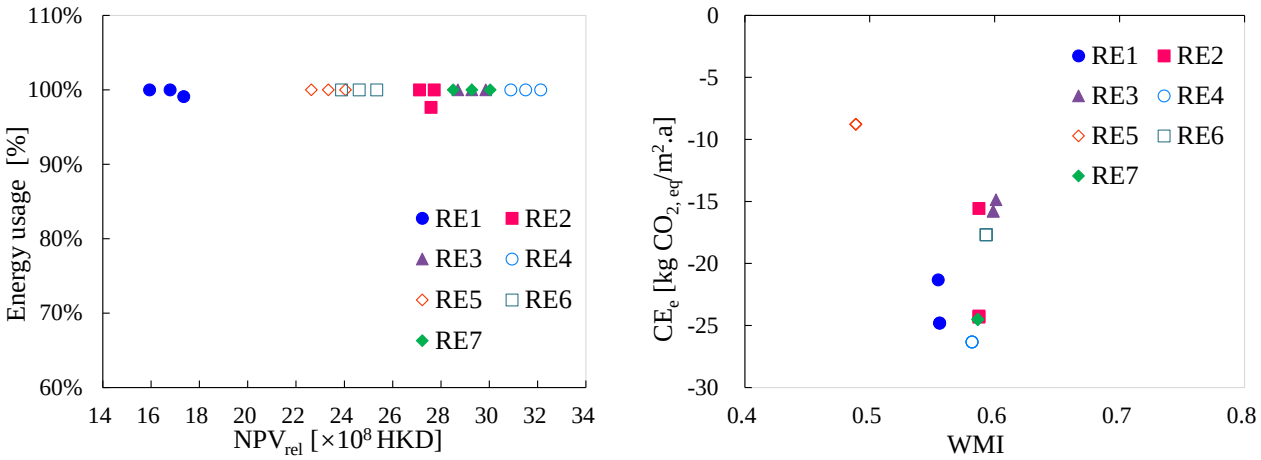

(a) (b)

Fig. 4.25 Energy usage and relative net present values of selected combinations [Publication IV].

The analysis of the results reveals that the energy usage ratio for RE1 and RE2 is less than 100% only when the submarine cable operates at 20% of its maximum cable capacity. Specifically, the energy usage ratios for RE1 and RE2 were 99% and 98%, respectively. In this scenario, all other combinations achieved an energy usage ratio of 100%. When the submarine cable capacity increased from 20% to 40%, the highest NPV_{rel} was observed at 30% of the maximum cable capacity, but only for RE2, reaching a value of 2.77×10^9 HKD. For the remaining combinations, the optimal economic performance occurred at 20% of the maximum cable capacity. Among all the combinations, RE4 exhibited the highest NPV_{rel} at 3.21×10^9 HKD, while RE1 had the lowest NPV_{rel} at 1.73×10^9 HKD. Even though the economic performance of RE4 at 40% capacity limit was lower compared to the cases at 20% and 30% of the maximum cable capacity, it still outperformed all other combinations. Furthermore, RE4 demonstrated the lowest CO_2 emissions, indicating its superior environmental performance. It is important to note that RE4 comprised an all-nearshore combination with wind turbines in both Macau and Hong Kong, while RE1 was an all-offshore combination with wind turbines on the Hong Kong subsystem and FPV on the Macau subsystem. The investment cost of the wind turbine system was lower than that of the FPV system, and the offshore system incurred higher investment costs. These cost differences explain why RE4 achieved the highest economic performance while RE1 demonstrated the lowest economic performance.

Following the analysis of S1CS1, it became evident that constantly charging the batteries to the upper limit may not be the most optimal strategy. Subsequently, a second charging strategy was devised, incorporating varying FSOC levels. This strategy, known as S1CS2, aimed to set the target FSOC as the level that would fulfil the requirements of the subsequent trip, and if the current FSOC exceeded the level necessary for the next trip, no charging process would be conducted, and if the charging process is needed, the target is to charge to the FSOC level that can satisfy the next trip. This approach aimed to optimise the charging process by aligning it with the specific FSOC needs for each trip, thus enhancing overall

operational efficiency. For the car carrier ferry, the minimum FSOC that can fulfil the next trip was 0.6. Considering the lower limit FSOC of the battery was 0.2, the target FSOC of the ferry was 0.8. The 10 EVs have trips in both cities; the minimum FSOC that can satisfy the next trip was 0.14 on the Hong Kong side and 0.04 on the Macau side, including the lower limit FSOC. The target FSOC was 0.34 and 0.24, respectively. The results are shown in Table 4.5.

Table 4.5 Energy matching, operational tariff, relative net present values, energy usage and emission results of S1CS2 cases [Publication IV].

	WMI	**Operational tariff**	**NPV_{rel}**	**Energy usage ratio**	**CE_a**
		[$\times 10^7$ HKD]	[$\times 10^8$ HKD]	%	kg/m^2. a
20% of submarine cable capacity upper limit					
RE1	0.54	4.56	17.33	99%	-25.69
RE2	0.58	4.15	27.58	98%	-18.80
RE3	0.60	4.16	29.85	100%	-17.22
RE4	0.58	4.16	32.12	100%	-28.04
RE5	0.47	4.95	24.04	100%	-15.80
RE6	0.58	4.18	25.33	100%	-23.28
RE7	0.58	4.15	30.03	100%	-27.36
30% of submarine cable capacity upper limit					
RE1	0.55	4.56	16.78	100%	-29.20
RE2	0.58	4.15	27.71	100%	-27.67
RE3	0.59	4.16	29.27	100%	-18.21
RE4	0.58	4.16	31.50	100%	-28.64
RE5	0.47	4.95	23.34	100%	-15.80
RE6	0.58	4.18	24.60	100%	-23.28
RE7	0.58	4.15	29.27	100%	-27.93
40% of submarine cable capacity upper limit					
RE1	0.55	4.56	15.93	100%	-29.20
RE2	0.58	4.15	27.10	100%	-27.75
RE3	0.59	4.16	28.69	100%	-18.21
RE4	0.58	4.16	30.89	100%	-28.64
RE5	0.47	4.95	22.63	100%	-15.80
RE6	0.58	4.18	23.87	100%	-23.28
RE7	0.58	4.15	28.51	100%	-27.93

Upon analysing the results, it was observed that the energy usage outcomes for the second charging strategy mirrored those of the first strategy. Only RE1 and RE2 exhibited energy usage ratios below 100% when the submarine cable operated at 20% of its capacity limit, with values of 99% and 98%, respectively. However, when compared to the first charging strategy, the restriction of the target FSOC to the level required for the next trip did not have a significant impact on the annual operational tariff and NPV_{rel}. Across all scenarios, the annual operational tariff and NPV_{rel} values remained comparable to those obtained under the first charging strategy, with differences of less than 0.1%. Considering that the FSOC of the electric ferry only experienced a reduction of 0.15, and although the reduction in the FSOC of electric cars reached approximately 0.5, the overall capacity of electric cars was smaller. The total capacity and energy reduction resulting from adjusting the charging BSOC target for electric ferries and electric cars remained insignificant compared to the energy scale of the harbour building. Consequently, no substantial differences in economic performance were observed. These

findings indicate that this charging strategy, which solely adjusted the FSOC target value, did not enhance the overall system performance. Therefore, the subsequent charging strategy will focus on adjusting the charging power and duration through the grid, aiming to achieve more noticeable improvements.

Both the first and second charging strategies focused only on controlling the FSOC. However, upon analysing the charging power curves, it was observed that when the batteries of the ferry and EVs were charged using grid electricity, the charging process would be completed within a limited number of time steps. Charging would cease before the entire duration of the ferry or EVs' parking period. This behaviour resulted in high energy demand concentrated in the initial time steps of the charging process. Considering that the electricity tariff models in both Hong Kong and Macau include demand charges, this concentration of energy demand led to higher electricity tariffs and poorer economic performance. Consequently, control strategies need to be devised to optimise this phenomenon. In the third charging strategy, known as S1CS3, the control of FSOC will be the same as in the second strategy. If the battery is being charged from the grid, the charging power during a single time step would be limited to the average value of the entire parking period. This approach would flatten out the demand curve, ensuring that the total energy demand is evenly distributed throughout the parking period with a more balanced power profile. The key results of this strategy are summarised in Table 4.6.

Table 4.6 Energy matching, operational tariff, relative net present values, energy usage and emission results of S1CS3 cases [Publication IV].

	WMI	**Operational tariff**	**NPV_{rel}**	**Energy usage ratio**	**CE_a**
		[$\times 10^7$ HKD]	[$\times 10^8$ HKD]	%	kg/m^2. a
20% of submarine cable capacity upper limit					
RE1	0.55	4.44	17.52	99%	-25.41
RE2	0.58	4.02	27.79	98%	-18.69
RE3	0.60	4.04	30.06	100%	-17.24
RE4	0.58	4.03	32.34	100%	-28.06
RE5	0.47	4.83	24.24	100%	-15.78
RE6	0.58	4.06	25.53	100%	-23.29
RE7	0.58	4.03	30.25	100%	-27.34
30% of submarine cable capacity upper limit					
RE1	0.55	4.44	16.98	100%	-28.92
RE2	0.58	4.02	27.93	100%	-27.67
RE3	0.59	4.04	29.48	100%	-18.23
RE4	0.58	4.03	31.72	100%	-28.67
RE5	0.47	4.83	23.54	100%	-15.78
RE6	0.58	4.06	24.80	100%	-23.29
RE7	0.58	4.03	29.49	100%	-27.94
40% of submarine cable capacity upper limit					
RE1	0.55	4.44	16.12	100%	-28.92
RE2	0.58	4.02	27.32	100%	-27.76
RE3	0.59	4.04	28.90	100%	-18.23
RE4	0.58	4.03	31.11	100%	-28.67
RE5	0.47	4.83	22.83	100%	-15.78
RE6	0.58	4.06	24.07	100%	-23.29
RE7	0.58	4.03	28.73	100%	-27.94

The results of this charging strategy indicate that the energy usage ratios align with those observed in the first two charging strategies. Only in the case of the two all-offshore combinations, when the submarine cable operates at 20% of its capacity limit, the energy usage ratios of RE1 and RE2 fall below 100%, specifically at 99% and 98%, respectively. However, for all other combinations, the energy usage ratios remain at 100%. This outcome can be attributed to the fact that energy usage is primarily determined by the capacity ratio and the energy management approach, while the charging strategy itself has minimal influence on energy usage. On the other hand, different charging strategies do impact the operational tariffs of the overall system and NPV_{rel}. In comparison to the first charging strategy, the operational tariffs experience reductions exceeding 1 million HKD across all scenarios. The largest reduction percentage of 3.1% is observed in RE2, while the smallest reduction of 2.3% occurs in RE5. Notably, the variations in submarine cable capacities do not significantly affect the percentages of operational tariff reduction. The increases in NPV_{rel} are less pronounced, ranging between 0.6% and 1.3%. The combination with the most substantial increase in NPV_{rel} is RE1, while RE4 exhibits the smallest increase. Furthermore, when the submarine cable capacity is augmented, there is a trend of increasing NPV_{rel} for the same RE combination. Although the percentage changes in operational tariffs and NPV_{rel} may appear modest, the actual reductions and increases exceed 1 million and 10 million, respectively. These seemingly small percentage values are a consequence of the substantial magnitudes associated with the two large-scale ferry terminal buildings. Overall, the findings demonstrate the influence of different charging strategies on operational tariffs and NPV_{rel}, highlighting the importance of optimising charging approaches to achieve cost savings and improved economic performance in the context of large-scale energy systems.

4.4.2 Scenario with energy sharing V2B function

Scenario 2 builds upon the system established in Scenario 1 by incorporating V2B functionality. This functionality allows vehicle-carrying ferries and electric cars to discharge power to buildings during periods of shortage. The aim is to assess the feasibility of the designed controls and evaluate the impact of V2B functionality on the energy-sharing function and the techno-economic performance of the system. Several stepwise optimised control strategies were developed and analysed to achieve these objectives. In the following paragraphs, we will discuss the details of the first control strategy (S2CS1) and present the results and analysis.

In the first control strategy, S2CS1, the settings largely follow those of the best-performing approach in Scenario 1, S1CS3, with the addition of the V2B function. The target FSOC for charging and discharging the car carrier ferry and EVs was set to meet the FSOC value required for their next trips. When the car carrier ferry and EVs were docked at the ferry terminal building, the V2B function would be activated to discharge power to the building if there was a shortage, provided that the

FSOC was higher than the target value. If the FSOC was lower than the target value, the B2V or Grid-to-Vehicle (G2V) function would be activated to charge the car carrier ferry and EVs. For the car carrier ferry, the minimum FSOC required to meet the next trip's demands was set at 0.6. Considering the lower limit FSOC of the battery at 0.2, the target FSOC for the ferry was set at 0.8. In the Hong Kong subsystem, the minimum FSOC required to meet the next trip's demands was 0.14, while on the Macau side, it was 0.04. The target FSOC for the ferry on the Hong Kong and Macau sides was set at 0.34 and 0.24, respectively. Table 4.7 and Fig. 4.26 present the results and variations of the respective parameters under this control strategy, highlighting the differences and impacts of the V2B function compared to the scenario without V2B functionality.

Table 4.7 Energy matching, operational tariff, relative net present values, energy usage and emission results of the S2CS1 cases and their variations [Publication IV].

	WMI	**WMI increase**	**Operational tariff**	**Operational tariff reduction**	**NPV_{rel}**	**NPV_{rel} increase**	**Energy usage ratio**	**CE_a**
		%	[$\times 10^7$ HKD]	%	[$\times 10^8$ HKD]	%	%	kg/m^2. a
20% of submarine cable capacity upper limit								
RE1	0.55	0.04%	4.44	0.15%	17.54	0.06%	99%	-25.48
RE2	0.58	0.05%	4.01	0.20%	27.80	0.04%	98%	-18.74
RE3	0.60	0.06%	4.03	0.22%	30.08	0.05%	100%	-17.32
RE4	0.58	0.05%	4.02	0.20%	32.35	0.04%	100%	-28.14
RE5	0.47	0.03%	4.83	0.14%	24.26	0.05%	100%	-15.86
RE6	0.58	0.04%	4.06	0.20%	25.55	0.05%	100%	-23.38
RE7	0.58	0.05%	4.02	0.20%	30.26	0.04%	100%	-27.43
30% of submarine cable capacity upper limit								
RE1	0.55	0.04%	4.44	0.15%	16.99	0.07%	100%	-28.99
RE2	0.58	0.05%	4.01	0.20%	27.95	0.05%	100%	-27.74
RE3	0.59	0.07%	4.03	0.22%	29.50	0.05%	100%	-18.32
RE4	0.58	0.05%	4.02	0.20%	31.74	0.04%	100%	-28.74
RE5	0.47	0.03%	4.83	0.14%	23.55	0.05%	100%	-15.86
RE6	0.58	0.04%	4.06	0.20%	24.82	0.06%	100%	-23.38
RE7	0.58	0.05%	4.02	0.20%	29.51	0.05%	100%	-28.03
40% of submarine cable capacity upper limit								
RE1	0.55	0.04%	4.44	0.15%	16.13	0.07%	100%	-28.99
RE2	0.58	0.05%	4.01	0.20%	27.34	0.05%	100%	-27.84
RE3	0.59	0.07%	4.03	0.22%	28.92	0.05%	100%	-18.32
RE4	0.58	0.05%	4.02	0.20%	31.12	0.04%	100%	-28.74
RE5	0.47	0.03%	4.83	0.14%	22.84	0.05%	100%	-15.86
RE6	0.58	0.04%	4.06	0.20%	24.09	0.06%	100%	-23.38
RE7	0.58	0.05%	4.02	0.20%	28.74	0.05%	100%	-28.03

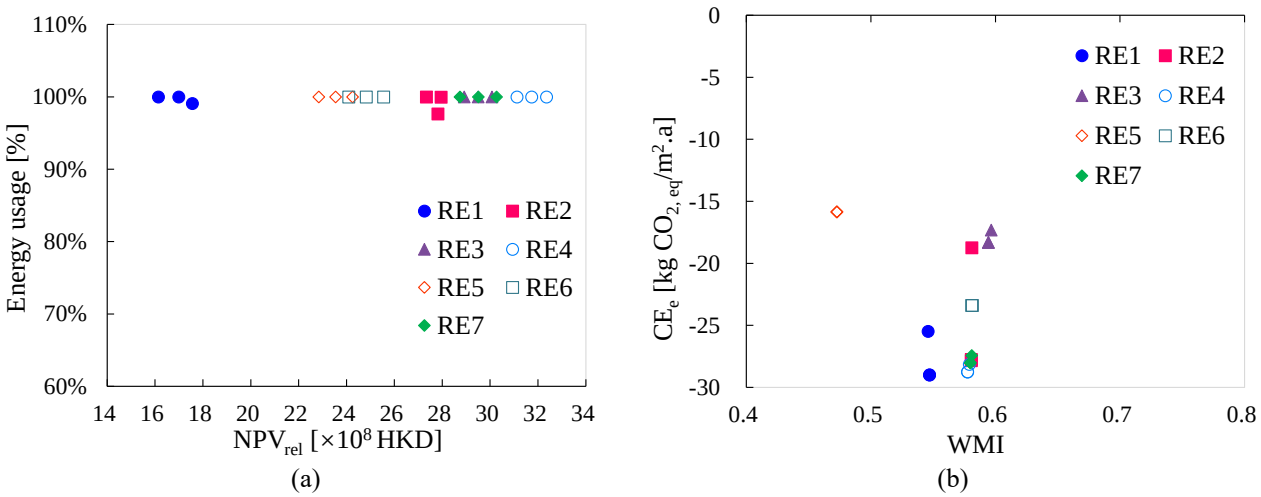

Fig. 4.26 Energy usage and relative net present values of all the combinations under S2CS1 [Publication IV].

Based on the findings, when comparing S1CS3 without V2B function to the renewable energy combinations in Scenario 2, all combinations exhibit a reduction in operational tariffs. The most substantial percentage reduction is observed in RE3 at 0.22%, while the smallest reduction is seen in RE5 at 0.14%. RE2, RE4, RE6, and RE7 all show a decrease of 0.2%, whereas RE1 experiences a reduction percentage of 0.15%. Since there is only one stakeholder who owns the entire system in this study, reducing operational costs leads to decreased economic expenditure and improved economic performance for this stakeholder. The subsystem on the Macau side achieves a higher reduction in operational costs compared to the subsystem in Hong Kong. Changes in submarine cable capacity do not have an impact on the changes in operational tariffs. Additionally, the inclusion of the V2B function does not affect the overall energy usage results of the system. Regarding energy-matching performance, the WMI results for S2CS1, with the V2B function, show insignificant enhancements compared to the results of S1CS3 without the V2B function. The percentage increase in WMI varies between 0.03% and 0.07%. Moreover, the results for NPV_{rel} remain similar and do not exhibit significant changes. These findings indicate that the introduction of the V2B function does not significantly alter the energy-matching performance or the economic performance of the system. Overall, the results suggest that incorporating the V2B function in Scenario 2 leads to reductions in operational tariffs across various renewable energy combinations. The Macau subsystem experiences greater cost reductions than the Hong Kong subsystem, while changes in submarine cable capacity do not affect operational tariff changes. Furthermore, the inclusion of the V2B function has minimal impact on energy usage, energy-matching, and NPV_{rel}.

In the second control strategy, S2CS2, different FSOC values were established for different energy sources during the charging process, as compared to S2CS1. When ocean renewable energy served as the energy source for charging, the target FSOC was set to the maximum value of 0.95 for the battery. On the other hand, when the charging process used

imported energy from the grid, the target FSOC was determined based on the FSOC value required for the car carrier ferry and EVs to meet their next trips. The settings for the discharge process remained the same. Table 4.8 presents the energy-sharing, matching, environmental, and economic results, along with the variations of their respective parameters, in relation to the scenario without the V2B function under this control strategy. It provides a comprehensive overview of how the system performed in terms of energy-sharing dynamics, energy-matching efficiency, environmental considerations, and economic aspects.

Table 4.8 Energy matching, operational tariff, relative net present values, energy usage and emission results of S2CS2 cases and their variations [Publication IV].

	WMI	**WMI increase**	**Operational tariff**	**Operational tariff reduction**	**NPV_{rel}**	**NPV_{rel} increase**	**Shared energy**	**CE_a**
		%	[$\times 10^7$ HKD]	%	[$\times 10^8$ HKD]	%	[$\times 10^7$ kWh]	kg/m^2.a
20% of submarine cable capacity upper limit								
RE1	0.56	2.52%	4.43	0.36%	17.56	0.22%	4.38	-20.23
RE2	0.59	1.77%	4.00	0.46%	27.82	0.11%	4.72	-14.96
RE3	0.60	1.37%	4.02	0.50%	30.10	0.11%	4.71	-14.54
RE4	0.59	1.21%	4.01	0.46%	32.37	0.10%	4.72	-25.74
RE5	0.48	2.43%	4.82	0.39%	24.28	0.13%	3.94	-11.59
RE6	0.60	2.53%	4.04	0.42%	25.57	0.13%	4.71	-17.70
RE7	0.59	1.56%	4.01	0.46%	30.28	0.10%	4.72	-24.12
30% of submarine cable capacity upper limit								
RE1	0.56	2.53%	4.43	0.36%	17.01	0.19%	4.38	-23.69
RE2	0.59	1.71%	4.00	0.46%	27.96	0.11%	4.73	-24.07
RE3	0.60	1.05%	4.02	0.50%	29.52	0.12%	4.72	-16.36
RE4	0.58	1.00%	4.01	0.46%	31.75	0.10%	4.73	-26.88
RE5	0.48	2.43%	4.82	0.39%	23.57	0.14%	3.94	-11.59
RE6	0.60	2.53%	4.04	0.42%	24.84	0.13%	4.71	-17.70
RE7	0.59	1.38%	4.01	0.46%	29.52	0.11%	4.73	-25.18
40% of submarine cable capacity upper limit								
RE1	0.56	2.53%	4.43	0.36%	16.16	0.20%	4.38	-23.69
RE2	0.59	1.71%	4.00	0.46%	27.36	0.12%	4.73	-24.18
RE3	0.60	1.05%	4.02	0.50%	28.94	0.12%	4.72	-16.36
RE4	0.58	1.00%	4.01	0.46%	31.14	0.10%	4.73	-26.88
RE5	0.48	2.43%	4.82	0.39%	22.86	0.14%	3.94	-11.59
RE6	0.60	2.53%	4.04	0.42%	24.11	0.14%	4.71	-17.70
RE7	0.59	1.38%	4.01	0.46%	28.76	0.11%	4.73	-25.18

Changing the target FSOC level only during the charging process does not affect the energy usage ratio of the entire system. As a result, the energy usage ratio obtained from this charging strategy remains the same as that of the first strategy. However, for all other combinations, the energy usage ratio is 100%. When comparing the energy-matching performance of S1CS3 without the V2B function to S2CS2, the maximum percentage increase in the WMI results is 2.53%, while the minimum increase is 1%. By adjusting the target charging FSOC level for renewable energy sources, such as electric ferries and electric vehicles, the system can absorb surplus energy to its maximum capacity and retain electricity that can be released during periods of shortage in the building. This optimisation leads to enhanced energy-matching performance

for the entire system, resulting in reduced operational tariffs and improved economic performance by reducing the reliance on grid supply to cover shortages. Compared to the first strategy that incorporates the V2B function (S2CS1), the percentage reduction in operational tariffs more than doubles in S2CS2, with a minimum decrease of 0.36% in RE1 and a maximum reduction of 0.5% in RE4.

Meanwhile, increasing the capacity of the submarine cables does not have a significant impact on the operational tariffs or their percentage reduction. The largest percentage increase in NPV_{rel} results is observed in RE1 at 0.12%, while the smallest increase occurs in RE4 and RE7 at 0.06%. When the percentage of maximum submarine cable capacity is set at 20%, RE4 achieves the highest NPV_{rel} result at 3.24×10^9 HKD, whereas RE1, with a 40% of maximum submarine cable capacity, has the lowest value at 1.62×10^9 HKD. Similar to Scenario 1, increasing the capacity ratio consistently decreases NPV_{rel} for all combinations except RE2, where NPV_{rel} initially increases and then declines. Although the percentage change in economic performance is not significant in absolute terms, it is relatively substantial considering the scale of the entire system. The minimum decrease in operational tariffs is 1.65×10^5 HKD, and the smallest increase in NPV_{rel} is 3.10×10^6 HKD across all cases.

4.4.3 Scenario without the middle submarine cable, ferry and EV incorporate the V2B function, Impact of ferry schedule and ferry energy consumption

The results of Scenario 2 reveal that when the submarine cable connects all sites, facilitating the transfer of renewable energy generation to the required locations, the energy-sharing within the system primarily occurs through the submarine cable. The electric ferry and electric vehicles, equipped with B2V and V2B functions, contribute to a certain level of energy-sharing. However, due to the control strategy and the limited battery capacity, the enhancement of the techno-economic performance of the entire system is insignificant. Consequently, in this subsection, the submarine cable that connects Hong Kong and Macau has been removed, focusing solely on energy-sharing through the electric ferry and electric vehicles. We aim to investigate the impact of energy-sharing exclusively through these components on the techno-economic performance of the system under this new setup. Additionally, the initial setting for energy consumption per kilometre by the electric car-carrying ferry was high, resulting in an FSOC level of 0.8 required for a one-way journey, with only 0.15 FSOC available for energy-sharing. This limitation significantly restricts the potential for energy-sharing and hampers the enhancement of techno-economic performance. To address this and for illustrative purposes only, a set of illustrative cases with a reduced energy consumption rate of 25 kWh/km was created for each control strategy in this scenario. These cases serve to demonstrate the impact of such a change in energy consumption on the overall system performance [120].

This economic performance-based control principle was introduced in the previous section. To demonstrate the difference and enhancement of the V2B function on the techno-economic performance and energy-sharing performance, the results with only the B2V function and with both the B2V and V2B functions were discussed and compared in this section. The intermediate submarine cables were removed, resulting in a single flow of offshore renewable energy integrated with an offshore renewable energy system. To ensure that no excess energy was wasted, the capacity of the remaining submarine cable was maintained at 100% of its maximum capacity. The energy-matching, economic and environmental results under this control strategy are shown in Fig. 4.27 and Table 4.9.

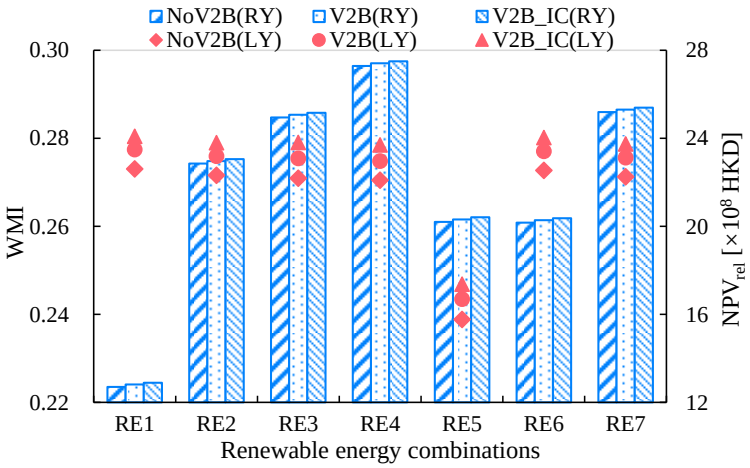

Fig. 4.27 Comparison of the combinations under conditions without V2B, with V2B and the illustrative cases [Publication IV].

Table 4.9 Techno-economic performance and variations of selected combinations under various conditions without V2B, with V2B and the illustrative cases [Publication IV].

Groups	Parameters	Units	RE1	RE2	RE3	RE4	RE5	RE6	RE7
No V2B	WMI		0.27	0.27	0.27	0.27	0.24	0.27	0.27
	Operational tariff	×10^7 HKD	7.36	7.36	7.37	7.34	7.71	7.35	7.35
	NPV$_{rel}$	×10^8 HKD	12.70	22.86	24.95	27.29	20.20	20.17	25.19
	CE$_a$	kg/m^2. a	-6.09	-10.17	-5.41	-10.70	-5.51	-6.50	-10.58
V2B	WMI		0.28	0.28	0.28	0.27	0.24	0.28	0.28
	WMI increase		1.60%	1.60%	1.67%	1.60%	1.94%	1.59%	1.60%
	Operational tariff	×10^7 HKD	7.29	7.29	7.29	7.26	7.64	7.27	7.27
	Operational tariff reduction		0.98%	0.98%	1.03%	1.05%	0.91%	1.00%	1.00%
	NPV$_{rel}$	×10^8 HKD	12.81	22.97	25.07	27.41	20.31	20.28	25.31
	NPV$_{rel}$ increase		0.87%	0.48%	0.48%	0.45%	0.55%	0.57%	0.46%
	CE$_a$	kg/m^2. a	-8.23	-12.30	-7.42	-12.66	-7.59	-8.52	-12.60
V2B_IC	WMI		0.28	0.28	0.28	0.28	0.25	0.28	0.28
	WMI increase		2.72%	2.73%	3.00%	2.95%	3.37%	2.75%	2.76%
	Operational tariff	×10^7 HKD	7.24	7.24	7.24	7.21	7.59	7.23	7.23
	Operational tariff reduction		1.63%	1.63%	1.74%	1.74%	1.64%	1.64%	1.64%
	NPV$_{rel}$	×10^8 HKD	12.89	23.05	25.16	27.50	20.41	20.37	25.39
	NPV$_{rel}$ increase		1.53%	0.85%	0.85%	0.77%	1.03%	0.98%	0.78%
	CE$_a$	kg/m^2. a	-10.19	-14.27	-9.61	-14.90	-9.70	-10.48	-14.56

In this control strategy, the primary objective is to maximise the feed-in tariff, resulting in all generations in Macau being sent to the grid. Therefore, the building demand in Macau is entirely met by the grid, leading to low WMI results that

represent energy-matching performance. However, when comparing cases with and without the V2B function, the introduction of the V2B function improves energy-matching performance. The improvement ranges from a minimum percentage increase of 1.60% in RE1, RE2, RE4, and RE7 to a maximum percentage increase of 1.94% in RE5. Regarding the WMI results, RE5 exhibits the most significant percentage improvement, with a WMI value of 0.24, while RE1, RE2, RE3, RE6, and RE7 all have WMI values of 0.28, and RE4 has a WMI value of 0.27. Furthermore, the inclusion of the V2B function enhances economic performance. The annual operational tariff is reduced by a percentage ranging from 0.91% to 1.05%, resulting in an actual reduction in operational tariff ranging from 7.05×10^5 to 7.69×10^5 HKD. Compared to Scenario 2, the percentage reduction in annual operational tariffs more than doubled. NPV_{rel} also shows an increase, with the most significant percentage increase occurring in RE1 at 0.87% and the smallest increase occurring in RE7 at 0.46%. The actual increase in NPV_{rel} values ranges from 1.10×10^7 to 1.23×10^7 HKD. RE4 achieves the maximum NPV_{rel} result of 2.74×10^9 HKD, while RE1 has the minimum NPV_{rel} result of 1.28×10^9 HKD. The greater percentage increase in NPV_{rel} for RE1 is due to its smaller original benchmark, making the percentage increase more pronounced than in other combinations.

By implementing a reduced energy consumption rate for the electric ferry, further improvements in energy-matching and economic performance can be achieved. In terms of the WMI parameter for energy-matching performance, the minimum percentage increase compared to cases without the V2B function rises to 2.72%, while the maximum percentage increase reaches 3.37% relative to cases with the original energy consumption. In terms of the operational tariff for economic performance, the minimum percentage reduction increases to 1.63%, and the maximum percentage reduction increases to 1.74%. For NPV_{rel}, the minimum percentage increase improves to 0.77%, and the maximum percentage increase improves to 1.53%.

When energy-sharing and exchange occur through mobile electric transport, the changes in energy-matching and economic results capture variations in energy-sharing. However, these indicators do not directly reflect specific energy-sharing and exchange levels. To calculate and demonstrate the amount of shared energy exchanged between Hong Kong and Macau via electric ferries and electric vehicles, certain assumptions need to be made. Firstly, we assume that the energy in the battery is adequately mixed and that energy from both sides is presented in proportion. When the battery is discharged, the source of the discharged energy is calculated based on this ratio. The energy discharged from Macau in Hong Kong and the energy discharged from Hong Kong in Macau are considered shared energy. In this control strategy, the actual energy transferred from Hong Kong to Macau and Macau to Hong Kong is detailed in Table 4.10, providing a comprehensive view of the energy exchange dynamics.

Table 4.10 Shared energy through electric ferry and cars with V2B function and the illustrative cases [Publication IV].

[$\times 10^3$ kWh]		**Electric vehicles**				**Electric car-carrying ferry**			
		Energy for use		Energy shared		Energy for use		Energy shared	
		HK2MO	MO2HK	HK2MO	MO2HK	HK2MO	MO2HK	HK2MO	MO2HK
V2B_IC	RE1	9.48	10.97	457.41	5.32	405.73	191.81	0.00	6.36
	RE2	9.48	10.97	457.41	5.32	405.73	191.81	0.00	6.36
	RE3	8.74	13.95	388.94	1.86	315.47	318.35	0.00	11.81
	RE4	8.80	13.71	384.73	1.51	314.44	319.78	0.00	8.94
	RE5	9.03	12.79	428.95	1.51	322.07	309.11	0.00	12.19
	RE6	9.13	12.37	413.34	2.97	388.99	215.28	0.00	6.82
	RE7	9.13	12.37	413.34	2.97	388.99	215.28	0.00	6.82
V2B	RE1	9.38	11.40	436.09	4.26	292.91	89.80	147.69	12.68
	RE2	9.38	11.40	436.09	4.26	292.91	89.80	147.69	12.68
	RE3	8.74	13.94	349.31	1.64	259.86	136.20	66.59	16.20
	RE4	8.78	13.81	352.05	1.39	258.59	137.97	67.61	13.74
	RE5	9.03	12.82	395.76	1.28	264.89	129.15	78.91	18.27
	RE6	9.08	12.62	383.93	1.98	284.23	102.00	127.16	12.27
	RE7	9.08	12.62	383.93	1.98	284.23	102.00	127.16	12.27

The results reveal that in the scenario where energy-sharing is achieved totally through mobile electric transport, electric cars play a crucial role in both Hong Kong and Macau. In the case of an electric ferry, excluding its own energy usage, energy-sharing can only occur from Macau to Hong Kong, resulting in zero energy discharged from Hong Kong to Macau. However, when considering the energy usage of the electric ferry itself, the energy-sharing becomes bidirectional. In this scenario, the energy used in the Macau region from Hong Kong is more significant than the energy used in the Hong Kong region from Macau. On the other hand, for electric cars, energy-sharing is always bi-directional. In contrast to the electric ferry, when considering only the energy discharged to the buildings to meet the energy shortage, a larger amount of energy is shared from Hong Kong to the Macau side. However, when considering wholly the energy used by electric vehicles, a greater amount of energy from Macau is utilized on the Hong Kong side. These findings highlight the dynamic nature of energy-sharing between the two regions in different scenarios.

Travel energy consumption, the FSOC level requirement for a single trip, and the length of time docked at a building were factors that would limit energy-sharing in this scenario, a series of hypothetical cases was conducted to investigate the impact of ferry travel schedules on energy-sharing performance. In this group of cases, adjustments will be made to the travelling schedule. The electric ferry and electric cars now travel directly from either Hong Kong or Macau to the other side without passing through the offshore site and without a one-hour stop. The total distance travelled in a single trip will be reduced from 50km to 45km, allowing for an additional 4 hours of stopping time at the harbour building within a day. The schedules for business trips on land by electric vehicles will remain unchanged. Moreover, with the modified travel schedule, in addition to one group of cases where the original energy consumption of the electric ferries is maintained, an

additional group of cases with minor energy consumption of the electric ferry are also included. The techno-economic and environmental performance of the cases with the new travel schedule and the illustrative cases are shown in Fig. 4.28 and Table 4.11.

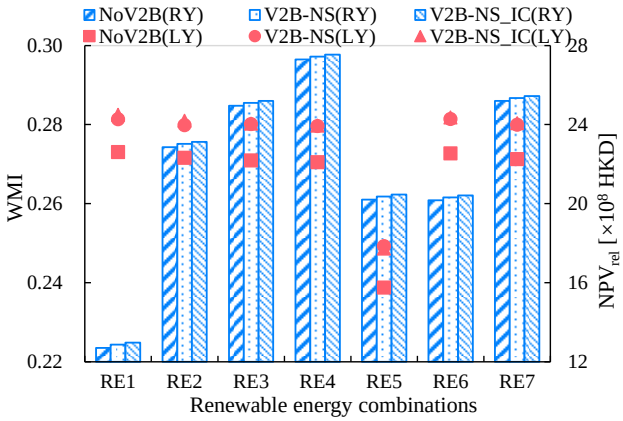

Fig. 4.28 Comparison of the of the cases with new travel schedule (NS) and the illustrative cases (IC) [Publication IV].

Table 4.11 Techno-economic performance and variations of the cases with new travel schedule and the illustrative cases [Publication IV].

Groups	Parameters	Units	RE1	RE2	RE3	RE4	RE5	RE6	RE7
NS_IC	WMI		0.28	0.28	0.28	0.28	0.25	0.28	0.28
	WMI increase		3.44%	3.45%	3.44%	3.42%	4.12%	3.34%	3.35%
	Operational tariff	$\times 10^7$ HKD	7.20	7.20	7.22	7.19	7.55	7.19	7.19
	Operational tariff reduction		2.21%	2.21%	2.00%	2.03%	2.04%	2.08%	2.08%
	NPV_{rel}	$\times 10^8$ HKD	12.97	23.13	25.19	27.54	20.46	20.42	25.45
	NPV_{rel} increase		2.11%	1.17%	0.98%	0.90%	1.27%	1.25%	1.00%
	CE_a	kg/m^2. a	-9.50	-13.57	-9.05	-14.55	-9.22	-10.01	-14.09
NS	WMI		0.28	0.28	0.28	0.28	0.25	0.28	0.28
	WMI increase		2.31%	2.32%	2.36%	2.25%	2.78%	2.20%	2.21%
	Operational tariff	$\times 10^7$ HKD	7.25	7.25	7.28	7.25	7.61	7.25	7.25
	Operational tariff reduction		1.44%	1.44%	1.22%	1.24%	1.30%	1.30%	1.30%
	NPV_{rel}	$\times 10^8$ HKD	12.8	23.03	25.09	27.44	20.36	20.32	25.35
	NPV_{rel} increase		1.33%	0.74%	0.57%	0.53%	0.77%	0.75%	0.60%
	CE_a	kg/m^2. a	-7.51	-11.58	-7.18	-12.50	-7.18	-7.99	-12.07

The analysis of the results reveals that modifying the travel schedule of the electric ferry and electric cars to include longer docking times leads to improved energy-matching and economic performance compared to the original operation schedule. The parameter for energy-matching performance, WMI, exhibits a percentage increase ranging from 2.20% to 2.78% when compared to the scenario without the V2B function. The reduction percentage in the operational tariff, an economic parameter, has increased from 1.22% to 1.44% compared to the original schedule. Additionally, the increase in the other economic parameter, NPV_{rel}, has risen from 0.53% to 1.33% compared to the cases with the original schedule. These findings demonstrate that extending the interaction time between mobile electric vehicles and harbour buildings effectively enhances energy-matching and economic performance.

In addition to the modified travel schedule, illustrative cases were considered with a lower energy consumption rate for the electric ferry. Consistent with previous findings, the reduction in energy consumption per kilometre allows for a larger battery capacity available for energy-sharing. Thus, this leads to further improvements in energy-matching and economic performance compared to the previous cases. These observations reinforce the notion that reducing the energy consumption of the electric ferry positively impacts energy-sharing and overall system performance.

To provide a comprehensive understanding of the energy dynamics, Table 4.12 presents the actual shared energy for covering building shortages and for the electric ferry's own travel purposes.

Table 4.12 Shared energy through electric ferries and cars in illustrative cases [Publication IV].

[$\times 10^3$ kWh]		**Electric vehicles**				**Electric car-carrying ferry**			
		Energy for use		Energy shared		Energy for use		Energy shared	
		Use_ HK2MO	Use_ MO2HK	HK2MO	MO2HK	Use_ HK2MO	Use_ MO2HK	HK2MO	MO2HK
NS_IC	RE1	6.20	7.98	419.68	22.14	314.13	94.11	0.00	30.93
	RE2	6.20	7.98	419.68	22.14	314.13	94.11	0.00	30.93
	RE3	6.51	7.93	390.98	23.31	312.67	95.64	0.00	36.93
	RE4	6.24	7.97	424.39	21.92	314.49	93.76	0.00	30.78
	RE5	5.83	8.07	477.21	19.11	321.53	86.76	0.00	36.72
	RE6	6.23	8.00	424.38	21.93	314.34	93.91	0.00	30.84
	RE7	6.23	8.00	424.38	21.93	314.34	93.91	0.00	30.84
NS	RE1	6.14	8.01	399.67	24.15	366.56	247.73	0.00	27.22
	RE2	6.14	8.01	399.67	24.15	366.56	247.73	0.00	27.22
	RE3	6.35	7.87	388.80	25.36	366.16	248.50	0.00	32.70
	RE4	6.18	7.98	394.09	24.11	366.62	247.67	0.00	27.16
	RE5	5.58	8.13	454.37	21.26	374.24	240.81	0.00	37.00
	RE6	6.16	8.02	398.58	24.12	366.59	247.70	0.00	27.19
	RE7	6.16	8.02	398.58	24.12	366.59	247.70	0.00	27.19

The results indicate that when the new travel schedule was implemented, no energy was shared from the Hong Kong side to the Macao side via the electric ferry in all cases. However, when it comes to electric vehicles, the energy shared from the Hong Kong side to the Macao side was greater in the cases with the new travel schedule compared to those with the original schedule. The implementation of the new travel schedule, which included longer interaction times with the two harbour buildings, resulted in increased energy sharing both from Hong Kong to Macau and from Macau to Hong Kong, involving both electric ferries and electric cars. Furthermore, the cases that considered the new travel schedule and featured reduced energy consumption of the electric ferry exhibited further improvements in the total amount of shared energy. These illustrative cases demonstrated enhanced energy-sharing capabilities compared to the previous cases, highlighting the positive impact of reducing the energy consumption of the electric ferry on the overall energy-sharing dynamics. The case results indicate that the energy sharing benefits from a navigation system with one electric ferry and ten EVs did not lead to a significant improvement in overall system performance. This is primarily due to the limited number of ferries

and EVs, along with constraints related to battery capacity and the specific purposes of cruising. These factors create a substantial difference in scale between a navigation system and a zero-emission building system. Despite the small percentage change, the economic gains can potentially reach millions. Moreover, this energy control strategy can leverage existing resources to enhance system performance without incurring additional investment costs. This highlights the significance of electric navigation systems. In future scenarios, increasing the number of ferries and EVs, as well as diversifying transportation routes and groups, could lead to more substantial improvements in performance.

Chapter 5. Conclusions and future research work

In this study, the ultimate research aim was to build zero energy buildings and systems and to maximise system feasibility, and with multiple directions of objectives, different scales of research systems were designed as well as energy management strategies orientated towards different purposes. In the initial part of the study, only single coastal office buildings were investigated and the techno-economic and environmental feasibility of reaching a zero-energy building was tested by composing several cases with different mixing ratios of ocean energy systems. Batteries were then utilised as energy storage devices to explore energy flexibility and demand response to enhance economic performance and to attempt to reduce the dependence of zero energy systems on FiT through energy management and market incentives. The scale and number of buildings were expanded to form a cross-harbour system that relies on both the nearshore and offshore ocean energy systems and utilises submarine cables to share energy between the buildings located in the two cities across the sea to enhance energy matching and economic performance. Finally, in this cross-harbour system, where the purpose of the building is a ferry terminal, a V2B function was added to the electric vehicles, which already existed as a means of transport to conduct energy sharing, as a removable battery to try out its impact on the performance of the system.

In the first part of the study, the coastal office building utilised heat exchangers submerged in the sea instead of traditional cooling towers to form a sea-source cooling system. Meanwhile, placing the heat exchanger on the shore and using seawater directly as cooling water were designed as other sea-source chillers for comparison. The results indicated that the sea-sourced cooling system with a heat exchanger submerged in the sea is feasible to achieve better COP values than the traditional cooling tower and reduce the energy consumption from the cooling system, Furthermore, the hybrid ocean renewable energy system including FPV and TSG system was incorporated into the coastal office building. Totally 11 cases with different mixing ratios of FPV and TSG systems based on similar total energy generation were designed. Considering the energy matching performance, C3 consisting of 2 TSGs and 3967 FPV panels achieved the optimal energy matching. The best economic performance was obtained by the C1 consisting only of the FPV system. The annual operational equivalent CO_2 emissions of all cases were significantly reduced compared with the reference case. As different numbers of batteries were added to the system, the energy-matching performance was gradually enhanced as the number

of batteries increased and the parameters approached 1. However, the CO_2 emissions also increased with the number of batteries, indicating that the increase in the number of batteries is less cost-effective and can compromise environmental performance.

The research proceeded to an exploration of energy flexibility and demand response aiming to minimize the mismatch between renewable energy generation and the building demand and improve the performance. The energy flexibility control methodology was the peak shaving and valley filling by batteries and conducted based on the annual or monthly charging and discharging line. Both flexibility control methods were effective in reducing operating costs. The flexibility control approach with monthly charging and discharging lines could achieve better techno-economic performance because the energy demand varied from month to month throughout the year. The control based on the monthly demand condition enabled better energy flexibility control to reduce the operational tariffs. Meanwhile, the energy flexibility control allowed the system to participate in the PDM programme to obtain incentives, and specific control for the PDM programme could achieve further improvement of incentives and enhance economic performance. However, without the FiT, the renewable energy penetration could only achieve 20% to 30% with neutral NPV_{rel} values, indicating the unfeasibility of the zero-energy system without the FiT. Furthermore, several modifications based on the benchmark in the PDM programme and grid exporting tariffs were proposed, and the results indicated that both modifications could achieve the enhancement of economic performance.

As the scale and number of buildings expanded from a single coastal office building to two large public buildings in cities across the sea, submarine cables were applied to conduct energy sharing enhancing technical and economic performance and trying to avoid dumped energy. Two potential integration FiT policies and several representative renewable energy combinations were designed. The results indicated that if the middle submarine cable did not exist, with the presence of an offshore FPV system, the submarine cable capacity does not need to be 100% and reducing the submarine cable capacity by a certain percentage could improve the economic performance without any dumped energy. If the middle submarine cable connected two offshore renewable energy sites, 40% of the maximum submarine cable capacity was sufficient to avoid any dumped energy. Renewable energy combinations that include only wind turbine systems had better economic performance, while the addition of tidal stream generators had a negative impact on economic performance. RE5, consisting entirely of the nearshore wind turbines could achieve the optimum NPV_{rel} values when the same land price was applied to both nearshore and offshore sites, which were 25.63×10^8 and 30.78×10^8 HKD, respectively. However, offshore battery installation could not replace part of the submarine cable capacity owing to the high investment and O&M cost. Compared to the boundary-based FiT policy, source-based FiT can better encourage energy sharing between the two

regions. Nevertheless, applying the actual land price made the cases with nearshore renewable energy systems difficult to obtain a positive economic performance.

Based on the hybrid cross-harbour system consisting of two large-scale zero-emission ferry terminal buildings, a car-carrying electric ferry and ten electric cars with transport tasks that incorporate the V2B function were utilized as the mobile energy storage to conduct further energy sharing. Adjusting the target FSOC value for charging and averaging the charging power could reduce the operational tariff and improve the NPV_{rel} results, with a maximum reduction of 1.24% in operational tariff and a maximum improvement of 1.02% in NPV_{rel} when the electric ferry and the electric car has B2V function and only as part of energy demand. If electric ferries and cars were equipped with the V2B function, energy-matching and economic performance could obtain certain improvements. Further adjustments on the charging FSOC upper limit, when the charging sources were renewable energy or grid, can achieve more enhancement, with reductions in operational tariffs of up to 0.5% and increases in NPV_{rel} of up to 0.22%. When the intermediate submarine cables were removed, together with the new travel schedule without docking at the offshore site and smaller travel energy consumption, the increase of energy matching could be 3.44%, the decrease in operational tariff could be 1.42×10^6 HKD and 2.74%, and the increase in NPV_{rel} could be 3.16×10^7 HKD and 3.40%. All the results indicated that moveable electric vehicles could perform a portion of the energy exchange to enhance performance, but are limited by factors such as battery capacity, energy requirements necessary for transport, and so on.

Future research should focus on the following aspects. Firstly, considering ocean energy systems, new and more advanced technologies with higher energy conversion efficiencies and fewer negative economic and environmental impacts could be applied in the future to reach the goal of a zero-energy system. Second, renewable energy systems can be combined with some lower-cost energy storage devices under certain conditions, such as hydroelectric storage devices that rely on height differences to enhance performance. Furthermore, given the current economic dependence on FiT to achieve zero-energy systems, incentives and policies that rely more on the market could be examined to enhance the viability of zero-energy buildings themselves. Finally, if we focus on electric vehicles combined with zero-energy buildings, a smart charging framework that determines the best routes and charging options based on actual traffic conditions, charging station congestion, charging costs, etc. is also a future research direction.

References

[1] IEA. Tracking Buildings [Online] Available: https://www.iea.org/energy-system/buildings
[2] EIA. Energy use for transportation [Online] Available: https://www.eia.gov/energyexplained/use-of-

energy/transportation.php
[3] Electrical & Mechanical Services Department. Hong Kong Energy End-use Data 2023 [Online] Available: https://www.emsd.gov.hk/filemanager/en/content_762/HKEEUD2023.pdf
[4] CNBC. G-20 leaders struggle to secure climate breakthrough at Rome summit [Online] Available: https://www.cnbc.com/2021/10/31/g-20-leaders-struggle-to-secure-climate-breakthrough-at-rome-summit-.html
[5] The Government of the HKSAR. Hong Kong's Climate Action Plan 2050 [Online] Available: https://www.climateready.gov.hk/files/pdf/CAP2050_booklet_en.pdf
[6] "Chapter 3 - From Efficient to Sustainable and Zero Energy Consumption Buildings," in *Handbook of Energy Efficiency in Buildings*, F. Asdrubali and U. Desideri Eds.: Butterworth-Heinemann, 2019, pp. 75-205.
[7] European Commission. "Renovation Wave." https://energy.ec.europa.eu/topics/energy-efficiency/energy-efficient-buildings/renovation-wave_en.
[8] Climate Cooperation China. "China Issues Action Plan for Energy Saving and Carbon Reduction (2024-2025)." https://climatecooperation.cn/climate/china-issues-action-plan-for-energy-saving-and-carbon-reduction-2024-2025/.
[9] California Energy Commission. "Building Energy Efficiency Standards." https://www.energy.ca.gov/programs-and-topics/programs/building-energy-efficiency-standards.
[10] IEA. IEA EBC - Annex 82 - Energy Flexible Buildings Towards Resilient Low Carbon Energy Systems [Online] Available: https://annex82.iea-ebc.org/
[11] A. Ghasempour, "Advanced metering infrastructure in smart grid: Requirements, challenges, architectures, technologies, and optimizations," 2017, pp. 77-127.
[12] European Commission. "Energy Efficiency Directive." https://energy.ec.europa.eu/topics/energy-efficiency/energy-efficiency-targets-directive-and-rules/energy-efficiency-directive.
[13] U.S. Department of Energy. "Grid Modernization Initiative." https://www.energy.gov/gmi/grid-modernization-initiative.
[14] IEA, "Tracking Demand Response," ed, 2023.
[15] U.S. Department of Energy, "Grid-Interactive Efficient Buildings," ed, 2024.
[16] UK Environment Committee e. "Community Energy." https://www.london.gov.uk/sites/default/files/2024-01/CommunityEnergyReport.pdf.
[17] R. F. De Masi, V. Festa, S. Ruggiero, A. Russo, and G. P. Vanoli, "Multi-domain approach for quality evaluation of building designed to be nearly zero energy: Case study in Mediterranean climate," *Energy and Built Environment,* 2024/05/14/ 2024, doi: https://doi.org/10.1016/j.enbenv.2024.05.004.
[18] S. Yoon and J. Lee, "Perspective for waste upcycling-driven zero energy buildings," *Energy,* vol. 289, p. 130029, 2024/02/15/ 2024, doi: https://doi.org/10.1016/j.energy.2023.130029.
[19] M. M. Oualid, M. Elmankibi, and N. Lamdouar, "The Net Zero Energy Building Definition Framework: An Overview Pathway to Enhancing Sustainable Development and Mitigating Climate Change in Morocco," *Procedia Computer Science,* vol. 236, pp. 281-288, 2024/01/01/ 2024, doi: https://doi.org/10.1016/j.procs.2024.05.032.
[20] S. Alqaed, J. Mustafa, S. M. Sajadi, and H. Ş. Aybar, "Enhancing energy efficiency in zero energy buildings: Analyzing the impacts of phase change material-filled enclosures and outlet air distance on solar wall performance," *Case Studies in Thermal Engineering,* vol. 58, p. 104342, 2024/06/01/ 2024, doi: https://doi.org/10.1016/j.csite.2024.104342.
[21] E. Ohene, M. Krarti, A. P. C. Chan, S.-C. Hsu, and M. K. Ansah, "Optimal design guidelines for net zero energy residential buildings in cooling-dominated climates: Case study of Ghana," *Building and Environment,* vol. 260, p. 111685, 2024/07/15/ 2024, doi: https://doi.org/10.1016/j.buildenv.2024.111685.
[22] J. Li and Z. Gou, "Addressing the development gap in net-zero energy buildings: A comparative study of China, India, and the United States," *Energy for Sustainable Development,* vol. 79, p. 101418, 2024/04/01/ 2024, doi: https://doi.org/10.1016/j.esd.2024.101418.
[23] S. Forrousso *et al.*, "Optimal sizing of off-grid microgrid building-integrated-photovoltaic system with battery for a net zero energy residential building in different climates of Morocco," *Results in Engineering,* vol. 22, p. 102288, 2024/06/01/ 2024, doi: https://doi.org/10.1016/j.rineng.2024.102288.
[24] H. Sady, S. Rashidi, and R. Rafee, "Towards a net-zero-energy building with smart control of Trombe walls, underground air ducts, and optimal microgrid composed of renewable energy systems," *Energy,* vol. 294, p. 130703, 2024/05/01/ 2024, doi: https://doi.org/10.1016/j.energy.2024.130703.
[25] H. Li, Z. Zhang, P. Xu, C. Jiang, and L. Yu, "A vortex-induced vibration device based on MG-TENG and research

of its application in ocean current energy harvesting," *Nano Energy,* vol. 124, p. 109457, 2024/06/01/ 2024, doi: https://doi.org/10.1016/j.nanoen.2024.109457.
[26] M. Bianchi and I. F. Fernandez, "A systematic methodology to assess local economic impacts of ocean renewable energy projects: Application to a tidal energy farm," *Renewable Energy,* vol. 221, p. 119853, 2024/02/01/ 2024, doi: https://doi.org/10.1016/j.renene.2023.119853.
[27] M. Bianchi, A. J. Arnal, M. Astorkiza-Andres, J. Clavell-Diaz, A. Marques, and M. Isasa-Sarralde, "Life cycle and economic assessment of tidal energy farms in early design phases: Application to a second-generation tidal device," *Heliyon,* vol. 10, no. 12, p. e32515, 2024/06/30/ 2024, doi: https://doi.org/10.1016/j.heliyon.2024.e32515.
[28] H. Yang, Q. Wu, and G. Li, "A multi-stage forecasting system for daily ocean tidal energy based on secondary decomposition, optimized gate recurrent unit and error correction," *Journal of Cleaner Production,* vol. 449, p. 141303, 2024/04/10/ 2024, doi: https://doi.org/10.1016/j.jclepro.2024.141303.
[29] C. Mo *et al.*, "Recognition method of turbine pollutant adhesion in tidal stream energy generation systems based on deep learning," *Energy,* vol. 302, p. 131799, 2024/09/01/ 2024, doi: https://doi.org/10.1016/j.energy.2024.131799.
[30] A. Rashid, T. H. Nakib, T. Shahriar, M. A. Habib, and M. Hasanuzzaman, "Energy and economic analysis of an ocean thermal energy conversion plant for Bangladesh: A case study," *Ocean Engineering,* vol. 293, p. 116625, 2024/02/01/ 2024, doi: https://doi.org/10.1016/j.oceaneng.2023.116625.
[31] C. Fan, C. Zhang, and W. Gao, "Improving the ocean thermal energy conversion by solar pond," *Solar Energy,* vol. 274, p. 112583, 2024/05/15/ 2024, doi: https://doi.org/10.1016/j.solener.2024.112583.
[32] Y. Zhang, Y. Chen, X. Qiu, Z. Tian, H. Peng, and W. Gao, "Experimental study and performance comparison of a 1 kW-class solar-ocean thermal energy conversion system integrated air conditioning: Energy, exergy, economic, and environmental (4E) analysis," *Journal of Cleaner Production,* vol. 451, p. 142033, 2024/04/20/ 2024, doi: https://doi.org/10.1016/j.jclepro.2024.142033.
[33] W. Gao, F. Wang, Z. Tian, and Y. Zhang, "Experimental investigation on the performance of a Solar-Ocean Thermal Energy Conversion system based on the Organic Rankine Cycle," *Applied Thermal Engineering,* vol. 245, p. 122776, 2024/05/15/ 2024, doi: https://doi.org/10.1016/j.applthermaleng.2024.122776.
[34] Y. Du *et al.*, "Performance analysis of ocean thermal energy conversion system integrated with waste heat recovery from offshore oil and gas platform," *Case Studies in Thermal Engineering,* vol. 54, p. 104027, 2024/02/01/ 2024, doi: https://doi.org/10.1016/j.csite.2024.104027.
[35] F. Chen, L. Liu, H. Zeng, J. Peng, Y. Ge, and W. Liu, "Theoretical and experimental study on the secondary heat recovery cycle of the mixed working fluid in ocean thermal energy conversion," *Renewable Energy,* vol. 227, p. 120142, 2024/06/01/ 2024, doi: https://doi.org/10.1016/j.renene.2024.120142.
[36] C. Zhang, J. Dai, K. K. Ang, and H. V. Lim, "Development of compliant modular floating photovoltaic farm for coastal conditions," *Renewable and Sustainable Energy Reviews,* vol. 190, p. 114084, 2024/02/01/ 2024, doi: https://doi.org/10.1016/j.rser.2023.114084.
[37] A. Alcañiz, N. Monaco, O. Isabella, and H. Ziar, "Offshore floating PV–DC and AC yield analysis considering wave effects," *Energy Conversion and Management,* vol. 300, p. 117897, 2024/01/15/ 2024, doi: https://doi.org/10.1016/j.enconman.2023.117897.
[38] A. S. Irshad, G. Ahmad Ludin, S. Ludin, M. H. Elkholy, S. Elias, and T. Senjyu, "Integration and performance analysis of optimal large-scale hybrid PV and pump hydro storage system based upon floating PV for practical application," *Energy Conversion and Management: X,* vol. 22, p. 100599, 2024/04/01/ 2024, doi: https://doi.org/10.1016/j.ecmx.2024.100599.
[39] R. C.J, K. H. Lim, J. C. Kurnia, S. Roy, B. J. Bora, and B. J. Medhi, "Design study on the parameters influencing the performance of floating solar PV," *Renewable Energy,* vol. 223, p. 120064, 2024/03/01/ 2024, doi: https://doi.org/10.1016/j.renene.2024.120064.
[40] S. K. A. Dzamesi *et al.*, "Comparative performance evaluation of ground-mounted and floating solar PV systems," *Energy for Sustainable Development,* vol. 80, p. 101421, 2024/06/01/ 2024, doi: https://doi.org/10.1016/j.esd.2024.101421.
[41] M. de-Borja-Torrejon, G. Mor, J. Cipriano, A.-L. Leon-Rodriguez, T. Auer, and J. Crawley, "Closing the energy flexibility gap: Enriching flexibility performance rating of buildings with monitored data," *Energy and Buildings,* vol. 311, p. 114141, 2024/05/15/ 2024, doi: https://doi.org/10.1016/j.enbuild.2024.114141.
[42] N. Maitanova, S. Schlüters, B. Hanke, and K. von Maydell, "An analytical method for quantifying the flexibility potential of decentralised energy systems," *Applied Energy,* vol. 364, p. 123150, 2024/06/15/ 2024, doi: https://doi.org/10.1016/j.apenergy.2024.123150.
[43] A. Erfani, T. Jafarinejad, S. Roels, and D. Saelens, "Assessing the impact of the dataset's size and quality on building thermal models for energy flexibility," *Energy and Buildings,* vol. 317, p. 114404, 2024/08/15/ 2024,

doi: https://doi.org/10.1016/j.enbuild.2024.114404.
[44] Z. Afroz, H. Wu, S. Sethuvenkatraman, G. Henze, R. Grønborg Junker, and M. Shepit, "A study on price responsive energy flexibility of an office building under cooling dominated climatic conditions," *Energy and Buildings,* vol. 316, p. 114359, 2024/08/01/ 2024, doi: https://doi.org/10.1016/j.enbuild.2024.114359.
[45] R. Förster, S. Harding, and H. U. Buhl, "Unleashing the economic and ecological potential of energy flexibility: Attractiveness of real-time electricity tariffs in energy crises," *Energy Policy,* vol. 185, p. 113975, 2024/02/01/ 2024, doi: https://doi.org/10.1016/j.enpol.2023.113975.
[46] W. Liang, H. Li, S. Zhan, A. Chong, and T. Hong, "Energy flexibility quantification of a tropical net-zero office building using physically consistent neural network-based model predictive control," *Advances in Applied Energy,* vol. 14, p. 100167, 2024/07/01/ 2024, doi: https://doi.org/10.1016/j.adapen.2024.100167.
[47] K. Zhang, E. Saloux, and J. A. Candanedo, "Enhancing energy flexibility of building clusters via supervisory room temperature control: Quantification and evaluation of benefits," *Energy and Buildings,* vol. 302, p. 113750, 2024/01/01/ 2024, doi: https://doi.org/10.1016/j.enbuild.2023.113750.
[48] F. Stegemerten, S. Leidolf, P. Stoffel, and D. Müller, "Exploring flexibility in building energy systems: Agent-based quantification and electricity tariff impacts," *Energy and Buildings,* vol. 334, p. 115500, 2025/05/01/ 2025, doi: https://doi.org/10.1016/j.enbuild.2025.115500.
[49] P. Fan, D. Wang, Y. Sun, and W. Wang, "A generalized flexibility potential quantification method of active thermal energy storage system for grid-interactive efficient buildings," *Journal of Energy Storage,* vol. 117, p. 116120, 2025/05/01/ 2025, doi: https://doi.org/10.1016/j.est.2025.116120.
[50] A. Atefi and V. Gholaminia, "Flexible demand-side management program in accordance with the consumers' requested constraints," *Energy and Buildings,* vol. 309, p. 114013, 2024/04/15/ 2024, doi: https://doi.org/10.1016/j.enbuild.2024.114013.
[51] H. Sun, X. Cui, and H. Latifi, "Optimal management of microgrid energy by considering demand side management plan and maintenance cost with developed particle swarm algorithm," *Electric Power Systems Research,* vol. 231, p. 110312, 2024/06/01/ 2024, doi: https://doi.org/10.1016/j.epsr.2024.110312.
[52] S. Yu *et al.*, "Demand side management full season optimal operation potential analysis for coupled hybrid photovoltaic/thermal, heat pump, and thermal energy storage systems," *Journal of Energy Storage,* vol. 80, p. 110375, 2024/03/01/ 2024, doi: https://doi.org/10.1016/j.est.2023.110375.
[53] R. Çakmak, "Design and implementation of a low-cost power logger device for specific demand profile analysis in demand-side management studies for smart grids," *Expert Systems with Applications,* vol. 238, p. 121888, 2024/03/15/ 2024, doi: https://doi.org/10.1016/j.eswa.2023.121888.
[54] M. A. S. T. Ireshika and P. Kepplinger, "Uncertainties in model predictive control for decentralized autonomous demand side management of electric vehicles," *Journal of Energy Storage,* vol. 83, p. 110194, 2024/04/01/ 2024, doi: https://doi.org/10.1016/j.est.2023.110194.
[55] A. Roshan and G. D, "Intelligent categorization and interactive mechanism for smart demand side management of residential consumers," *Sustainable Energy, Grids and Networks,* vol. 37, p. 101255, 2024/03/01/ 2024, doi: https://doi.org/10.1016/j.segan.2023.101255.
[56] B. Nilges, C. Reinert, and N. von der Assen, "Is demand-side management environmentally beneficial? Analyzing the greenhouse gas emissions due to load shifting in electric power systems," *Journal of Cleaner Production,* vol. 434, p. 140062, 2024/01/01/ 2024, doi: https://doi.org/10.1016/j.jclepro.2023.140062.
[57] Y. Manoharan, K. Olson, and A. J. Headley, "Sensitivity of energy storage system optimization program to the source of renewable energy in the presence of demand side management: A behind-the-meter case study," *Applied Energy,* vol. 388, p. 125557, 2025/06/15/ 2025, doi: https://doi.org/10.1016/j.apenergy.2025.125557.
[58] S. S. Kumaresan and P. R. Jeyaraj, "Smart building transferable energy scheduling employing reward shaping deep reinforcement learning with demand side energy management," *Journal of Building Engineering,* vol. 104, p. 112316, 2025/06/15/ 2025, doi: https://doi.org/10.1016/j.jobe.2025.112316.
[59] Y. Li, G. M. Senthil Kumar, S. Cao, and S. Wang, "Electric vehicle-based distant energy sharing between zero-emission coastal office and hotel buildings," *Journal of Building Engineering,* vol. 90, p. 109496, 2024/08/01/ 2024, doi: https://doi.org/10.1016/j.jobe.2024.109496.
[60] F. D. Minuto, M. Crosato, D. S. Schiera, R. Borchiellini, and A. Lanzini, "Shared energy in renewable energy communities: The benefits of east- and west-facing rooftop photovoltaic installations," *Energy Reports,* vol. 11, pp. 5593-5601, 2024/06/01/ 2024, doi: https://doi.org/10.1016/j.egyr.2024.05.054.
[61] A. Tiwari, B. K. Jha, and N. M. Pindoriya, "Multi-objective optimization based demand response program with network aware peer-to-peer energy sharing," *International Journal of Electrical Power & Energy Systems,* vol. 157, p. 109887, 2024/06/01/ 2024, doi: https://doi.org/10.1016/j.ijepes.2024.109887.
[62] L. Bokopane, K. Kusakana, H. Vermaak, and A. Hohne, "Optimal power dispatching for a grid-connected electric vehicle charging station microgrid with renewable energy, battery storage and peer-to-peer energy sharing,"

Journal of Energy Storage, vol. 96, p. 112435, 2024/08/15/ 2024, doi: https://doi.org/10.1016/j.est.2024.112435.
[63] M. A. Sayed, M. M. Ahmed, W. Azlan, and L. W. Kin, "Peer to peer solar energy sharing system for rural communities," *Cleaner Energy Systems,* vol. 7, p. 100102, 2024/04/01/ 2024, doi: https://doi.org/10.1016/j.cles.2023.100102.
[64] F. Minelli, I. Ciriello, F. Minichiello, and D. D'Agostino, "From Net Zero Energy Buildings to an energy sharing model - The role of NZEBs in Renewable Energy Communities," *Renewable Energy,* vol. 223, p. 120110, 2024/03/01/ 2024, doi: https://doi.org/10.1016/j.renene.2024.120110.
[65] Y. Bian, L. Xie, J. Ye, L. Ma, and C. Cui, "Peer-to-peer energy sharing model considering multi-objective optimal allocation of shared energy storage in a multi-microgrid system," *Energy,* vol. 288, p. 129864, 2024/02/01/ 2024, doi: https://doi.org/10.1016/j.energy.2023.129864.
[66] W. Ji, S. Guo, H. Sun, and D. Liu, "Optimal dispatching of multi-community electric-thermal integrated energy systems considering wind and solar uncertainties based on hydraulic stability and energy sharing," *Energy Conversion and Management,* vol. 308, p. 118335, 2024/05/15/ 2024, doi: https://doi.org/10.1016/j.enconman.2024.118335.
[67] Y. Zhou and P. D. Lund, "Peer-to-peer energy sharing and trading of renewable energy in smart communities ─ trading pricing models, decision-making and agent-based collaboration," *Renewable Energy,* vol. 207, pp. 177-193, 2023/05/01/ 2023, doi: https://doi.org/10.1016/j.renene.2023.02.125.
[68] X. Chen *et al.*, "Multi-objective optimization of battery capacity of grid-connected PV-BESS system in hybrid building energy sharing community considering time-of-use tariff," *Applied Energy,* vol. 350, p. 121727, 2023/11/15/ 2023, doi: https://doi.org/10.1016/j.apenergy.2023.121727.
[69] M. Algafri, A. Alghazi, Y. Almoghathawi, H. Saleh, and K. Al-Shareef, "Smart City Charging Station allocation for electric vehicles using analytic hierarchy process and multiobjective goal-programming," *Applied Energy,* vol. 372, p. 123775, 2024/10/15/ 2024, doi: https://doi.org/10.1016/j.apenergy.2024.123775.
[70] M. Garau and B. N. Torsæter, "A methodology for optimal placement of energy hubs with electric vehicle charging stations and renewable generation," *Energy,* vol. 304, p. 132068, 2024/09/30/ 2024, doi: https://doi.org/10.1016/j.energy.2024.132068.
[71] H. He, Y. Huang, and T. Senjyu, "Microgrid load forecasting and optimization for future remote island electric vehicle mass penetration: The case of Okinawa Island," *Energy Reports,* vol. 11, pp. 5532-5541, 2024/06/01/ 2024, doi: https://doi.org/10.1016/j.egyr.2024.05.024.
[72] W. Zhan, Z. Wang, J. Deng, P. Liu, and D. Cui, "Integrating system dynamics and agent-based modeling: A data-driven framework for predicting electric vehicle market penetration and GHG emissions reduction under various incentives scenarios," *Applied Energy,* vol. 372, p. 123749, 2024/10/15/ 2024, doi: https://doi.org/10.1016/j.apenergy.2024.123749.
[73] W. Lyu *et al.*, "Impact of battery electric vehicle usage on air quality in three Chinese first-tier cities," *Scientific Reports,* vol. 14, no. 1, p. 21, 2024/01/02 2024, doi: 10.1038/s41598-023-50745-6.
[74] M. Zand, M. Alizadeh, M. Azimi Nasab, M. Azimi Nasab, and S. Padmanaban, "Electric vehicle charger energy management by considering several sources and equalizing battery charging," *Renewable Energy Focus,* vol. 50, p. 100592, 2024/09/01/ 2024, doi: https://doi.org/10.1016/j.ref.2024.100592.
[75] N. K. Panda and S. H. Tindemans, "Efficient quantification and representation of aggregate flexibility in Electric Vehicles," *Electric Power Systems Research,* vol. 235, p. 110811, 2024/10/01/ 2024, doi: https://doi.org/10.1016/j.epsr.2024.110811.
[76] R. B. Roy, S. Alahakoon, S. J. Arachchillag, and S. Rahman, "Optimizing dynamic electric ferry loads with intelligent power management," *Energy Reports,* vol. 9, pp. 5952-5963, 2023/12/01/ 2023, doi: https://doi.org/10.1016/j.egyr.2023.05.029.
[77] Y. Feng, L. Dai, M. Yue, H. Hu, and S. Fang, "Assessing the decarbonization potential of electric ships for inland waterway freight transportation," *Transportation Research Part D: Transport and Environment,* vol. 129, p. 104151, 2024/04/01/ 2024, doi: https://doi.org/10.1016/j.trd.2024.104151.
[78] T. Song, L. Fu, L. Zhong, Y. Fan, and Q. Shang, "HP3O algorithm-based all electric ship energy management strategy integrating demand-side adjustment," *Energy,* vol. 295, p. 130968, 2024/05/15/ 2024, doi: https://doi.org/10.1016/j.energy.2024.130968.
[79] Y. Zhang, L. Sun, T. Fan, F. Ma, and Y. Xiong, "Speed and energy optimization method for the inland all-electric ship in battery-swapping mode," *Ocean Engineering,* vol. 284, p. 115234, 2023/09/15/ 2023, doi: https://doi.org/10.1016/j.oceaneng.2023.115234.
[80] J. Gao, H. Lan, X. Zhang, H. H. C. Iu, Y.-Y. Hong, and H. Yin, "A coordinated generation and voyage planning optimization scheme for all-electric ships under emission policy," *International Journal of Electrical Power & Energy Systems,* vol. 156, p. 109698, 2024/02/01/ 2024, doi: https://doi.org/10.1016/j.ijepes.2023.109698.

[81] M. Ganjian, H. Bagherian Farahabadi, M. A. Alirezapouri, and M. Rezaei Firuzjaei, "Optimal design strategy for fuel cell-based hybrid power system of all-electric ships," *International Journal of Hydrogen Energy,* vol. 50, pp. 1558-1571, 2024/01/02/ 2024, doi: https://doi.org/10.1016/j.ijhydene.2023.07.258.
[82] B. Pang, S. Liu, H. Zhu, Y. Feng, and Z. Dong, "Real-time optimal control of an LNG-fueled hybrid electric ship considering battery degradations," *Energy,* vol. 296, p. 131170, 2024/06/01/ 2024, doi: https://doi.org/10.1016/j.energy.2024.131170.
[83] UW-Madison. TRNSYS – Official Website [Online] Available: https://sel.me.wisc.edu/trnsys/features/features.html
[84] Thermal Energy System Specialists. "TRNSYS." https://www.trnsys.com/ (accessed.
[85] SEL. *TRANSSOLAR Energietechnik GmbH, CSTB – Centre Scientifique et Technique du Bâtiment, TESS – Thermal Energy Systems Specialists. Section 8.7 Meteonorm data. Volume 8 Weather Data. TRNSYS 18 document package*.
[86] MeteotestAG. Meteonorm [Online] Available: https://meteonorm.com/en/
[87] EPD. Marine quality introduction [Online] Available: https://www.epd.gov.hk/epd/misc/marine_quality/1986-2005/eng/introduction_content.htm
[88] Carrier. Water-Cooled Liquid Chillers 30XW-30XWH. Order No. 13457-20, 10.2009. Supersedes order No. 13457-20, 01.2009.
[89] Daikin. Water-Cooled Scroll-Compressor Chillers, Catalog 613. Model WGZ-D • 30 to 200 Tons • R-410A • 60Hz/50Hz. CAT 613 (4/13); 2013.
[90] M. Kumar, H. Mohammed Niyaz, and R. Gupta, "Challenges and opportunities towards the development of floating photovoltaic systems," *Solar Energy Materials and Solar Cells,* vol. 233, p. 111408, 2021/12/01/ 2021, doi: https://doi.org/10.1016/j.solmat.2021.111408.
[91] FuturaSun. FU 250 / 255 / 260 / 265 / 270 / 275 P Polycrystalline Photovoltaic Module - 60 Cells [Online] Available: http://www.futurasun.com
[92] PacificNorthwest, "Tidal Energy," ed, 2021.
[93] Tidalpower.co.uk. Tidal Stream Generator [Online] Available: http://tidalpower.co.uk/tidal-stream-generator
[94] A. Roberts, B. Thomas, P. Sewell, Z. Khan, S. Balmain, and J. Gillman, "Current tidal power technologies and their suitability for applications in coastal and marine areas," *Journal of Ocean Engineering and Marine Energy,* vol. 2, no. 2, pp. 227-245, 2016.
[95] HKHO. Hong Kong Tidal Stream Prediction System [Online] Available: https://current.hydro.gov.hk/en/map.html
[96] A. Kusiak, H. Zheng, and Z. Song, "On-line monitoring of power curves," *Renewable Energy,* vol. 34, no. 6, pp. 1487-1493, 2009/06/01/ 2009, doi: https://doi.org/10.1016/j.renene.2008.10.022.
[97] P. L. Fraenkel, "Tidal Current Energy Technologies," *Ibis,* vol. 148, no. s1, pp. 145-151, 2006/03/01 2006, doi: https://doi.org/10.1111/j.1474-919X.2006.00518.x.
[98] P. L. Fraenkel, "Power from marine currents," *Proceedings of the Institution of Mechanical Engineers, Part A: Journal of Power and Energy,* vol. 216, no. 1, pp. 1-14, 2002/02/01 2002, doi: 10.1243/095765002760024782.
[99] J. Hardisty, "The tidal stream power curve: a case study," *Energy and Power Engineering,* vol. 4, no. 3, pp. 132-136, 2012.
[100] F. Chen, *The Kuroshio power plant*. Springer, 2013.
[101] NREL. Cost of Renewable Energy [Online] Available: https://www.nrel.gov/analysis/tech-lcoe-re-cost-est.html
[102] Wind-turbine-models. AN Bonus 1000/54 [Online] Available: https://en.wind-turbine-models.com/turbines/396-an-bonus-1000-54
[103] Wind-turbine-models. Alstom ECO 122/2700 [Online] Available: https://en.wind-turbine-models.com/turbines/629-alstom-eco-122-2700
[104] D. Clayton. Wind Turbine Spacing: How Far Apart Should They Be? [Online] Available: https://energyfollower.com/wind-turbine-spacing/
[105] X. Pi, "Offshore Wind Power: High Demand, Clear Pattern, Quality Growth Race (in Chinese)," ed: Ping An Securities Group, 2022.
[106] S. Cao, "The impact of electric vehicles and mobile boundary expansions on the realization of zero-emission office buildings," *Applied Energy,* vol. 251, p. 113347, 2019, doi: https://doi.org/10.1016/j.apenergy.2019.113347.
[107] EMSD. Performance-based Building Energy Code [Online] Available: https://www.emsd.gov.hk/filemanager/en/content_724/pb-bec_2007.pdf
[108] HKGBC. "Hong Kong Green Office Guide." https://www.hkgbc.org.hk/eng/gog.aspx (accessed.

[109] CLP. CLP 2024 Electricity Tariff Tables [Online] Available: https://www.clp.com.hk/content/dam/clphk/documents/tariff-adjustment-2024/TariffTable2024_ENG.pdf
[110] CLP. Peak Demand Management [Online] Available: https://www.clp.com.hk/en/environment/funds-services/peak-demand-management.html
[111] Marine Department, HKSAR. Port of Hong Kong Statistical Tables [Online] Available: https://www.mardep.gov.hk/en/fact/pdf/portstat_ast_2018.pdf
[112] Marine and Water Bureau, Macao. Ferry Terminals Statistics [Online] Available: https://www.marine.gov.mo/subpage.aspx?a_id=1498191461#
[113] CEM Macau. Tariff Group B [Online] Available: https://www.cem-macau.com/en/customer-service/billing-service/tariff-group-b/
[114] J. Trillos, D. Wilken, U. Brand-Daniels, and T. Vogt, *HySeas III: The World's First Sea-Going Hydrogen-Powered Ferry – A Look at its Technical Aspects, Market Perspectives and Environmental Impacts*. 2019.
[115] EV-database. Tesla Model S Dual Motor [Online] Available: https://ev-database.org/car/1404/Tesla-Model-S-Dual-Motor
[116] Lands Department, The Government of the HKSAR. Land Sale Records [Online] Available: https://www.landsd.gov.hk/en/resources/land-info-stat/land-sale/land-sale-records.html
[117] S. Cao, A. Hasan, and K. Sirén, "On-site energy matching indices for buildings with energy conversion, storage and hybrid grid connections," *Energy and Buildings,* vol. 64, pp. 423-438, 2013.
[118] S. Cao, A. Mohamed, A. Hasan, and K. Sirén, "Energy matching analysis of on-site micro-cogeneration for a single-family house with thermal and electrical tracking strategies," *Energy and Buildings,* vol. 68, pp. 351-363, 2014.
[119] Electrek. Tesla slashes the price of the Powerpack by 27% on Battery Day [Online] Available: https://electrek.co/2020/09/22/tesla-slashes-price-powerpack-battery-day/
[120] Siemens Energy. Decarbonizing maritime transport A study on the electrification of the European Ferry Fleet [Online] Available: https://assets.siemens-energy.com/siemens/assets